INFRARED LASERS WITH NOVEL GEOMETRIES

Adrian Alles Leal

UNIVERSITAT ROVIRA i VIRGILI

Infrared lasers with novel geometries

Adrian Alles Leal

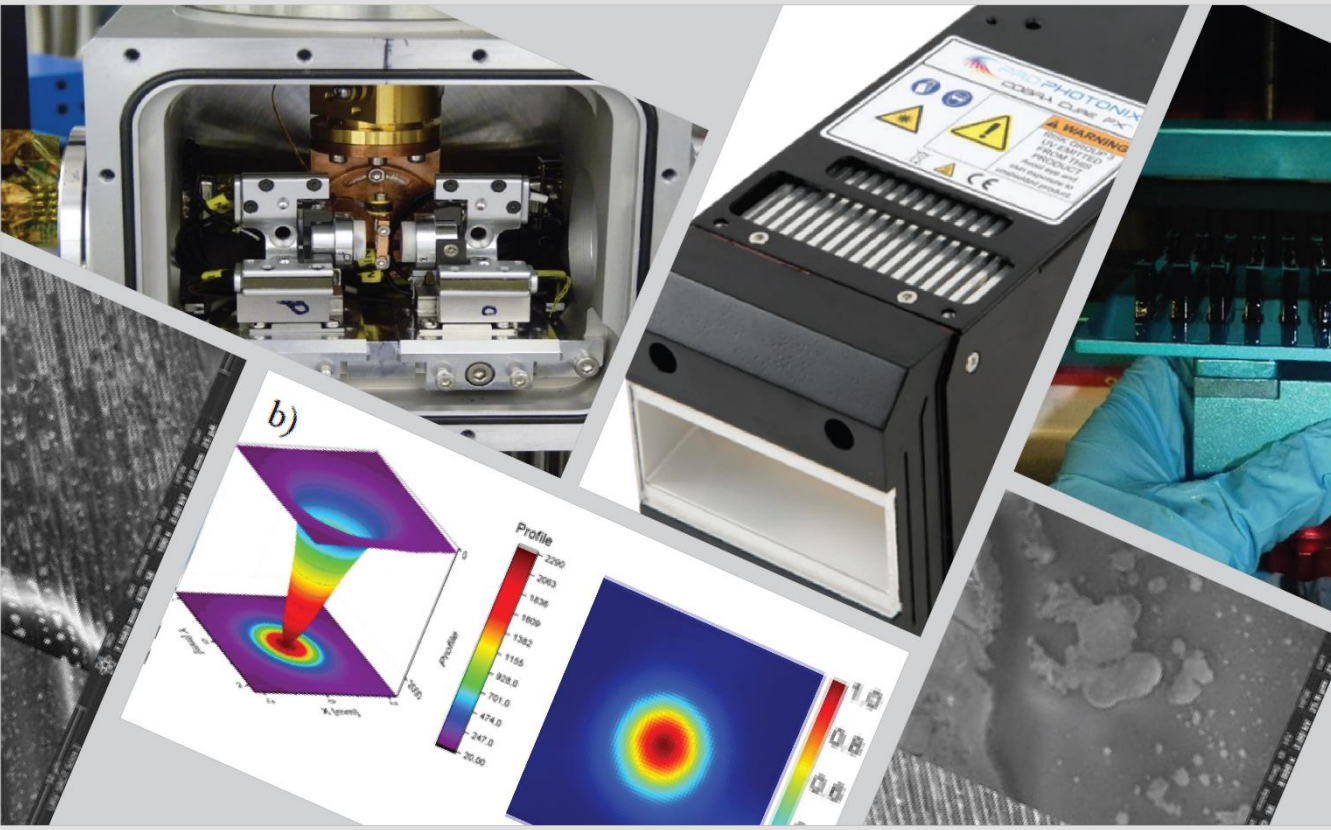

DOCTORAL THESIS

2023

UNIVERSITAT ROVIRA I VIRGILI
INFRARED LASERS WITH NOVEL GEOMETRIES
Adrian Alles Leal

UNIVERSITAT ROVIRA I VIRGILI
INFRARED LASERS WITH NOVEL GEOMETRIES
Adrian Alles Leal

UNIVERSITAT ROVIRA I VIRGILI
INFRARED LASERS WITH NOVEL GEOMETRIES
Adrian Alles Leal

Adrian Alles Leal

Infrared lasers with novel geometries

Doctoral thesis

Supervised by:

Dr. Josep Maria Serres

Prof. Dr. Xavier Mateos

Prof. Dr. Francesc Díaz

Doctoral Programme in Nanoscience, Materials and Chemical Engineering

Department of Physical and Inorganic Chemistry

Physics and Crystallography of Materials and Nanomaterials (FiCMA-FiCNA)

UNIVERSITAT ROVIRA i VIRGILI

TARRAGONA, 2023

Infrared lasers with novel geometries

Adrian Alles Leal

Física i Cristal·lografia de Materials i Nanomaterials (FiCMA -FiCNA)
Departament de Química Física i Inorgànica
Universitat Rovira i
Virgili, Tarragona,
Spain

UNIVERSITAT ROVIRA I VIRGILI
DEPARTAMENT DE QUÍMICA FÍSICA I INORGÀNICA
Campus Sescelades
Marcel·lí Domingo, s/n
43007 Tarragona
Tel. +34 977 55 81 37
Fax +34 977 55 95 63
www.quimica.urv.es

DECLARATION

Dr. Josep Maria Serres, Prof. Dr. Xavier Mateos and Prof. Dr. Francesc Diaz,

WE STATE that the present study, entitled **"Infrared lasers with novel geometries"**, presented by **Adrian Alles Leal** for the award of the degree of Doctor, has been carried out under our supervision at the **Department of Quimica Fisica i Inorgánica** of this university.

_____

Tarragona, 29/06/2023

Doctoral Thesis Supervisor/s

UNIVERSITAT ROVIRA I VIRGILI
INFRARED LASERS WITH NOVEL GEOMETRIES
Adrian Alles Leal

Abstract

Infrared lasers with novel geometries

Adrian Alles Leal

The development of laser light sources is continuously growing where historically efforts have focused on increasing laser power and reducing cost per watt by using only certain wavelengths in the electromagnetic spectrum.

A part of this thesis focused on the characterization of materials for the development of new compact lasers, generating emissions at different wavelengths of ~1.06 μm for Yb^{3+} and ~1.95 μm for Tm^{3+}; in continuous wave; and both at room temperature and cryogenic. This work intends to contribute in a relevant way to a solution that involves the development of compact lasers that operate at 1 micron and around 2 microns with high level performance. The novelty lies mainly in the spectral range of 2 microns and the cooling strategy of the laser crystal to achieve the desired results.

Finally, from the knowledge acquired and due to the potential of high-power infrared lasers, with novel geometries, it was applied to a study on additive manufacturing, opening new research opportunities, and improving the properties of existing devices and reducing manufacturing costs, as well as new light sources. The preliminary results obtained will serve as the basis and continuation of future projects in the line of photonics and advanced manufacturing systems of the Eurecat technology center.

Keywords: Infrared solid-state lasers, Diode-pumped, Laser materials, Cryogenic cooling, Additive Manufacturing.

Preface

This PhD thesis was carried out within the Physics and Crystallography of Materials and Nanomaterials (FiCMA – FiCNA) research group, at the Department of Physical and Inorganic Chemistry of the Universitat Rovira i Virgili (URV), Tarragona, Spain, between January 2020 and June 2023. It was supervised by Dr. Josep Maria Serres, Prof. Dr. Xavier Mateos and Prof. Dr. Francesc Díaz.

The study has been possible thanks to the financial support provided by Eurecat with the Vicente López grant under the project LASUV3D.

The research has been carried out in collaboration with international research groups:

- Dr. Venkatesan Jambunathan, and Dr. Tomas Mocek at the HiLASE Center, Institute of Physics ASCR (Dolní Brezany, Czech Republic).
- Dr. Pavel Loiko at the Centre de Recherche sur les Ions, les Matériaux et la Photonique (CIMAP), Université de Caen, Caen, France.

I am very pleased to have been able to work at HiLASE for three months and to have worked in close contact with all these excellent people. Without their contribution, I could not have written this thesis.

Adrian Alles Leal
Tarragona, 2023

Acknowledgments

"Gratitude is the heart's memory."

To, Dr. Josep Maria Serres, director, and supervisor of this doctoral thesis, for giving me this unique opportunity for my academic training and personal development. For his expertise, considerations, and support until the end of this investigation. El meu infinit agraïment.

To my supervisors, especially Prof. Dr. Xavier Mateos for his knowledge, valuable contributions, and thoughtful comments in the corrections of each result obtained. Moltes gràcies.

To Dr. Venkatesan Jambunathan my sincere gratitude for his professional leadership, scientific passion, and patience during my research stay in Czech Republic. Namasté.

To Dr. Victor Llamas, who was always there when I needed him, for his innumerable contributions and his love for Physics. Muchas gracias.

To Mailyn Ceballos for these first 15 years of friendship. For all the encouragement and good energy. Eres importante para mi.

To my friend Dra. Anna Volokitina for the beautiful and unforgettable memories in Tarragona. Spasiba!

To my PhD colleagues who gave me their solidarity hands on countless occasions and the friendship. Thank you, Sami, Ghassen, David and Antonio.

My gratitude to Gemma and Nicole, for their technical assistance, always with a smile and motivation.

To the Eurecat Foundation for the Vicente López scholarship, mobility grants and to the AMS group for their contributions.

To the URV for the opportunity to accomplish my doctoral studies.

A mi familia y amigos en Cuba y alrededor del mundo, que son mi inspiración y el motor que impulsa mi vida.

A todos, mi corazón les agradece.

A mis padres, con toda mi ilusión

Table of contents

Chapter 1

Motivation for the work

Continuous or pulsed laser generation[1], [2] [3] are very interesting in different application sectors. Two of the interesting sectors where this type of laser is used can be found in the medical sector [4] for tissue or eye treatments and in the industrial sector for advanced manufacturing applications for the additive manufacturing of 3D pieces [5]. The development of laser light sources is in continuous growth where historically efforts have focused on increasing laser power and reducing cost per watt by using only certain wavelengths in the electromagnetic spectrum. In recent years, it has been shown that different laser wavelengths with the same working power have different effects, which allows for much more effective treatment and processing compared to treatments performed up to now [6] [7]. A part of this work focuses on the characterization of laser materials for the development of new compact devices, generating emissions at different wavelengths, energy, and power, in continuous wave. Mainly, the potential of this work is focused on the development of

lasers for the industrial sector in advanced additive manufacturing, however, there are other sectors of interest with other applications [8] [9] [10].

The potential of 3D printing, for example, is booming, with many applications in different sectors ranging from its uses in the medical area and dentistry, architecture, electronic engineering, automotive, mechatronics, civil, production and automation. There are not a few artists, designers and merchants who use 3D printers to print their sculptures, luxurious jewelry, sports shoes, clothing, and decoration pieces [11] [12] [13] [14]. To optimize manufacturing and transportation times, NASA has sent its 3D printing machines into space that allow a personalized pieces to be available instantly [15]. Currently, Laser Focus World forecasts a skyrocketing increase in global sales of lasers and according to a study by Markets and Markets, the 3D printing market will move close to 32.7 billion dollars per year until 2023, growing close to a 25% per year [16] [17]. The numbers are an indicator of guaranteed success and motivate the search for innovations within this area, considering that it is a growing technology and that it is still far from its culminating point. The main characteristic of additive manufacturing is the flexibility it provides, making it an invaluable tool for short series. However, there are still limitations that slow down the manufacturing of pieces, and commercial machines only work on certain specific materials [18].

As will be seen in the following chapters, the thesis investigates new

laser materials for different continuous wave light sources, both at room temperature and in cryogenic cooling conditions [19]. This work represents a challenge in the field of diode-pumped solid-state lasers (SSLs) research with industrial applications. All these 2-micron laser applications are relatively new and constantly looking for improvements. Cryogenic temperatures [20] have been applied in SSLs primarily, although not only, in the 1-micron spectral range based on Yb ions [21]–[25] because there are known improvements over lasers operating at room temperature [26] [27] [28] [29]. Cryogenic temperatures significantly improve the thermo-optic properties of the active medium, increase thermal conductivity, decrease the variation of the refractive index with temperature, dn/dT, and the coefficient of thermal expansion, thus minimizing thermo-optic effects. Furthermore, laser materials under cryogenic conditions [30] [31] significantly increase the absorption cross section and lastly, the radiative lifetime of the emitting electronic level increases significantly at cryogenic temperatures.

This thesis is carried out with the motivation of developing a prototype machine for additive laser printing incorporating a set of laser light sources that allow the laser of the equipment to be customized with the material with which it is desired to work. In addition, the combination of two technologies is also proposed to accelerate the manufacturing process of 3D pieces, using the large area sintering technique (LAS) [32] with the laser technique, combining the benefits that each of these presents separately to

avoid the drawbacks that they present individually.

Chapter 2

Introduction

This second chapter provides an overview of solid-state lasers, their evolution over time, and the current state of the art of lasers, as well as future challenges associated with SSLs. Information on the active media (laser matrix) is described in a basic way, the active ions studied (Yb^{3+}, $Tm3^{+}$) and the cryogenic cooling systems are described. Finally, a description of the industrial applications of lasers and particularly in additive manufacturing is shown.

2. Introduction

2.1. State of the Art of Lasers

The discovery of the laser [7] [33] was without a doubt a significant event that was forever permeated as one of the great milestones in the history of science and technology.

Years of research, important discussions, and valuable contributions [34] from prestigious scientists from around the world precede it, but it was May 16, 1960, at the Hughes Research Laboratories in Malibu, west of Los Angeles, California, the day that is marked as the date the threshold of the laser age was crossed.

The optimistic 32-year-old American physicist and electrical engineer, Dr. Theodore Harold Maiman [35], and his assistant Irnee D'Haenens were experimenting very hard, until the ingenious idea sparked the first laser in history that Monday afternoon. Essentially, the device, still in use today, consisted of a small rod of pink synthetic ruby [36] [37] with 0.05% chromium, placed inside a flash tube as a medium of optically pumping the crystal. Silver mirrors at both ends of the glass were placed. The atoms in the crystal were excited by the intense light from the helical xenon lamp. After a pulse of light bounced between the mirrors, a bright red laser beam was displayed in full view of its creator, who would then begin an exhaustive effort to document their finding, to which the world is still indebted.

In honor of the discovery of the laser, UNESCO would declare May 16 as the International Day of Light.

2. Introduction

Figure 1. a) Theodore Maiman's first laser, removed from aluminum cylinder used during operation, and **b)** photo of Maiman behind a larger ruby laser

The laser, which in its beginnings was considered as "a solution that was looking for a problem" [38] as a joke, soon made headlines, causing the international scientific community to focus on developing the potential that lasers would certainly have. The prolific 1960s undoubtedly made possible new patents, publications, and inventions in telephony, the Internet, space exploration, medicine, and more [39][40][41][42].

The laser emerged as a new light for the coming centuries, as a discovery that, unlike other inventions that covered a single purpose, was a way of generating coherent light [43] that would open a range of possibilities in the most dissimilar areas and with a

2. Introduction

promising path in their contribution to knowledge. Laser beams traveled to the Moon before any human. More than sixty years of development since then have served to have a huge variety of lasers grouped into three large families: gas, solid-state, and semiconductor [44], and attempts to vastly improve the performance of all of them and find applications in scientific research, telecommunications, engineering, medicine, the military, materials science, and many others.

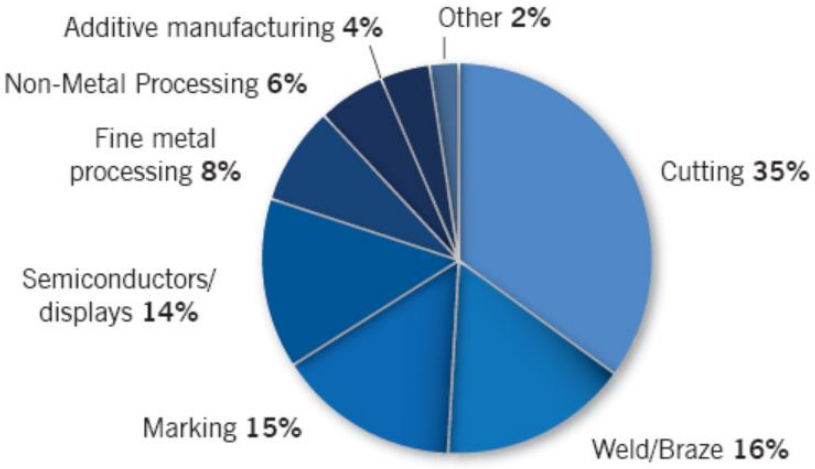

Figure 2. Industrial laser applications

It would be rigorous to reference all the relevant facts associated with lasers or give credit to all the people who made important contributions during that time, many of whom have been laureates of the world's most prestigious awards and recognitions [45], for example the Nobel Prizes [46] [47]. Like every evolving branch of

science, the world of lasers faces new challenges in the current era and for the future. Work is being done with a view to building increasingly intense, efficient, and safe lasers. Significant challenges remain, including developing extreme optics and cooling systems that can operate reliably in all kinds of conditions, and designing lasers that are mobile and affordable.

In this context, photonics [48] together with interdisciplinary research are more important than ever in the development of powerful precision lasers for the materials processing and manufacturing industry of the future, additive manufacturing of human organs and tissues in the laboratory, quantum technology and laser-based nuclear fusion [49].

2.2. Solid-State Lasers

Laser is an acronym for Light Amplification by Stimulated Emission of Radiation [6]. A laser can be defined as a device capable of generating a monochromatic, coherent, and directional beam using the stimulated emission [50] of radiation in a suitable medium.

The operating principle of a solid-state laser is based on the excitation of the active medium (amplifying material) through an optical pump mechanism. Due to the bombardment, the material absorbs the incident radiation, favoring the inversion of the population in the active medium. A resonant cavity is responsible for capturing the light that travels between the mirrors from one end to the other, increasing the accumulation of energy and the possibility of achieving stimulated emission (gain). This cavity

should be designed in such a way that the gains exceed the losses due to absorption, scattering or diffraction.

2.2.1. Laser active medium

Solid-state lasers [51][52], [53] are those that have a solid material in different geometries as the active medium. As previously mentioned, the first material used was synthetic ruby crystal [36]. In the same decade, uranium-doped calcium fluoride [54] was used, emitting at 2.5 μm. In later years, the use of glasses, ceramics, and crystals doped with transition or rare-earth[55] metals in small proportions for solid-state lasers became common. These ions can be divalent (Tm^{2+}, Ni^{2+}, Co^{2+}, Sm^{2+}, Dy^{2+}, and V^{2+}) or trivalent (Er^{3+}, Nd^{3+}, Ho^{3+}, Ce^{3+}, Tm^{3+}, Pr^{3+}, Gd^{3+}, Eu^{3+}, Yb^{3+} and Cr^{3+}) with internal energy levels that allow transitions favoring population inversion.

Rare earths [56] are used because the excited state of their ions is not strongly linked to the thermal variations of their phonons, or crystalline lattices, so the thresholds of this type of laser can be reached at low pumping intensities. The interaction between the hosts and dopants is known as the active medium.

The active medium determines the possible wavelengths that the laser can emit. Those wavelengths are determined by the specific transitions between the laser energy levels in this material. Although it is true that the fundamental and excited energy levels are usually considered, for practical purposes the laser can use up to four levels.

There are many active mediums that allow laser generation. Due

to its widespread use in multiple applications, NdYAG [57][58] [59] is the most common of all, with four energy levels. With a cubic crystalline structure of yttrium aluminum oxide, and neodymium as a dopant, forming a garnet. This laser can emit continuous and pulsed wavelengths at different wavelengths, which makes it possible to use it in medicine, material processing, and many others.

The titanium sapphire lasers [60] [61] [62] have the widest curve of the SSLs from 660 to 1180 nm, covering a wide range of the electromagnetic spectrum and use intense pulses of a few femtoseconds with high peak powers for the emission of X-rays and generation of harmonics. It is considered the most widely used ultra-fast laser.

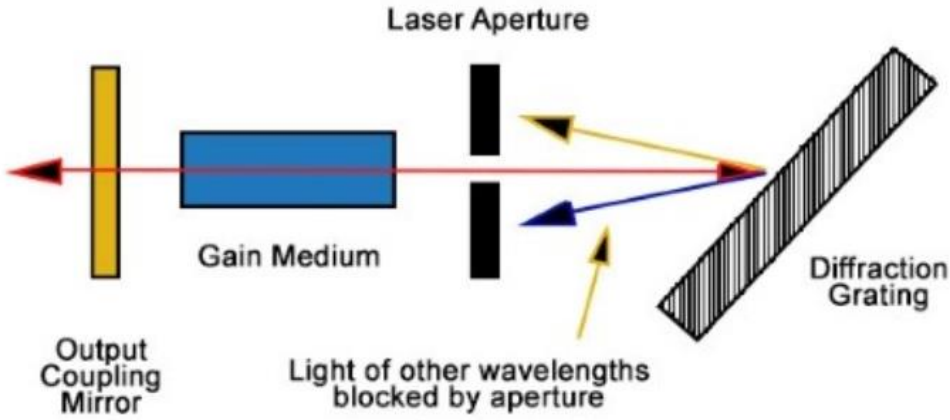

Figure 3. Schematic of a Ti:Sapphire Laser

2.2.2. Host Materials

The host material [63] for a solid-state gain medium must possess both unique microscopic and macroscopic properties, as well as favorable mechanical, thermal, and optical properties. It should be noted the transmission, dispersion, absorption, refractive index variation, charge compensation to maintain electricity, hardness, tension, and elasticity.

Optimum host properties ensure proper laser operation by allowing more extreme shelling that does not damage material, more accessible cutting and polishing, and excellent beam profile quality to be achieved. These host materials are often grouped as crystals and glasses.

Crystals are isotropic and anisotropic (uniaxial and biaxial), that is, the former have the same refractive index in all optical directions, while the latter are those whose refractive index depends on the direction of light propagation. They are characterized by being structurally ordered, having low laser thresholds, and by their high thermal conductivity and hardness.

On the other hand, the glasses are isotropic, have lower melting temperatures and, therefore, are easier to manufacture, have a high optical quality and can be doped homogeneously in higher concentrations. However, they have a much lower thermal conductivity than crystals and have an inhomogeneous broadening.

Among the most attractive isotropic materials are cubic crystals,

such as garnets, spinels or sesquioxides [56] [64], [65], due to their simple crystalline structure, high thermal conductivity, and small thermal expansion.
In the case of anisotropic, there are fluorides, monoclinic double tungstates (MDT) [66] [67], among others.

2.2.3. Rare-Earth ions

The active dopant ions used in solid-state lasers are ions of transition metals (Ti, Cr) and rare earths (lanthanide metals), between lanthanum and lutetium, located in the penultimate row of the periodic table. Of the latter, the most common ions are neodymium (Nd), ytterbium (Yb), erbium (Er), thulium (Tm) and holmium (Ho).
Lanthanide materials have the electronic configuration [Xe] $6s^2$ $5d^0$ $4f^n$ (where n is the number of 4f electrons from $0 < n < 14$, with some exceptions). It is common to find them as trivalent cations. In this oxidation state, the electronic configuration is [Xe] $4f^n$. Electrons are only completed in the 4f shell, and electrons in the 6s and 5d shells are missing. In fact, valence electrons are responsible for its absorption and emission transitions.
The two active rare earth ions that were used in this thesis are briefly described below: Tm and Yb.

The atomic number of Yb is 70 and it has the simplest system because only one excited state corresponding to the transition is possible. $^2F_{7/2} \rightarrow {}^2F_{5/2}$.

At room temperature, this corresponds to a nearly 4-level laser system. It is mainly used for laser generation at 1 μm. The absorption bandwidth for Yb^{3+} is between 880-1000 nm depending on the host. This band-pumping system shows very efficient laser generation, reducing fractional heat load (low losses by non-radiative processes) and very low quantum defect providing high slope efficiencies.

The simple energy level scheme avoids up-conversion and excited state absorption. It is also widely used as a sensitizing ion for lanthanide ions such as Er, Ho, Tm, and Pr because it exhibits very high absorption and transfers some energy to active ions [68][69][70].

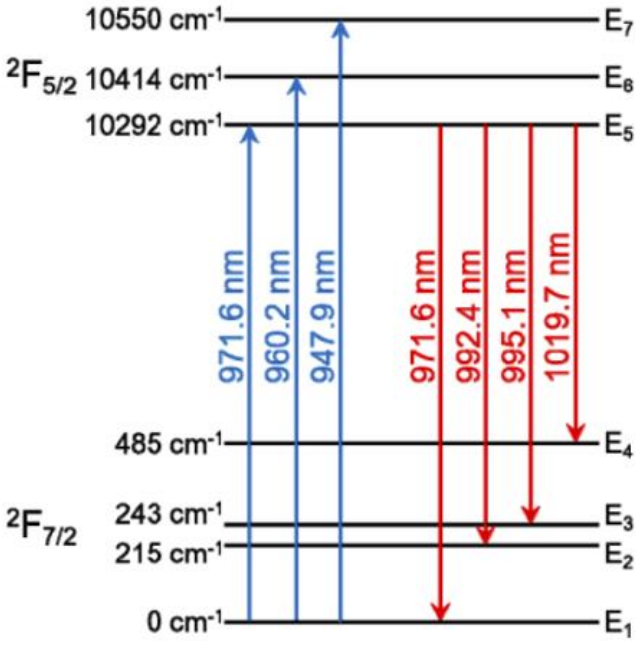

Figure 4. Energy diagram of Yb^{3+} in the host material YLF with

corresponding absorption and emission lines

The atomic number of Tm is 69 and it is one of the most suitable and efficient for lasers at 2 μm due to the high quantum efficiency caused by the so-called cross relaxation (CR), which reduces the heat load. The emission of ~2 μm corresponds to the $^3F_4 \rightarrow {}^3H_6$ transition. The CR mechanism allows to excite Tm ions to the $^3F_4$ level with only one pump of photons [71]–[73].

2.3. Cryogenic cooling

From practically the beginning of the use of lasers, ways were sought that would allow improvements in their performance. Among them, avoiding overheating of the resonant cavity that would prevent laser operation or reduce its efficiency, using cooling systems that dissipate heat.

Although it is true that the first laser operated at room temperature, for the second laser, demonstrated in history by Peter Sorokin and Mirek Stevenson, CaF_2 doped with U^{3+}, a cryogenic liquid, helium, was introduced, which allowed the inversion of population be reduced and therefore the threshold of the laser. Other types of cryogenic liquids may be suitable, for example liquid hydrogen, liquid neon, or liquid nitrogen.

2. Introduction

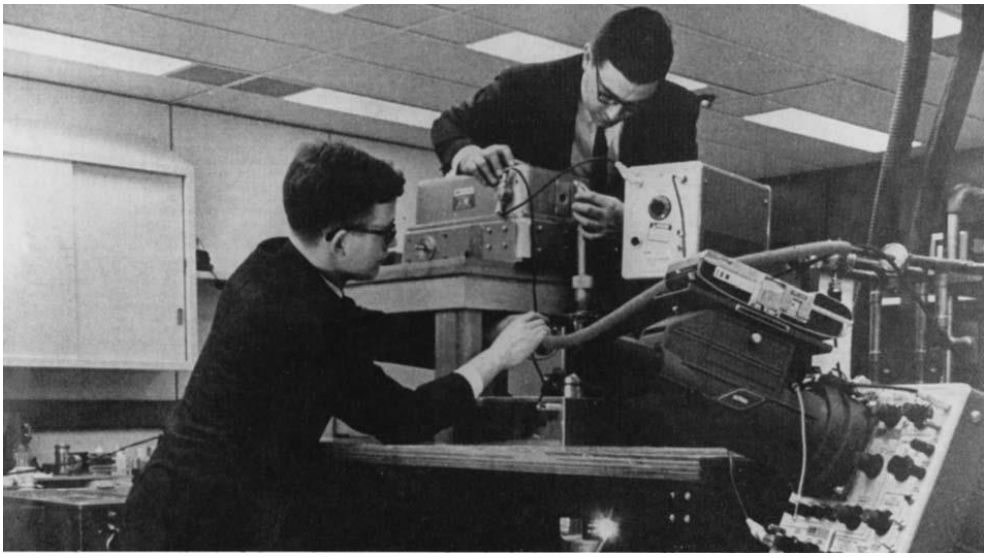

Figure 5. Peter Sorokin (left) and Mirek Stevenson (right) adjust their cryogenically cooled uranium-CsF_2 laser at the IBM T. J. Watson Research Center

From this crucial moment, scientists from the most prestigious institutions and laser centers in the world have found attractive numbers and have given rise to cryogenic lasers starting a revolution in the search for high powers and notable improvements in the beam quality.

Numerous publications [28], [30], [74] [75] endorse these advantages and serve as motivation to continue contributing scientific knowledge in the area.

The importance of cryogenic cooling systems is mainly due to several reasons. First, cryogenic temperatures significantly improve

key thermo-optical properties of the active medium, such as increasing thermal conductivity, decreasing the variation of the refractive index with temperature, dn/dT, and decreasing the coefficient of thermal expansion, thus minimizing non desired thermo-optical effects such as aberration, thermal lensing, thermally induced mechanical stress, among others. Second, laser materials in cryogenic conditions significantly increase the absorption cross section. Finally, the radiative lifetime of the emitting electronic level is significantly increased at cryogenic temperatures.

Cryogenic temperatures have been applied in SSLs primarily in the 1-micron spectral range based on Yb ions because there are demonstrated improvements over lasers operating at room temperature.

However, in recent years, novel contributions have been published in the 2-micron spectral range. In one of our most recent contribution [76] we present the laser characteristics of a 5 at.% Tm:YLF crystal using a modular setup at cryogenic temperatures and a maximum output power of 6.5 W at 80 K corresponding to an efficiency of 66 0.0% slope with respect to absorbed power with excellent beam quality.

Quantitative values of absorption and emission cross sections for Yb-doped laser materials (Yb:YAG and Yb:LuAG) as a function of temperature between 80 and 340 K are given in [77] . Note that for both materials, the emission cross section at 80 K is about 5 times that at room temperature, while the bandwidth is greatly reduced.

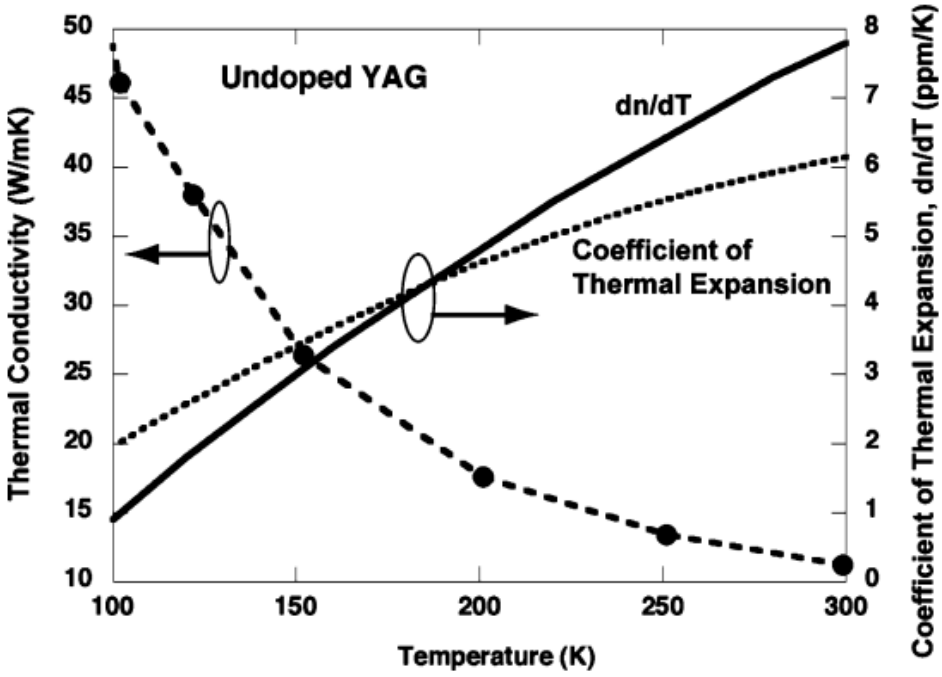

Figure 6. Thermal conductivity κ, coefficient of thermal expansion ζ, and dn/dT for undoped YAG from data in [78]

In [79] the pulsed and continuous wave laser characteristics of the transparent ceramic Yb:Y_2O_3 at cryogenic temperatures are reported. At 100K, a maximum CW output power of 12W was achieved, about three times that of 300K, and a slope efficiency of 54.4%, 2.4 times that of 300K.

2.4. Lasers in industrial applications

Lasers has been closely linked to advanced industrial manufacturing processes. Undoubtedly, the industrial sector is the world leader in terms of sales, only surpassed by telecommunications. There are various applications in the welding of parts, cutting, processing of materials and nanomaterials, perforation and drilling, laser engraving and marking, surface treatments, as well as inspection and metrological control, and many others. Among the main industries that benefit from these laser applications are the automotive, textile, naval or aerospace industries [80] [81], [82] [83].

2.4.1. Lasers in additive manufacturing

Additive manufacturing technologies (AM Additive Manufacturing) are a set of technologies that allow complex geometries to be obtained through a process of adding layers of material.

Today it is unthinkable not to consider the high potential of 3D printing and the most diverse applications and sectors of modern society. For short series it offers unique feasibility, as it is a highly flexible technology. However, there are still limitations in layer-by-layer manufacturing and the time required to have a piece. Similarly, commercially available kits do not cover specific materials of manufacture.

One of the technologies that uses a laser to melt, fuse or sinter particles together to end up forming an object, is the so-called SLS (Selective Laser Sintering) technology [84]–[86].

The laser in an SLS printer will vary in power, which determines what materials the machine can print. The SLS process can be described schematically as shown in Figure 7.

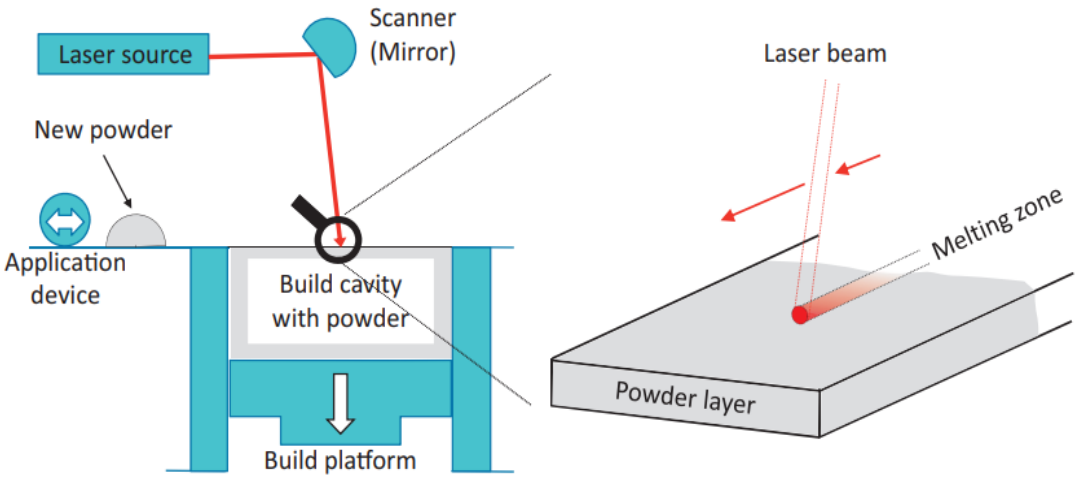

Figure 7. Physical schematic of SLS technology

A build area is coated step by step with polymer powder [87]. In each freshly applied layer, the laser introduces spatially different geometric information into the powder layer (see Figure 7, right). The powder melts homogeneously, in this case at the location where the laser hits the powder. Through layer-by-layer fusion and subsequent solidification, a piece is created by the overlapping and joining of many individual layers.

Chapter 3

Objectives and tasks of the Thesis

The general objective of this thesis is to design and develop compact, efficient, and robust SSLs in continuous wave using different ion-host combinations that can be applied in industry, and especially in additive manufacturing. This study focuses on lasers at various laser wavelengths, particularly at 1 and 2 µm. The general objective described above can be subdivided into four specific objectives:

- ✓ CW laser generation on active materials using microchip setup at room temperature.
- ✓ CW laser generation in active materials using a modular compact

3. Objectives and task of the Thesis

cavity at cryogenic temperatures in 1 and 2 µm.

- ✓ Characterization of materials for additive manufacturing.
- ✓ Development of a prototype 3D printing machine with the combination of LAS technology (UV projector) + UV laser.

To achieve these objectives, the study of new laser materials for different continuous wave light sources was carried out. The best materials for additive manufacturing were selected, and the most appropriate technologies for the projector, custom and/or commercial lasers that met the proposed requirements were also selected. Previously unstudied rare earth doped crystals were examined and all optical characterization was carried out in the laboratory. These were optical absorption and emission spectroscopy, Raman, power, wavelength, laser beam profile, among others; and thus, we obtained the results that were discussed and published. In addition, its functionality in industrial applications was validated by studying different emission ranges in the electromagnetic spectrum.

To first achieve the goal, the development of a new laser crystal with broadband emission properties at ~2 µm was studied: a gallium-tantalum-calcium garnet codoped with Tm^{3+}, Li^{+} (Tm:CLTGG) in a plane-plane linear cavity. The study largely focused on spectroscopy and laser operation of the Tm:CLTGG [88].

3. Objectives and task of the Thesis

The second objective was to demonstrate the operation of the laser in continuous wave applying the concept of compact modular cavity at cryogenic temperatures. The temperature would modify the thermo-optical and spectroscopic characteristics of the material, so the behavior of the laser was clearly different from that previously studied at room temperature. This objective allowed the collection of important data, such as the absorption of the material at different temperatures, the output laser power, the wavelength, the slope efficiency, the threshold of the laser, the spatial profile of the laser and its polarization. All this for the different samples that include different doping and thicknesses.

The last two objectives of this thesis include activities and tasks that were carried out within LASUV3D, the project's commercial name, *"Development of a new additive manufacturing technology combining LAS technology with UV laser. Study of new continuous and pulsed laser materials"*. LASUV is an internal recovery project of the AMS – Advanced Manufacturing Systems group of the Technological Center of Catalonia (Eurecat) [89] led by two main researchers and another group of multidisciplinary specialists. At the same time, the project was the subject of a master's degree thesis [90] of one of the participants and the author of this doctoral thesis.

The general Work Plan pursued by the LASUV3D project during the two-year period is detailed below. A schedule of activities was

planned, making a distribution of the activities and multiple follow-up meetings, consultations with external experts, as well as technical visits were carried out.

Note that as it is a multidisciplinary team, the activities were distributed according to the technical capacities of those responsible involved. It should be noted that for the development of this doctoral thesis, both the author and his supervisors focused on Activities 1 and 2, fundamentally, although not exclusively.

Activity 1: Technological surveillance

It is essential to constantly sketch and monitor emerging technologies, light sources and all kinds of new materials that arise, both to evaluate and diagnose the new technology and for the future and evolution of this and other projects of a similar nature.

Activity 2: Light sources and materials

Task 2.1: Study of new materials. Continuous wave light.

Within this task, the search and selection of additive manufacturing materials and the study of new laser materials for different continuous wave light sources will be carried out. The investigations carried out will be the basis from which those materials that we consider optimal will be selected, as well as the most appropriate technologies; customized and/or commercial lasers that meet the

required demands. We work based on being able to have a point laser, with a beam diameter of less than 100 µm and capable of emitting in an area with dimensions equal to or greater than 10x10 cm^2, with diffusive transmission optics, which allows it to be used as a project for the rapid curing of the pieces.

Task 2.2: Study of new materials. Pulsed wave light

This task will consist of the search for materials for the generation of pulses and those studied in the previous task, for different light sources. We will focus on investigating materials that are suitable for pulse generation, including saturable absorbers made of graphene, acousto-optic modulators, as well as mechanical modulators from an electromechanical chopper [91].

Task 2.3: Manufacture and characterization of different prototypes of compact lasers.

Within this task we will focus on studying the design and manufacture of compact solid-state lasers, from materials that have been previously studied and that presented a favorable optical response and that are encouraging for the industry. It is intended to study the possibility of having a prototype assembled with the solid-state laser, which allows its adaptation and combination of SLS and LAS technologies and observe the need to make changes in the work strategy, if necessary.

3. Objectives and task of the Thesis

As previously mentioned, the LASUV3D project is carried out in different stages, for two years. Activities 1 and 2 are accompanied by another series of tasks related to the design and conceptualization of the test bench to achieve proper positioning of the projector and laser, electronic and firmware conceptualization. In the same way, the project covers the assembly and start-up of all the pieces, the preliminary tests of the subsystems, the printing tests. Lastly, the manufacturing tests and the study of the patent approach.

Chapter 4

Equipment y Devices

This section briefly describes the most important equipment used to obtain the results in this study. Devices such as pump sources, output coupler mirrors, crystal holders, cavity setups, external devices, spectroscopy, and microscopy equipment are described, as well additive manufacturing materials and devices.

4.1. Pump sources

When we talk about generating lasers, pump sources [92] are essential elements. Optically pumping a medium basically means injecting light to electronically excite the medium or some of its components at other energy levels that are generally higher. The idea in question is to achieve a population inversion in the medium of gain. In this way, achieve optical amplification by stimulated emission for some range of optical frequencies. In the development of the thesis, the work has been done essentially with active ions Ytterbium and Thulium, for which it has been necessary to use different pumping sources, depending on the absorption band of these elements (energy levels of the active ions).

The pumping sources used in the study are described below:

For the pumping of the crystals, we use a set of commercial fiber-coupled laser diodes that operate at ~793 nm, ~976 nm and ~981 nm, in continuous wave regimes. Each of them was manipulated with different fibers to provide unpolarized light.

- ✓ The ~793 nm AlGaAs laser diode had a core diameter of 200 µm with a numerical aperture (NA) value of 0.22. The laser diode temperature was set at 12°C and emitted at 793 nm.

For the laser operation in cryogenic conditions, different diodes available in the Lab.03 facilities were used in HiLASE.

- ✓ Diode laser emitting around 793 nm was used as pump source, with a bandwidth of 0.5 nm stabilized by a Volume Bragg Grating [93]. The fiber-coupled diode had a core diameter of 105 μm and N.A. = 0.22 delivering a maximum output power of 25 W.

- ✓ A VBG diode with stabilized pump emitting at 976 nm matching the zero-phonon line of the gain medium.

4.2. Crystal holders for cooling

Crystals cooling holders are essential to minimize heating of the active material and thus help to dissipate the heat generated in the holders more efficiently. With these cooling systems we try to reduce all possible losses and gain stability and prevent unwanted thermal and mechanical effects that can cause damage to the crystals. Different sets of holders made of copper were necessary that allow the cooling of the faces of the active medium and their respective crystal holders considering the dimensions and thickness of the crystals. In all cases, very thin sheets of indium were used, and it was cooled with water.

.

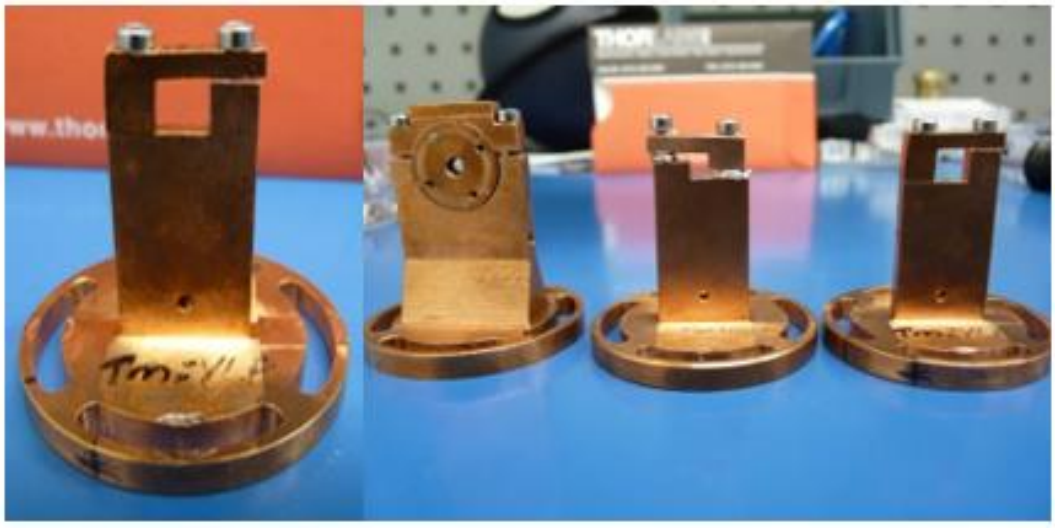

Figure 8. Crystal holders for cooling

4.3. Cavity for laser set-ups

This section shows the configurations used in laser generation. These include pump sources, optics, active materials, and cooling systems.

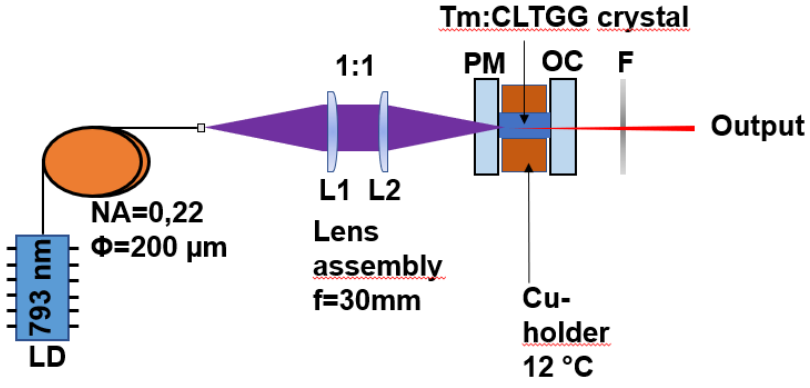

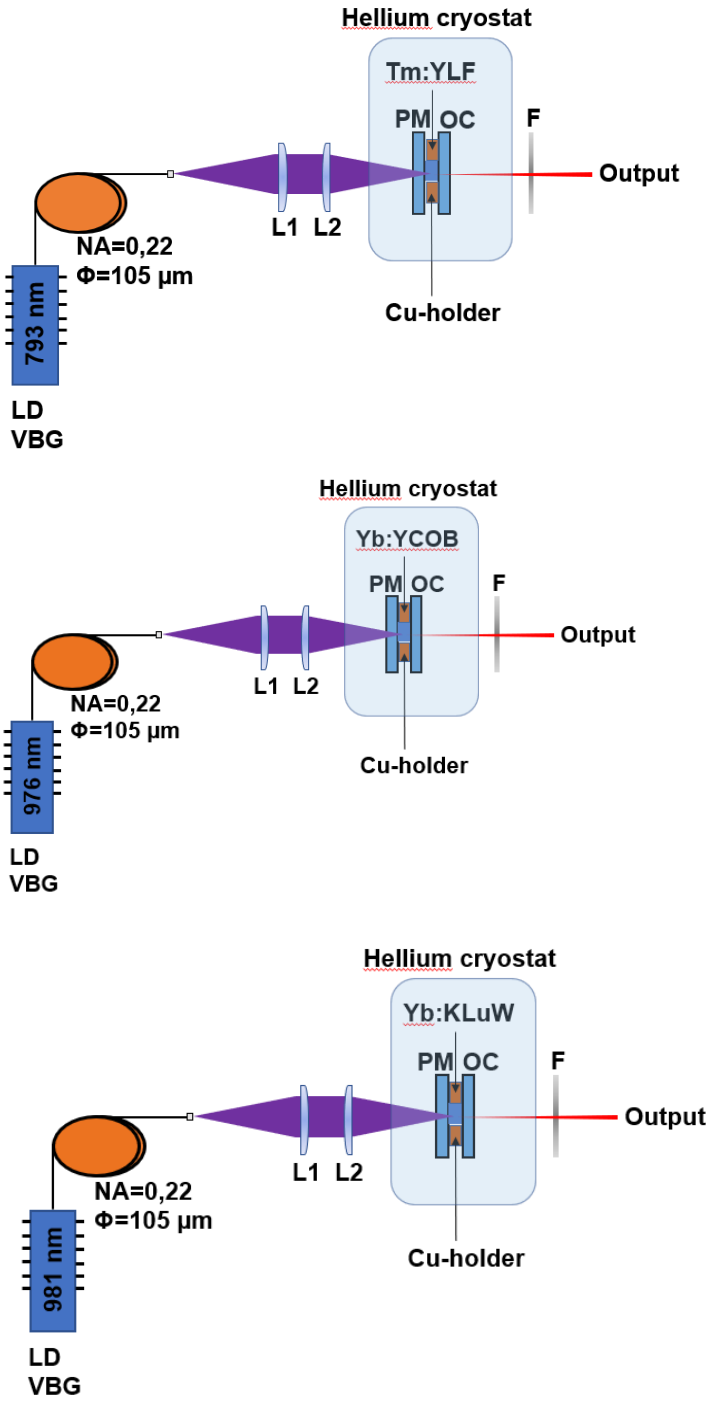

Figure 9. Laser setups used in this thesis

Note that for the crystals studied under cryogenic conditions, the design, as shown in Figure 10, consisted in all cases of a compact modular cavity, adapting the optical elements and diodes in correspondence with the active materials to be studied.

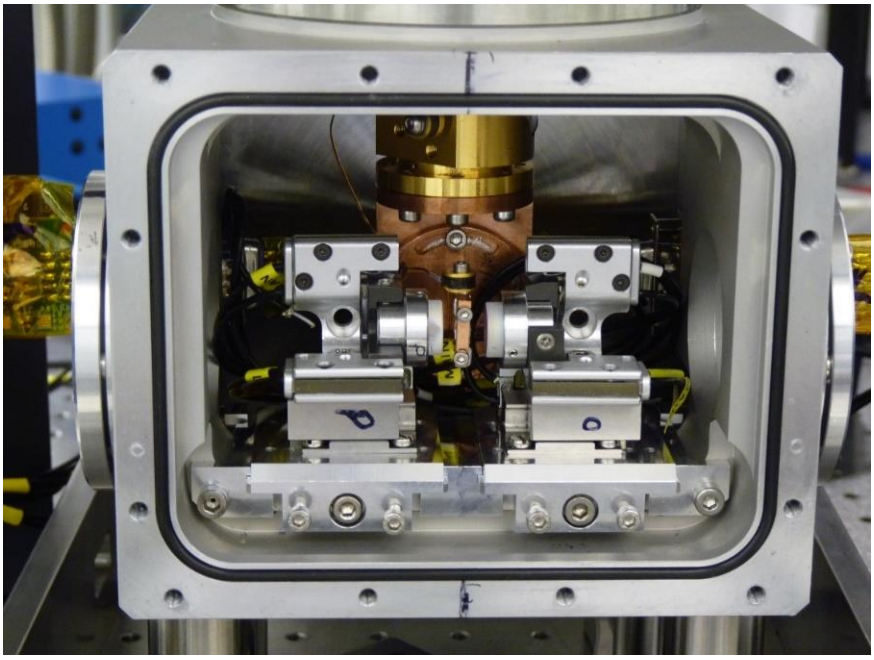

Figure 10. Cryogenic compact laser setup

4.4. External devices for laser operation

To characterize the laser beam, various optical detectors are needed, such as a power meter detector, spectrometers, and a CW visible-NIR camera. A laser power/energy meter was used to characterize the output beam. This provided good signal stabilization with low noise. Spectrophotometers were used to

detect the wavelength emission from the laser. Two different devices in different working ranges, from 800 to 1600 nm and from 1000 to 2600 nm, were used with an optical bandpass of <0.2 nm and <0.5 nm, respectively, and a precision wavelength. of ±0.2nm. A model FIND-R-SCOPE 85706 near-infrared camera operating in the 400 to 2000 nm region helped detect the NIR emission, quality, and profile of the laser beam. The camera provided high resolution 25mm f:1.4 manual iris lens. The video image was easily convertible with the help of a computer.

For the experiments at cryogenic temperatures, was used an equipment that allowed maintaining such working conditions for laser operation and other external devices. A closed-cycle helium cryostat (CH-204, JANIS) was used, with a cooling power of 13.5 W at 100 K; a Lake Shore temperature controller (DT 670) to monitor and maintain the sample temperature, which has 2 silicon diode sensors and a 50 Ω heater.

Two chillers, differently polarized, and infrared cameras, and wave-scans were used to measure the relevant wavelengths.

Figure 11. Lake Shore temperature controller (DT 670)

Figure 12. Vacuum

4. Equipment and Devices

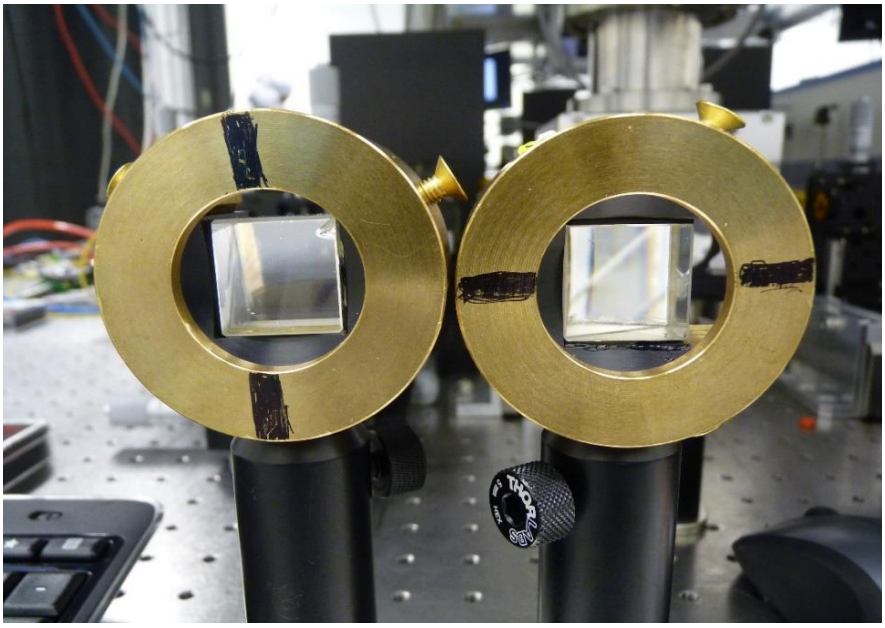

Figure 13. Light polarizers

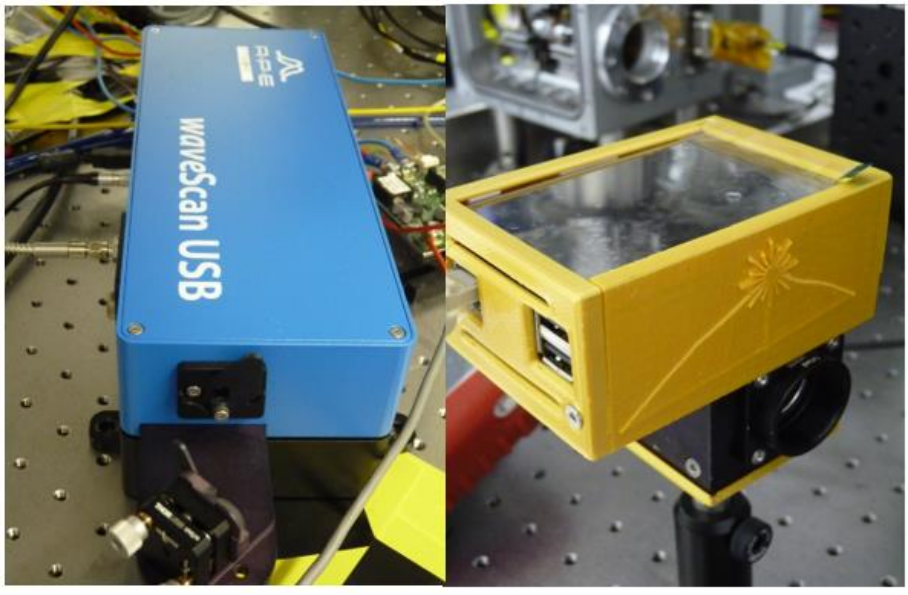

Figure 14. Wavescan (left); Infrared camera (right)

Figure 15. Chiller

4.5. Spectroscopic characterization

Spectroscopic characterization [94] was achieved using a VARIAN CARY-5E-UV-VIS-NIR 500 Scan spectrophotometer at URV. Both, the absorption, and transmission measurements were carried out to accurately know the absorption bands and the absorption wavelength, which is essential when selecting the most relevant pumping source.

It is possible to perform calculations of the emission cross sections of the ions and the gain sections. With this equipment we can make measurements along a spectral range from 400 to 2200 nm and

optical densities (O.D) from 0 to 10 with linear response.

Using this technique, we can compare the intensity between the incoming (I_0) and transmitted (I) beams of a given wavelength according to the Beer-Lambert law [95]:

$$I = I_0 e^{-\alpha d}$$

where d represents the thickness of the sample and α is the absorption coefficient that accounts for the variation of the radiation intensity through the medium.

The transmittance and absorbance (or O.D.) are defined as:

$$T = \frac{I}{I_0}$$

$$O.D = -ln\,\mathrm{T}$$

$$\alpha = \frac{O.D}{d\ log\ e}$$

To conclude, the absorption can be expressed by a quantity that will only depend on the nature of the material, the absorption cross section (σ_a) that accounts for the effective area of each absorbent center ($\sigma_a = \frac{\alpha}{N}$), where N the concentration of absorbing ions.

A quartz halogen lamp is used as the source of the visible and NIR spectral range. Because of the selective polarization of the samples, before the sample it is necessary to place a polarizer and a photomultiplier for visible radiation will be in charge of detecting the transmitted beam.

4.6. Microscopic techniques

Raman spectroscopy [96] is used to obtain chemical and structural information through vibrational and rotational analysis of chemical substances (organic and inorganic, liquid and solid). This technique is supplementary to infrared spectroscopy, where lines that are not visible in Raman spectroscopy may be active in infrared spectroscopy and vice versa. Raman mapping provides information about the distribution of different compounds contained in one plane or at different depths in a sample.

The Renishaw InVia Raman confocal microscope is equipped with three gratings of 2400 lines/mm, 1200 lines/mm and 600 lines/mm, three lasers available with wavelengths of 514 nm, 633 nm and 785 nm, and NExT filters for studies in ranges below 100 cm^{-1}.

Figure 16. Confocal Raman microscope

FESEM-FIB [97] is a field emission scanning electron microscope that integrates a focused electron beam and a gallium ion beam. The technique is used for ultra-high-resolution imaging, sample preparation for transmission microscopy, and 3D characterization of all types of materials, including magnetic and insulating materials. It features an X-ray energy dispersive spectrometry detector, a micromanipulator, and four gas injectors to design high-resolution nanostructures or exfoliate specific regions.

The equipment used under the control and supervision of the

technicians from the Scientific and Technical Resources Service of URV was the Scios 2 of FEI Company.

This equipment is characterized by a NiCol electron column (Non-Immersion Column) with electrostatic lenses that allow ultra-high resolution, and suitable for magnetic samples. It has 3 detectors on the column with high image contrast, an ion column, an ETD secondary electron detector on the chamber, a segmented backscattered electron (CBS/ABS) detector for composition and materials contrast, and for information on surface and topographic contrast, a segmented STEM (bright field, dark field, and high angle annular) detector, a fully automated micromanipulator, and an X-ray detector.

Figure 17. Operation of the FESEM-FIB

4.7. Additive manufacturing materials and devices

Numerous additive manufacturing materials [98], [99], as well as complementary equipment, devices and elements were used. One of the light sources used was a COBRA Cure™ FX3 lamp, as shown in Figure 18. The lamp consists of a radiation source based on LEDs, which are commonly used from a system such as a printing machine.

Figure. 18. Lamp COBRA Cure™ FX3

4. Equipment and Devices

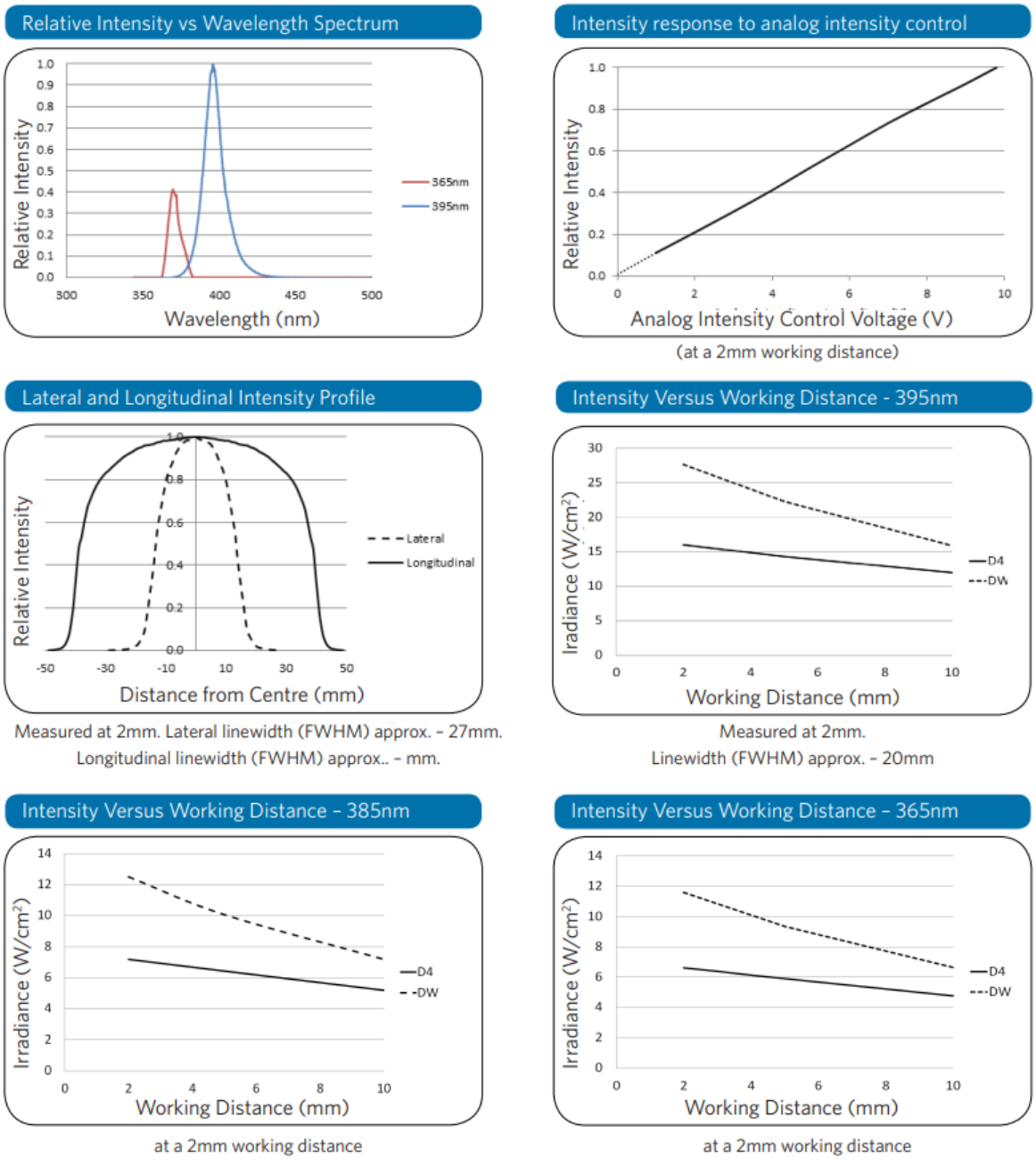

Figure 19. Optical characteristics of the lamp

It is worth mentioning the use of AnyCubic and AnyCubic Photon 0 resin printers, photosensitive UV resins, different polyamides, PLA plastic materials.

Different LCD [100] and mono LCD screens were used to achieve cooling of both through integration systems. In the same way, we use an AnyCubic pieces washing and curing machine and an EZ50 universal testing machine [101].

Figure 20. Washing/curing machine

Chapter 5

Results

In this doctoral thesis, special attention has been paid to laser operation at ~1 and ~2 μm in a continuous wave regime; both, at room temperature and under cryogenic conditions; which are discussed in this chapter. The results developed at FiCMA are exposed, as an interdisciplinary research group with extensive and proven experience in microchip lasers at room temperature, and on the other hand, the close collaborations with prestigious European institutions such as the HiLASE Center [102] where the experiments were carried out in the cryogenic laboratory at two different wavelengths of the electromagnetic spectrum.

5. Results

5.1. Continuous-wave laser operation at room temperature

Operation of solid-state lasers was carried out using various crystalline matrixes doped with rare earth ions using a microchip configuration.

5.1.1. Laser generation around ~2 μm from Tm^{+3} doped Tm:CLTGG

To complement these results, this section will show the scientific publications resulting from the work carried out for this thesis: research articles [P1] and [C1] [88]. It should be noted that the work is the result of the valuable collaboration of different multidisciplinary research groups from universities laboratories and research centers, composed of authors with extensive experience from various European and Asian countries, and the author of this thesis. In [P1] we report on the development of a novel laser crystal with broadband emission properties at ~2 μm that generates 1.08 W with a slope efficiency of 23.8 %. The main contribution of the main author consisted of the assembly and laser operation of the diode-pumped crystal and optical spectroscopy. Both studies were carried out in the FiCMA group, using the equipment and devices we have and the support of laboratory technicians. These results were enriched with the contributions of the other authors of the work such as crystal growth, X-ray diffraction and the study of thermal properties.

5. Results

5. Results

Tm^{3+}-doped calcium lithium tantalum gallium garnet (Tm:CLTGG): Novel laser crystal

Optical Materials Express, 11(9), 2938-2951.

ADRIAN ALLES,[1,2] ZHONGBEN PAN,[3,4] PAVEL LOIKO,[5] JOSEP MARIA SERRES,[1,2] SAMI SLIMI,[1] SHAWUTI YINGMING[3], KAIYANG. TANG,[3] YICHENG WANG,[4] YONGGUANG ZHAO,[4,6] ELENA DUNINA,[7] ALEXEY KORNIENKO,[7] PATRICE CAMY,[5] WEIDONG CHEN,[4,8] LI. WANG,[4] UWE GRIEBNER,[4] VALENTIN PETROV,[4] ROSA MARIA SOLÉ,[1] MAGDALENA AGUILÓ,[1] FRANCESC DÍAZ[1] AND XAVIER MATEOS[1,*]

[1]Universitat Rovira i Virgili, FiCMA-FiCNA, Marcel·lí Domingo 1, 43007 Tarragona, Spain
[2]Eurecat, Centre Tecnològic de Catalunya, Advanced Manufacturing Systems Unit (AMS), Marcel·lí Domingo 2, 43007 Tarragona, Spain
[3]Institute of Chemical Materials, China Academy of Engineering Physics, 621900 Mianyang, China
[4]Max Born Institute for Nonlinear Optics and Short Pulse Spectroscopy, Max-Born-Str. 2a, 12489 Berlin, Germany
[5]Centre de Recherche sur les Ions, les Matériaux et la Photonique (CIMAP), UMR 6252 CEA-CNRS-ENSICAEN, Université de Caen Normandie, 6 Boulevard du Maréchal Juin, 14050 Caen Cedex 4, France
[6]Jiangsu Key Laboratory of Advanced Laser Materials and Devices, Jiangsu Normal University, 221116 Xuzhou, China
[7]Vitebsk State Technological University, 72 Moskovskaya Ave., 210035 Vitebsk, Belarus
[8]Key Laboratory of Optoelectronic Materials Chemistry and Physics, Fujian Institute of Research on the Structure of Matter, Chinese Academy of Sciences, Fuzhou, 350002 Fujian, China
**xavier.mateos@urv.cat*

5. Results

Abstract:

We report on the development of a novel laser crystal with broadband emission properties at ~2 μm – a Tm^{3+} ,Li^{+} -codoped calcium tantalum gallium garnet (Tm:CLTGG). The crystal is grown by the Czochralski method. Its structure (cubic, sp. gr. $Ia\bar{3}d$, a = 12.5158(0) Å) is refined by the Rietveld method. Tm:CLTGG exhibits a relatively high thermal conductivity of 4.33 $Wm^{-1}K^{-1}$. Raman spectroscopy confirms a weak concentration of vacancies due to the charge compensation provided by Li^{+} codoping. The transition probabilities of Tm^{3+} ions are determined using the modified Judd-Ofelt theory yielding the intensity parameters Ω_2 = 5.185, Ω_4 = 0.650, Ω_6 = 1.068 [10^{-20} cm^2] and α = 0.171 [10^{-4} cm]. The crystal-field splitting of the Tm^{3+} multiplets is revealed at 10 K. The first diode-pumped Tm:CLTGG laser generates 1.08 W at ~2 μm with a slope efficiency of 23.8%. The Tm^{3+} ions in CLTGG exhibit significant inhomogeneous spectral broadening due to the structure disorder (a random distribution of Ta^{5+} and Ga^{3+} cations over octahedral and tetrahedral lattice sites) leading to smooth and broad gain profiles (bandwidth: 130 nm) extending well above 2 μm and rendering Tm:CLTGG suitable for femtosecond pulse generation.

5. Results

1. Introduction

An ordered crystal is an ideal solid material exhibiting lattice periodicity in all directions. The certain location of atoms in the unit-cell is repeated forming a translationally invariant crystal structure in the long-range. The structure disorder is a deviation from a perfect crystalline order. Weak disorder can be represented as a perturbation of the crystalline structure, e.g., caused by dopants, defects, vacancies and / or dislocations. Strong disorder is a marked departure from the crystalline order. The length scale over which order, or disorder persists is also relevant. The local disorder can be revealed at a length of several unit-cells.

In laser physics, structurally disordered crystals constitute an important class of gain materials [1]. In such crystals, one or several host-forming cations are randomly distributed over two or more different crystallographic sites. Two situations for the dopant (laser-active) ions can be thus distinguished: (i) the dopant ions are distributed over several lattice sites [1] or (ii) they are present at one site while other cations experience a random site distribution [2]. In both cases, the spectral bands of dopant ions will experience an inhomogeneous broadening either due to the presence of several crystal-fields or due to the different cation multi-ligands around the dopant ions. Such spectral broadening is favorable for broadband tuning of the laser wavelength and / or the generation of ultrashort

5. Results

pulses in mode-locked (ML) lasers. Note that there also exists compositional disorder in “mixed” (solid-solution) materials $A_{1-x}B_x$, even when the parent compounds (A and B) are ordered [3]. In this case, the spectral broadening is also observed. The main drawback of disordered crystals is the deterioration of their thermal properties. Thus, the search of disordered crystals showing high thermal conductivity is relevant.

Among the host crystals for doping with laser-active rare-earth ions (RE^{3+}), cubic multicomponent garnets with general chemical formula $\{A\}_3[B]_2(C)_3O_{12}$ where A = Y, Gd, Lu or Ca, Mg, Fe, Sr, etc., and B and C = Al, Sc, Ga, Ta, etc., attract an important attention. Note that the ordered garnet $Y_3Al_5O_{12}$ (YAG) is the most widespread laser host crystal. Crystals belonging to the cubic garnet family combine good thermo-mechanical behavior with attractive spectroscopic properties of the dopant RE^{3+} ions. They are optically isotropic. Finally, cubic garnets can be grown by the well-developed Czochralski (Cz) method.

Among the structurally disordered multicomponent garnets, the crystal of calcium niobium gallium garnet (CNGG) is known [4,5]. The structure disorder of CNGG originates from a random site distribution of Nb^{5+} and Ga^{3+} cations over [B] and (C) lattice sites leading to a significant inhomogeneous broadening of the emission bands of the RE^{3+} dopant ions. The latter are expected to replace for the divalent Ca^{2+} cations; the charge compensation is provided

5. Results

by vacancies [6] or by intentional codoping by univalent alkali ions (Na^+, Li^+ or their combination) [7,8] further affecting the spectral broadening [9].

Recently, CNGG-type crystals doped with thulium (Tm^{3+}) [10] and holmium (Ho^{3+}) [11] ions have been proven to be very suitable for the generation of ultrashort pulses (sub-100 fs) at ~2 μm owing to their smooth and very broad gain profiles extending well above 2 μm [12] and avoiding the effect of the structured absorption of water vapors in the atmospheric air on the ML laser performance. Pan et al. reported on a Tm:CNNGG laser mode-locked by a single-walled carbon nanotube saturable absorber (SA)delivering 84 fs pulses at 2018 nm. In the continuous-wave (CW) regime, the same work reports on a broad tuning range of 1879 – 2086 nm [10]. Zhao et al. achieved shorter pulses (67 fs, i.e., 10 optical cycles at 2083 nm) from a Tm,Ho:CLNGG laser mode-locked by the same SA because of the combined gain bandwidths from both active ions [13].

There exists another disordered multicomponent garnet similar to CNGG, namely calcium tantalum gallium garnet (CTGG) [14]. Ma et al. has shown that CTGG exhibits higher thermal conductivity (κ = 3.76 $Wm^{-1}K^{-1}$) as compared to its niobium counterpart [14]. There exist studies on CTGG-type crystals doped with Nd^{3+} and Yb^{3+} ions for laser operation at ~1 μm [15,16]. However, Tm^{3+}-doped crystals working in the ~2 μm spectral range have not been studied yet.

In the present work, we aimed to reveal the potential of Tm^{3+}, Li^+-codoped calcium tantalum gallium garnet (Tm:CLTGG) as a

5. Results

broadband laser gain material at ~2 μm and beyond.

2. Crystal growth

A Tm^{3+}, Li^{+}-codoped calcium tantalum gallium garnet (abbreviated: CLTGG) single crystal was grown by the Czochralski (Cz) method in an iridium crucible using argon atmosphere. The starting materials, $CaCO_3$ (purity: 4N), Ta_2O_5, Ga_2O_3, Li_2CO_3 and Tm_2O_3 (5N), were weighed according to the chemical formula $Ca_3Ta_{1.88}Li_{0.20}Ga_{2.80}O_{12}$. To compensate the volatilization of Ga_2O_3 during the synthesis of the polycrystalline material and the crystal growth, an excess of 1.0 wt% Ga_2O_3 was added. The equation of the chemical reaction was as follows:

$3CaCO_3 + 0.94Ta_2O_5 + 1.525Ga_2O_3 + 0.075Tm_2O_3 + 0.1Li_2CO_3 \rightarrow Ca_3Ta_{1.88}Li_{0.20}Ga_{2.80}O_{12}\cdot 0.05Tm_3Ga_5O_{12} + 3.1CO_2\uparrow$.

The raw materials were mixed, ground, and heated at 900 ℃ for 10 h in a platinum crucible to decompose $CaCO_3$. After the crucible was cooled down to room temperature (RT, 20 ℃), the mixture was pressed into tablets and again reheated at 1200 ℃ for 15 h to form the cubic garnet phase through a solid-state reaction. The synthesized polycrystalline material was placed in an iridium crucible and melted by an intermediate-frequency heater. The first crystal was grown using an [111] oriented seed from undoped YAG. From this first crystal, another seed with the same orientation was cut and used for the growth of laser-quality crystals. During the crystal growth, the pulling rate varied from 0.5 to 1.0 mm/h and the

5. Results

crystal rotation speed was kept at 8 to 15 revolutions per minute. After the growth was completed, the crystal was removed from the melt and cooled down to RT at a stepped rate of 15 to 25 ℃/h. The crystal was annealed in air, the maximum temperature was 1200 ℃ and the hold duration was 24 h, the heating and cooling rates were about 50 ℃/h.

Fig. 1. Photograph of the as-grown Tm:CLTGG crystal boule, the growth direction is [111].

Figure 1 shows a photograph of an as-grown Tm:CLTGG crystal boule. It has a cylindrical shape (diameter: 20 mm, length of the central part: 30 mm). The crystal does not contain cracks and inclusions and no scattering centers are observed under illumination by a He-Ne laser indicating good optical quality. The as-grown crystal shows a slight greenish coloration.

By using X-ray fluorescence, the actual concentration of Tm^{3+} ions was measured to be 3.17 at.% with respect to Ca^{2+} ions (N_{Tm} =

5. Results

5.03×1020 cm^{-3}) leading to a segregation coefficient K_{Tm} of 0.67.

3. Crystal structure

3.1. X-ray diffraction

The X-ray powder diffraction (XRD) pattern was measured at RT using a Bruker D2 Phaser diffractometer, Cu Kα1 radiation (1.54184 Å) with a step size of 0.02° and a step time of 1.0 s, in the range of 2θ from 10° to 90°. The measured diffraction pattern, Fig. 2(a), agrees well with the theoretical one for cubic $Al_{1.23}Ca_3Fe_{0.99}Hf_2Si_{0.99}O_{12}$ garnet (Crystallography Open Database (COD) card #96-901-3967). No other phases are found.

The structure of Tm:CLTGG was refined using the Rietveld method. The Match3! software was used and a total of 196 reflections were analyzed. The obtained reliability factors are R_p = 4.94%, R_{wp} = 6.38%, R_{exp} = 2.21% and the reduced chi squared $\chi^2 = (R_{wp}/R_{exp})^2$ = 8.37. Tm:CLTGG crystallizes in the cubic class (sp. gr. $Ia\bar{3}d$, No. 230) with a lattice constant a = 12.5158(0) Å, the volume of the unit-cell is V = 1960.54 $Å^3$, the calculated density is ρ_{calc} of 5.893 g/cm^3 and the number of formula units in the unit-cell is Z = 8. The fractional atomic coordinates, the site occupancy factors (O.F.) and the isotropic displacement parameters obtained during the Rietveld refinement are listed in Table 1.

5. Results

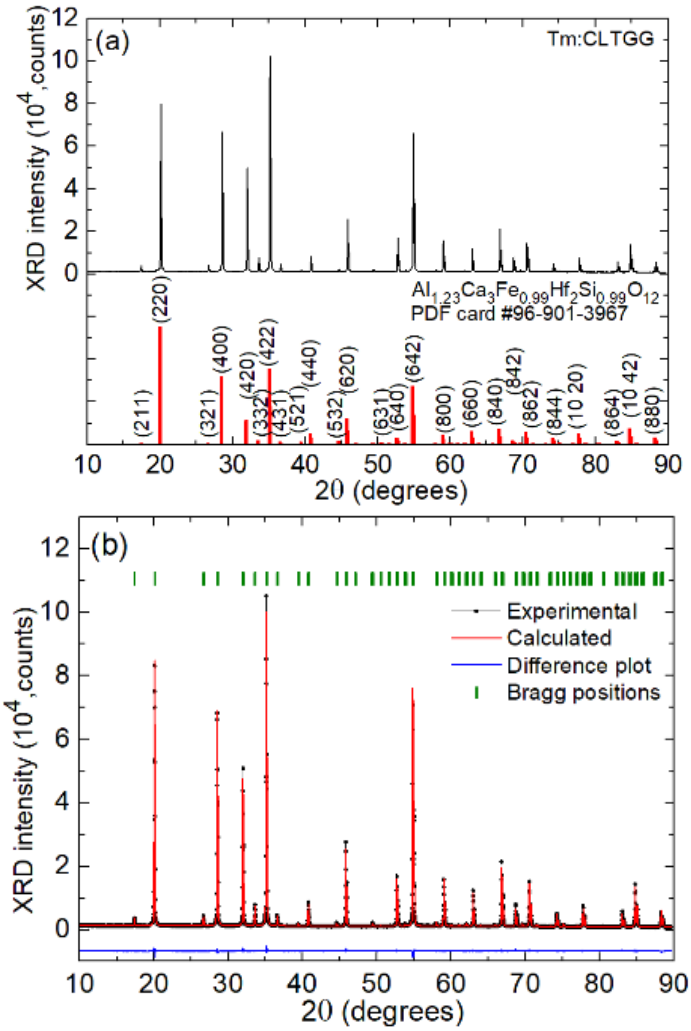

Fig. 2. X-ray powder diffraction study of Tm:CLTGG: **(a)** XRD pattern, (hkl) are Miller's indices, vertical bars – theoretical pattern for $Al_{1.23}Ca_3Fe_{0.99}Hf_2Si_{0.99}O_{12}$ garnet; **(b)** Rietveld structure refinement: experimental (black), calculated (red) and differential (blue) XRD profiles, vertical dashes mark the Bragg reflections.

5. Results

Table 1. Fractional Atomic Coordinates, Occupancy Factors and Isotropic Displacement Parameters for Tm:CLTGG Crystal

Atoms	Wyckoff	*x/a*	*y/b*	*z/c*	*O.F.*	B_{iso}, $Å^2$
Ca	24*c*	1/8	0.0000(0)	1/4	0.963	0.722(7)
Tm	24*c*	1/8	0.0000(0)	1/4	0.031	0.722(7)
Ta1	16*a*	0.0000(0)	0.0000(0)	0.0000(0)	0.660	0.253(1)
Ga1	16*a*	0.0000(0)	0.0000(0)	0.0000(0)	0.340	0.253(1)
Ga2	24*d*	0.3750(0)	0.0000(0)	1/4	0.789	0.481(4)
Ta2	24*d*	0.3750(0)	0.0000(0)	1/4	0.068	0.481(4)
Li	24*d*	0.3750(0)	0.0000(0)	1/4	0.115	0.481(4)
O	96*h*	-0.0295(1)	0.0492(1)	0.1482(9)	1	0.826(0)

The structure of Tm:CLTGG is illustrated in Fig. 3. This crystal belongs to the family of multicomponent garnets with a general formula $\{A\}_3[B]_2(C)_3O_{12}$, where {A}, [B], and (C) stand for dodecahedral (Wyckoff symbol: 24c), octahedral (16a) and tetrahedral (24d) sites, respectively [5]. The stoichiometric CTGG, in analogy to CNGG [4], is expected to have a chemical formula of $Ca_3Nb_{1.5}Ga_{3.5}O_{12}$ which is equivalent to $\{Ca_3\}[Nb_{1.5}Ga_{0.5}](Ga_3)O_{12}$. The composition of the real crystal (even undoped) deviates from the stoichiometric one. The Ca^{2+} cations are located in the {A} sites.

5. Results

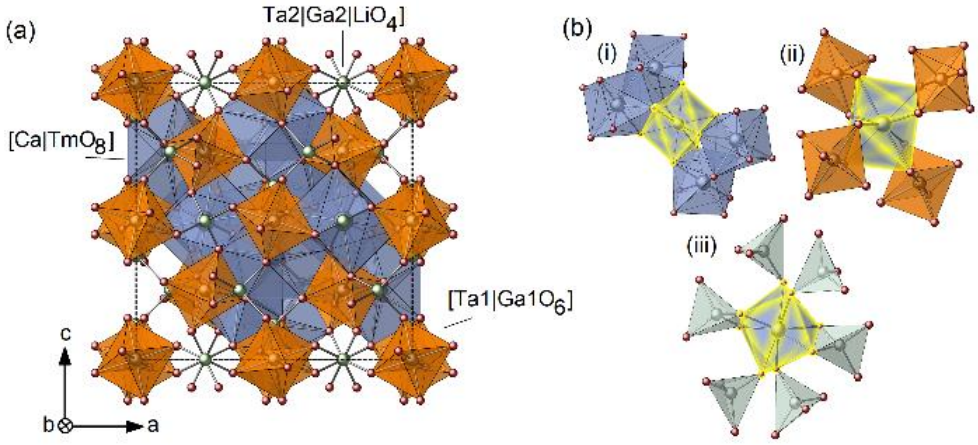

Fig. 3. Crystal structure of Tm:CLTGG: (a) a fragment of the crystal structure within one unit-cell (dashed lines) in projection to the a-c plane; (b) the variety of cationic distributions around Ca^{2+} | Tm^{3+} ions occupying the dodecahedral 24c sites: nearest-neighbor cations at: (i) dodecahedral 24c sites, (ii) octahedral 16a sites and (iii) tetrahedral 24d sites.

The Tm^{3+} ions replace for the Ca^{2+} ones (the corresponding ionic radii are RCa = 1.12 Å and RTm = 0.994 Å for VIII-fold oxygen coordination). In the [Ca|TmO_8] dodecahedrons, there are four shorter (2.3966(2) Å) and four longer (2.5577(0) Å) metal-to-oxygen (M-O) interatomic distances. The Ta^{5+} and Ga^{3+} cations are randomly distributed over the [B] and (C) sites with VI-fold and IV-fold oxygen coordination, respectively, according to the occupancy factors listed in Table 1. The M-O bond lengths are 1.990(0) Å (×6) and 1.8526(1) Å (×4), respectively. The Li^{+} ion incorporation in this garnet takes place only at 24d sites. The charge compensation is ensured by both, Li^{+} ions and cationic vacancies □ in the 24c and

5. Results

24d sites. Their calculated percentages are 0.6% and 2.8%, respectively. The chemical formula of the crystal can be thus expressed as follows:

$\{Ca_{2.889}Tm_{0.093}\square_{0.018}\}[Ta_{1.32}Ga_{0.68}](Ga_{2.367}Ta_{0.204}Li_{0.345}\square_{0.084})O_{12}$.

In the Tm:CLTGG structure, each $[Ca|TmO_8]$ dodecahedron shares edges with four other dodecahedra where the shortest interatomic distance Ca|Tm—Ca|Tm is 3.8321(1) Å, and it is surrounded by four corner-sharing octahedra (Nb^{5+} and Ga^{3+} at 16a site) and by six tetrahedra (Ga^{3+}, Nb^{5+} and Li^{+} at 24d site), two of them sharing edges, and the remaining four are connected by shared corners.

3.2 Raman spectroscopy

The Raman spectrum of Tm:CLTGG was measured using a Renishaw inVia confocal Raman microscope with a ×50 Leica objective and an Ar^{+} ion laser (514 nm). It is shown in Fig. 4. In the same figure, for comparison, we also show the Raman spectrum of its niobium isomorph, Tm:CLNGG. A total of 18 bands are resolved in the Raman spectrum of Tm:CLTGG. Among them, the vibrations at high frequencies (700-900 cm^{-1}) forming two broad bands are typically analyzed as they are sensitive to the alteration of the structure of multicomponent garnets [4,5]. They are assigned to internal vibrations (symmetric stretching modes, vs) of $[M2O_4]$ tetrahedra. In our case, the 24d sites are occupied by Ta^{5+} and Ga^{3+} cations. The band at lower frequencies with two local maxima at 748

5. Results

cm^{-1} (C1) and 772 cm^{-1} (C2), is assigned to the $[Ga_2O_4]$ groups and it is only slightly distorted with respect to that in the Tm:CLNGG crystal. The band at higher frequencies, at 842 cm^{-1} (C4), is due to the $[Ta_2O_4]$ groups. The latter does not split, possesses much weaker intensity and is shifted to higher frequencies as compared to that in Tm:CLNGG crystal with $[Nb_2O_4]$ groups. The lack of the long-frequency component of the second band indicates weak structural distortion of the $[Ta_2O_4]$ tetrahedra and weak content of cationic vacancies, in agreement with the XRD study. This highlights the positive role of Li^+ ions in the charge compensation.

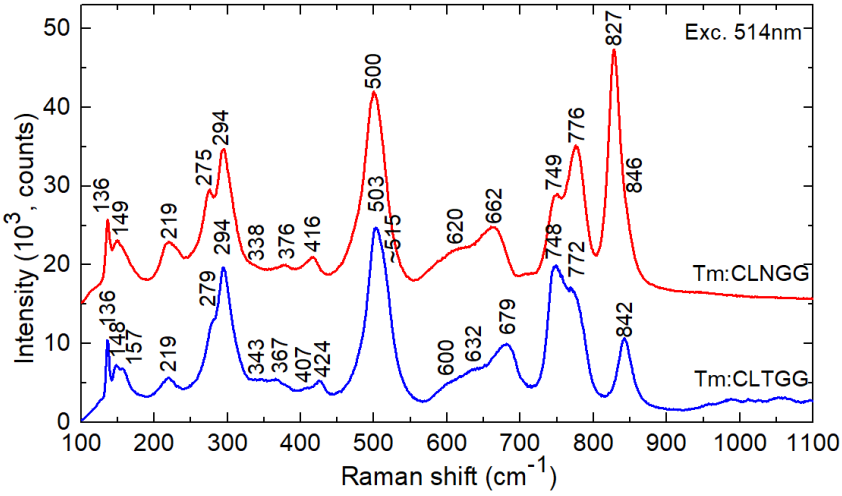

Fig. 4. Unpolarized RT Raman spectrum of the Tm:CLTGG crystal, λ_{exc} = 514 nm. Numbers indicate the band frequencies in cm^{-1}. The Raman spectrum of Tm:CLNGG is given for comparison.

4. Thermal properties

5. Results

The specific heat C_p and the thermal diffusivity λ were measured using a laser flash apparatus (NETZSCH LFA457). For this, a squared wafer was cut from the Tm:CLTGG crystal along the [111] direction having the dimensions of 4×4×1 mm^3. It was coated with graphite from two opposite sides.

The dependence of the specific heat of Tm:CLTGG on temperature is shown in Fig. 5(a). The Cp value increases monotonously with temperature, from 0.57 to 0.66 J g^{-1} K^{-1}, when the temperature is increased from 298.2 K to 571.9 K. Figure 5(b) shows the measured thermal diffusivities. The λ value along the [111] direction decreases with temperature. At 298.2 K, it amounts to 1.374 mm^2/s. Finally, the thermal conductivity along the [111] direction was calculated using the formula $\kappa = \lambda \times \rho \times C_p$ where ρ = 5.53 g/cm^3 is the crystal density measured using the buoyancy method. The thermal conductivity decreases with temperature, Fig. 5(c). At room temperature, it amounts to 4.33 $Wm^{-1}K^{-1}$, which is larger than for CNGG-type crystals [4,20].

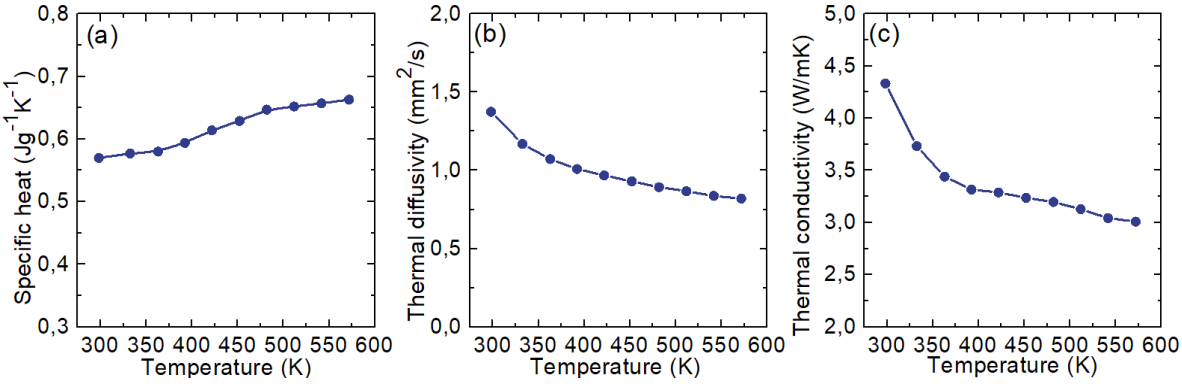

Fig. 5. Thermal properties of the Tm:CLTGG crystal as a function of temperature: (a) specific heat; (b) thermal diffusivity; (c) thermal conductivity.

5. Optical spectroscopy

5.1 Optical absorption

The absorption spectrum was measured using a Varian CARY 5000 spectrophotometer. The cubic Tm:CLTGG is optically isotropic. The unpolarized RT absorption spectrum of Tm:CLTGG is shown in Fig. 6(a). In the spectrum, the well-resolved absorption bands are related to transitions of Tm^{3+} ions from the ground-state ($^3H_6$) to excited-states (from $^3F_4$ to $^1D_2$, in increasing energy order).

5. Results

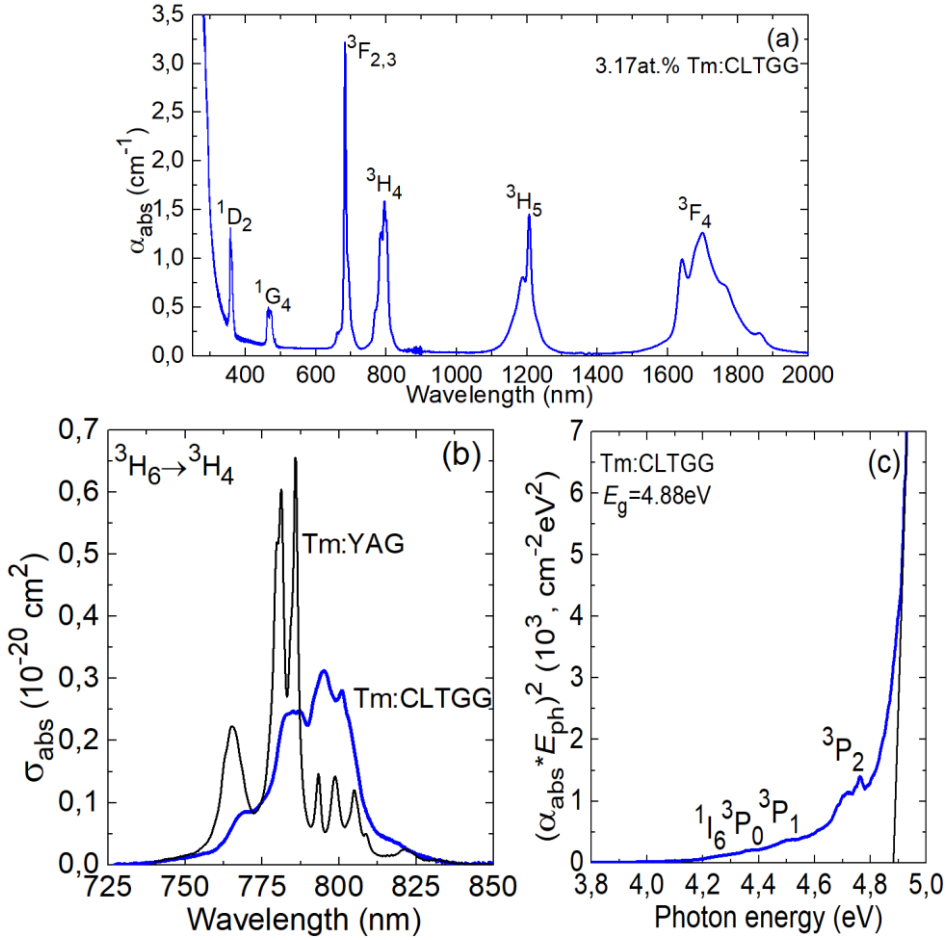

Fig. 6. Absorption of the Tm:CLTGG crystal: (a) RT absorption spectrum; (b) absorption cross-sections, σ_{abs}, for the $^3H_6 \rightarrow {}^3H_4$ Tm^{3+} transition; (c) Tauc plot for the evaluation of the optical bandgap (E_g).

The absorption cross-sections σ_{abs} for the $^3H_6 \rightarrow {}^3H_4$ Tm^{3+} transition which is suitable for pumping of laser crystals by AlGaAs diode lasers emitting at ~0.8 μm are shown in Fig. 6(b). The maximum σ_{abs} is 0.31×10^{-20} cm^2 at 795.0 nm and the absorption bandwidth (full

5. Results

width at half maximum, FWHM) is 26.7 nm. Compared to the widespread Tm:$Y_3Al_5O_{12}$ garnet crystal, Tm:CLTGG exhibits smoother and broader absorption at the expense of lower cross-section. This represents the effect of inhomogeneous broadening caused by the structural disorder and, in particular, the different cationic distributions around the Tm^{3+} ions, cf. Fig. 3(b).

The absorption spectrum of Tm:CLTGG reveals no significant absorption in the visible assigned to color centers related to cationic vacancies. This indicates charge compensation via Li^+ doping. Figure 6(c) shows the Tauc plot for the determination of the UV absorption edge (assuming indirect transitions). The optical bandgap energy E_g is 4.88 eV (0.254 μm). At the onset of the host absorption, weak absorption bands due to transitions of Tm^{3+} ions to higher-lying $^1I_6$ and $^3P_{0\text{-}2}$ states are found.

5.2. Judd-Ofelt analysis

The transition intensities for Tm^{3+} ions were calculated from the absorption spectrum using the standard Judd-Ofelt (J-O) theory [17,18], and its modification accounting for configuration interaction (mJ-O theory) [19]. This formalism was used to determine the contributions of electric dipoles (ED). The magnetic dipole (MD) contributions for transitions with $\Delta J = J - J' = 0, \pm 1$ were calculated independently within the approximation of Russell–Saunders on the

5. Results

wave functions of Tm^{3+} under an assumption of a free-ion. The refractive index of CLTGG was taken from [20].

The detailed procedure of the J-O calculations for Tm^{3+}-doped crystals is described in detail elsewhere [21]. Here, we only discuss the main approximations. For the standard J-O theory, the ED line strengths of the J → J' transition are given by:

$$S_{\mathrm{calc}}^{\mathrm{ED}}(JJ') = \sum_{k=2,4,6} U^{(k)}\Omega_k, \tag{1a}$$

$$U^{(k)} = \langle (4f^n)SLJ \| U^k \| (4f^n)S'L'J' \rangle^2. \tag{1b}$$

Here, $U^{(k)}$ are the reduced squared matrix elements which were calculated using the free-ion parameters from [22] and Ω_k are the intensity (J–O) parameters (for both, k = 2, 4, 6).

In the mJ-O theory, it is assumed that only the excited configuration of the opposite parity $4f^{n-1}5d^1$ contributes to the configuration interaction. The ED line strengths are then [19]:

$$S_{\mathrm{calc}}^{\mathrm{ED}}(JJ') = \sum_{k=2,4,6} U^{(k)}\tilde{\Omega}_k, \tag{2a}$$

$$\tilde{\Omega}_k = \Omega_k[1 + 2\alpha(E_J + E_{J'} - 2E_f^0)]. \tag{2b}$$

In other words, the intensity parameters $\tilde{\Omega}_k$ are linear functions of energies (E_J and $E_{J'}$) of the two multiplets, where Ef^0 is the mean energy of the 4fn configuration and $\alpha \approx 1/(2\Delta)$ where $\Delta \approx E(4f^{n-1}5d^1) - E(4f^n)$ is the average energy difference between the fundamental and first excited configurations.

Table 2 summarizes the experimental and calculated absorption oscillator strengths f (the latter are determined by both the J-O and

5. Results

mJ-O theories from the corresponding line strengths). The intensity parameters are Ω_2 = 1.715, Ω_4 = 0.943 and Ω_6 = 0.963 [10^{-20} cm^2] (J-O theory) and Ω_2 = 5.185, Ω_4 = 0.650, Ω_6 = 1.068 [10^{-20} cm^2] and α = 0.171 [10^{-4} cm] (mJ-O theory). The latter theory provides lower root mean square (r.m.s.) deviation between the experimental and calculated f values, so that it was selected for further analysis.

Table 2. Measured and Calculated Absorption Oscillator Strengths of Tm^{3+} ions in CLTGG crystal[a]

Transition $^3H_6 \rightarrow ^{2S+1}L_J$	$<E>$, cm^{-1}	Γ, nm×cm^{-1}	f_{exp}, 10^{-6}	f^{Σ}_{calc}, 10^{-6}	
				J-O	mJ-O
$^3F_4$	5823	215.51	1.641	1.649^{ED}	1.583^{ED}
$^3H_5$	8363	76.642	1.211	$1.317^{ED}+0.534^{MD}$	$1.058^{ED}+0.534^{MD}$
$^3H_4$	12628	51.696	1.859	2.139^{ED}	2.810^{ED}
$^3F_{3,2}$	14568	44.848	2.137	3.073^{ED}	2.521^{ED}
$^1G_4$	21182	7.750	0.791	0.568^{ED}	1.101^{ED}
$^1D_2$	27686	10.607	1.849	1.815^{ED}	1.783^{ED}
$^1I_6+^3P_0+^3P_1$	35239	13.677	3.811	$1.690^{ED}+0.029^{MD}$	$3.017^{ED}+0.029^{MD}$
$^3P_2$	38067	6.665	2.166	1.958^{ED}	2.270^{ED}
r.m.s. dev.				*1.078*	*0.689*

5. Results

[a]<E> - "center of gravity" of the absorption band, Γ – integrated absorption coefficient, f_{exp} and f^{Σ}_{calc} – experimental and calculated absorption oscillator strengths, respectively, ED electric-dipole, MD - magnetic-dipole.

The probabilities of spontaneous radiative transitions $A_{calc}(JJ')$, the luminescence branching ratios B(JJ') and the radiative lifetimes of the excited-states τ_{rad} were calculated using the mJ-O theory, the results are shown in Table 3. For the $^3F_4$ and $^3H_4$ states, τ_{rad} is 5.33 ms and 0.55 ms, respectively.

Table 3. Calculated Probabilities of Spontaneous Radiative Transitions of Tm^{3+} ions in CLTGG crystal (Obtained from the mJ-O Theory)[a]

Excited state	Terminal state	$\langle\lambda_{em}\rangle$, nm	$A_{calc}(JJ')$, %	$B(JJ')$, %	A_{tot}, s^{-1}	τ_{rad}, ms
$^3F_4$	$^3H_6$	1717.3	63.62^{ED}	1	187.51	5.33
$^3H_5$	$^3F_4$	3937.0	$8.81^{ED}+0.24^{MD}$	0.027	329.09	3.03
	$^3H_6$	1195.7	$212.78^{ED}+107.26^{MD}$	0.973		
$^3H_4$	$^3H_5$	2344.7	$16.59^{ED}+10.34^{MD}$	0.015	1801.71	0.55
	$^4F_4$	1469.5	$154.95^{ED}+25.61^{MD}$	0.100		
	$^3H_6$	791.9	1594.22^{ED}	0.885		
$^3F_2+^3F_3$	$^3H_4$	5154.6	$22.24^{ED}+0.32^{MD}$	0.005	4760.78	0.36
	$^3H_5$	1611.6	818.37^{ED}	0.172		
	$^3F_4$	1143.5	$1191.94^{ED}+74.14^{MD}$	0.266		
	$^3H_6$	686.4	2653.77^{ED}	0.557		

$^1G_4$	$^3F_2$+$^3F_3$	1511.9	28.52^{ED}	0.030	4524.78	0.22
	$^3H_4$	1169.0	103.11^{ED}+4.17^{MD}	0.142		
	$^3H_5$	780.1	600.49^{ED}+39.18^{MD}	0.359		
	$^3F_4$	651.1	1468.80^{ED}+156.71^{MD}	0.063		
	$^3H_6$	472.1	273.22^{ED}+12.88^{MD}	0.406		
$^1D_2$	$^1G_4$	1537.5	563.86^{ED}	0.008	72495.29	0.01
	$^3F_2$+$^3F_3$	762.3	5710.24^{ED}+183.16^{MD}	0.081		
	$^3H_4$	664.1	5340.29^{ED}	0.074		
	$^3H_5$	517.5	218.16^{ED}	0.003		
	$^3F_4$	457.4	50840.29^{ED}	0.701		
	$^3H_6$	361.2	9639.29^{ED}	0.133		

[a]$\langle\lambda_{em}\rangle$ - mean emission wavelength, $A_{calc}(JJ')$ – probability of radiative spontaneous transition, B(JJ') – luminescence branching ratio, A_{tot} – total probability of radiative transitions, τ_{rad} - radiative lifetime, ED electric-dipole, MD - magnetic-dipole.

5.3 Luminescence (emission spectra and lifetime)

The RT luminescence spectrum was measured using an optical spectrum analyzer (AQ6375B, Yokogawa) for which the spectral response was calibrated using a 20 W quartz iodine lamp. The pump source was a 795 nm Ti:Sapphire laser (excitation to the $^3H_4$ state). The luminescence spectrum is shown in Fig. 7(a). The broad and intense band at 1.6 - 2.3 μm is due to the $^3F_4 \rightarrow {}^3H_6$ transition, while the weaker band at 1.35 - 1.55 μm originates from the $^3H_4 \rightarrow {}^3F_4$ transition.

5. Results

The luminescence decay was studied at RT using an optical parametric oscillator (Horizon, Continuum), a 1/4 m monochomator (Oriel 77200), an InGaAs detector and an 8 GHz digital oscilloscope (DSA70804B, Tektronix). The sample was finely powdered to avoid the effect of radiation trapping. The decay curve from the $^3F_4$ state is well fitted using a single-exponential law yielding a luminescence lifetime τlum of 4.93 ms (for the powdered sample), Fig. 7(b). It is only slightly shorter than the radiative one, revealing a relatively high quantum yield $\eta_q = \tau_{lum}/\tau_{rad} = 92\%$. The decay from the $^3H_4$ state is not single-exponential revealing the effect of cross-relaxation for neighboring Tm^{3+} ions. The mean decay time $< \tau_{lum} >$ = 0.159 ms, Fig. 7(c).

5. Results

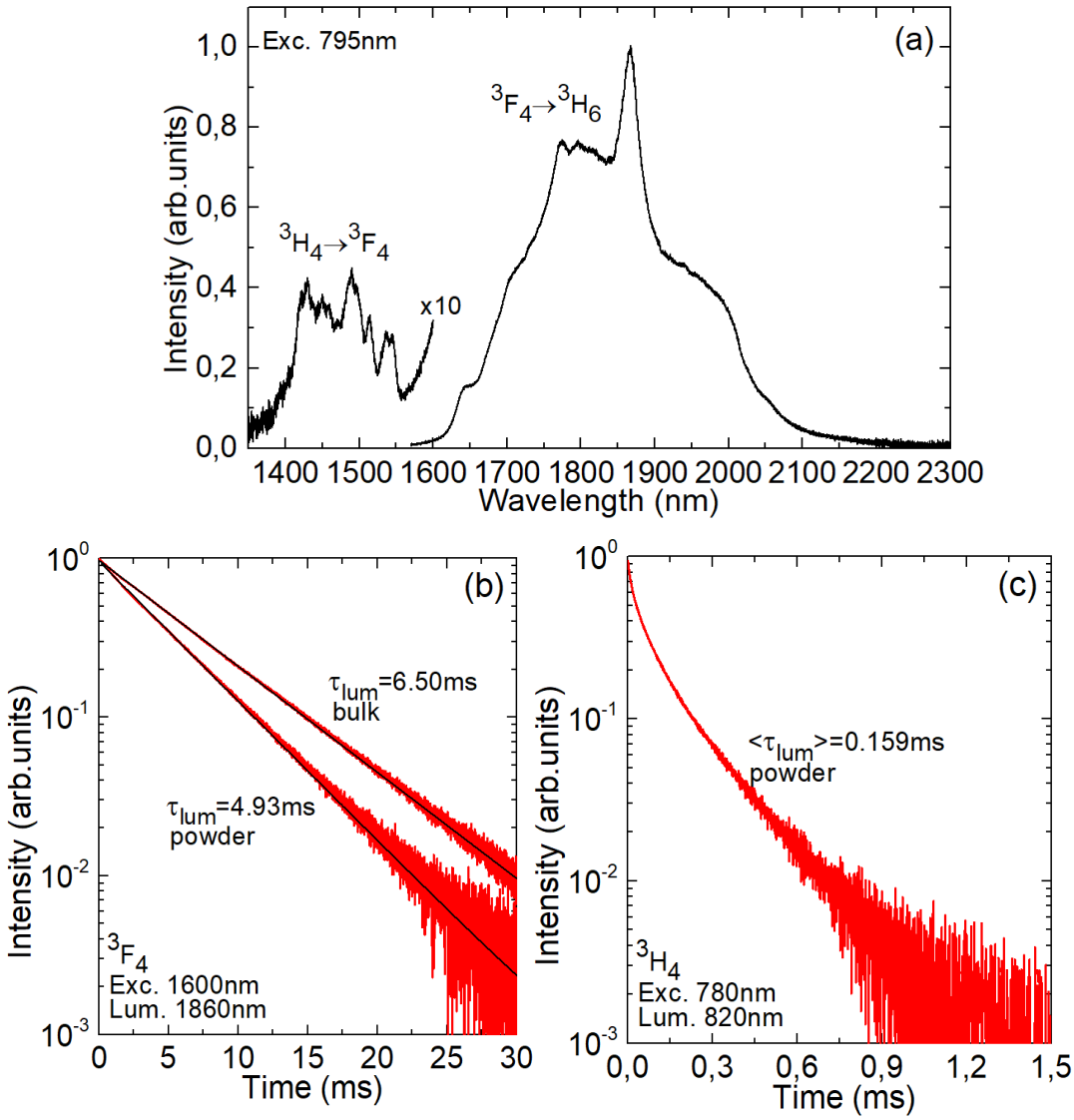

Fig. 7. Near-infrared emission properties of the Tm:CLTGG crystal: (a) luminescence spectrum, λ_{exc} = 795 nm; (b,c) luminescence decay curves from the (b) 3F4 and (c) 3H4 Tm3+ states.

5. Results

4.4. Low-temperature spectroscopy

The low temperature (LT, 10 K) absorption and luminescence spectra were measured using a cryostat (Oxford Instruments, model SU 12) with helium-gas close-cycle flow. In CLTGG, Tm^{3+} ions replace for the Ca^{2+} ones in dodecahedral sites with the D2 symmetry. These sites are distorted due to the presence of univalent Li^{+} cations serving for charge compensation and various cation coordinations around the {A} sites, cf. Fig. 3. Each $2^{S+1}L_J$ multiplet with integer J is thus split into *2J + 1* Stark sub-levels. For brevity, in Fig. 8, we only show the absorption and luminescence spectra revealing the splitting of the $^3F_4$ and $^3H_6$ states relevant for ~2 μm laser operation. The assignment of electronic transitions is after the work of Lupei et al. for ordered Tm^{3+}-doped $Gd_3Ga_5O_{12}$ (GGG) garnet [23]. Figure 8 reveals a significant inhomogeneous broadening of the absorption and luminescence bands of Tm^{3+} ions even at 10 K when the electron-phonon interaction is suppressed, which is a fingerprint of the structure disorder.

5. Results

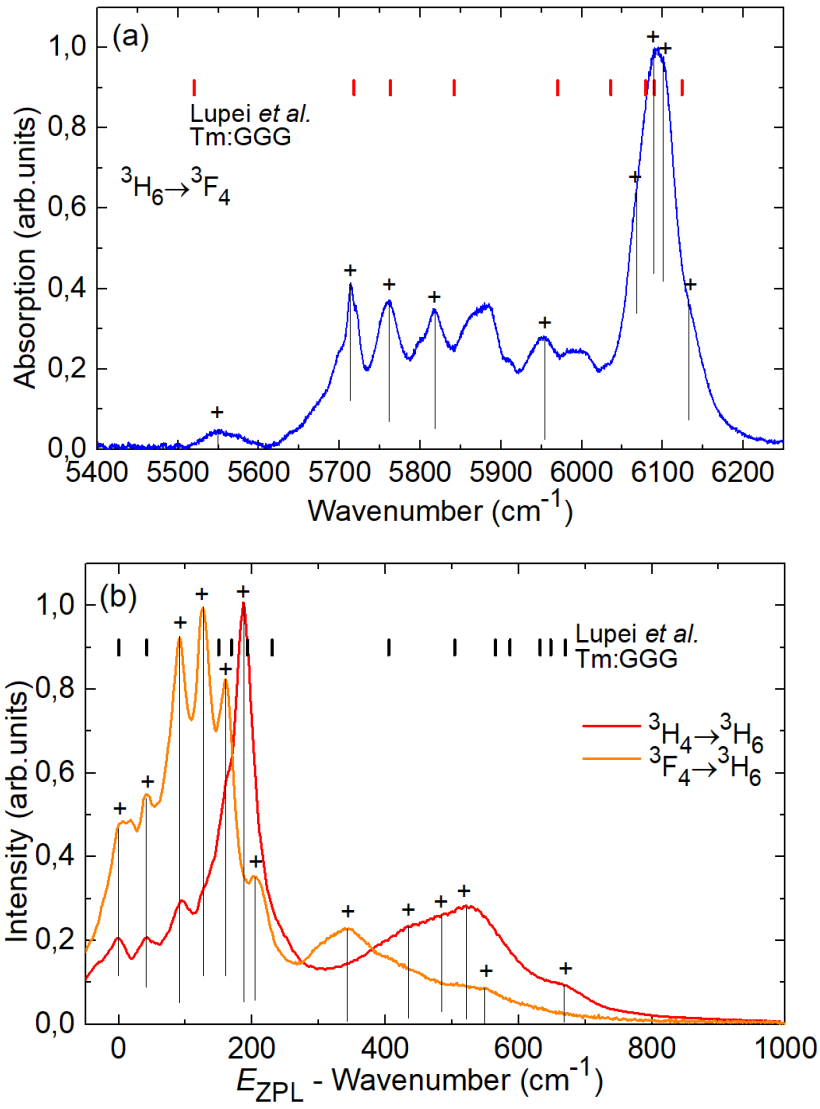

Fig. 8. Low-temperature (LT, 10 K) absorption and emission spectra for Tm^{3+} ions in the CLTGG crystal: (a) absorption, $^3H_6 \rightarrow {}^3F_4$ transition; (b) emission, $^3F_4 \rightarrow {}^3H_6$ and $^3H_4 \rightarrow {}^3H_6$ transitions.

5. Results

The symbol "+" marks the assigned electronic transitions. Vertical dashes – crystal-field splitting in Tm:GGG after [23].

The experimental energy-levels of Tm^{3+} ions in CLTGG are listed in Table 4 for the multiplets from $^3H_6$ up to $^1D_2$. For the $^3F_4 \rightarrow {}^3H_6$ transition of interest for ~2 μm laser operation, the zero-phonon line (ZPL), i.e., the transition between the lowest Stark sub-levels of both multiplets, occurs at 1806 nm (EZPL = 5538 cm^{-1}). The partition functions for the ground-state and the excited-state, calculated at RT, amount to $Z_1 = 4.786$ and $Z_2 = 2.402$, respectively, so that their ratio $Z_1/Z_2 = 1.992$.

Table 4. Experimental Energy Levels of Tm^{3+} ions in CLTGG crystal

Multiplet	*E*, cm^{-1}
$^3H_6$	0; 42; 91; 126; 160; 187; 206; 342; 433; 484; 522; 549; 668
$^3F_4$	5538; 5713; 5760; 5813; 5952; 6067; 6091; 6101; 6138
$^3H_5$	8299; 8314; 8396; 8412; 8426; 8458; 8567; 8606; 8683; 8773; 8809
$^3H_4$	12577; 12594; 12632; 12703; 12739; 12774; 12916; 12994; 13026
$^3F_3$	14552; 14573; 14621; 14644 (*3 missing*)
$^3F_2$	15096; 15129; 15149; 15230 (*1 missing*)
$^1G_4$	21071; 21116; 21205; 21284; 21304; 21461; 21489; 21648; 21707
$^1D_2$	27662; 27826; 27940; 28044; 28102

5. Results

5.5. Transition cross-sections

The absorption cross-section spectrum for the $^3H_6 \rightarrow {}^3F_4$ transition is shown in Fig. 9(a), the maximum σ_{abs} reaches 0.25×10^{-20} cm^2 at 1699 nm.

For the $^3F_4 \rightarrow {}^3H_6$ transition, the stimulated-emission (SE) cross-section, σ_{SE}, spectra were calculated by two methods: the Füchtbauer–Ladenburg (F-L) equation [24] and the reciprocity method (RM) [25]. For the F-L equation, the luminescence spectrum was used, cf. Fig. 7(a), the radiative lifetime of the $^3F_4$ state was determined from the mJ-O theory (τ_{rad} = 5.33 ms) and the refractive index of the crystal ($n \approx 1.92$) was taken from [20]. For the RM, we used the measured absorption spectrum and the determined crystal-field splitting, cf. Table 4. The results of both methods are shown in Fig. 9(a). They are in good agreement with each other. The maximum σ_{SE} reaches 0.35×10^{-20} cm^2 at 1866 nm and at longer wavelengths where the laser operation is expected, σ_{SE} reaches 0.18×10^{-20} cm^2 at 1992 nm (both values correspond to the F-L method).

The ~2 μm Tm laser represent a quasi-three-level scheme with reabsorption. Thus, gain cross-sections are usually calculated, $\sigma_{gain} = \sigma_{SE} - (1 - \beta)\sigma_{abs}$, where $\beta = N_2(^3F_4)/N_{Tm}$ is the inversion ratio. They are useful to conclude about the possible laser wavelength (in the free-running regime), the potential tuning range as well as the gain bandwidth for mode-locked oscillators. The gain spectra for

5. Results

Tm:CLTGG are shown in Fig. 9(b). The gain profiles of this disordered crystal are smooth and broad. For small and moderate inversion ratios ($\beta < 0.16$), a single local peak is observed in the spectra centered at ~1.99 μm. The gain bandwidth (FWHM) for an intermediate $\beta = 0.12$ is as broad as 130 nm. The gain profiles extend well beyond 2 μm owing to the large total ground-state splitting ($\Delta E(^3H_6) = 668\ cm^{-1}$) for Tm^{3+} ions and strong electron-phonon (vibronic) interaction with phonons of the host matrix. The longest purely electronic transition (neglecting the inhomogeneous broadening) for Tm^{3+} ions is 2053 nm.

5. Results

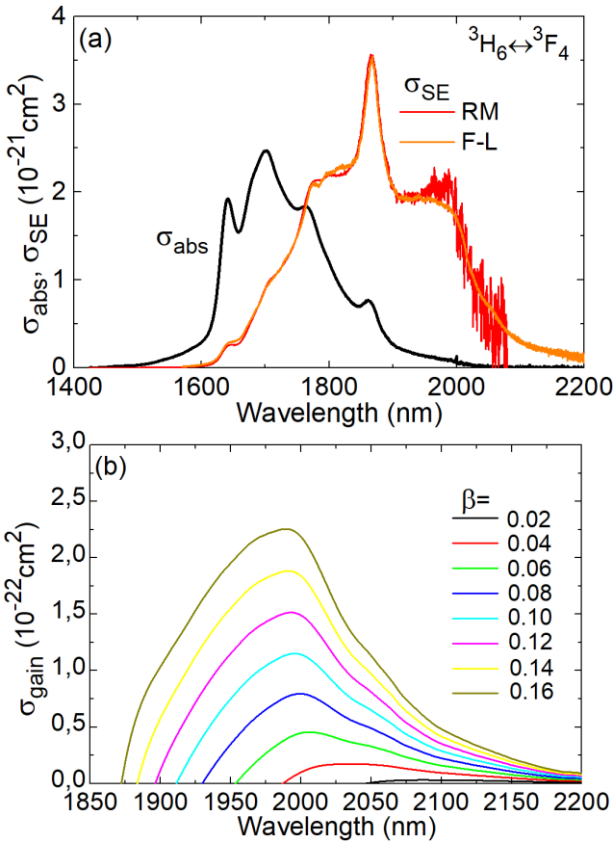

Fig. 9. $^3H_6 \leftrightarrow {}^3F_4$ transition of Tm^{3+} ions in CLTGG: (a) absorption, σ_{abs}, and stimulated emission (SE), σ_{SE}, cross-sections; (b) gain cross-sections, $\sigma_{gain} = \sigma_{SE} - (1 - \beta)\sigma_{abs}$, where $\beta = N_2(^3F_4)/N_{Tm}$ is the inversion ratio.

6. Diode-pumped laser operation

6.1. Laser set-up

Figure 10(a) shows the scheme of the compact diode-pumped Tm:CLTGG laser. The laser element was cut along the [111] direction. It had an aperture of 3.05×3.09 mm^2 and a thickness of

5. Results

8.19 mm. Both end faces of the element were polished to laser quality and left uncoated. To remove the heat released during pumping, the element was wrapped in indium foil and fixed in a Cu-holder cooled by circulating water; the water temperature was 12 °C.

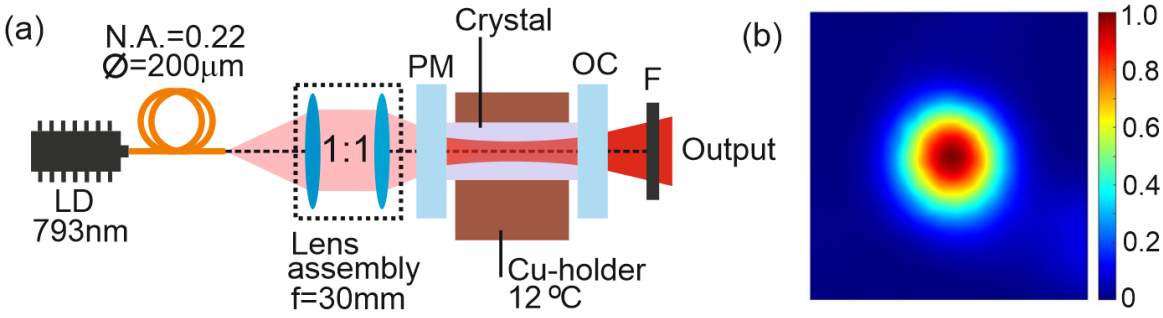

Fig. 10. (a) Scheme of the diode-pumped compact Tm:CLTGG laser: LD – laser diode, PM – pump mirror, OC – output coupler, F – cut-off filter; **(b)** far-field output profile of the laser mode, TOC = 5%, P_{abs} = 4.0 W.

The laser cavity consisted of a plane pump mirror (PM) coated for high transmission (HT) at 0.80 μm and high reflection (HR) at 1.8-2.1 μm and a set of plane output couplers (OCs) having transmissions TOC of 1.5%, 3%, 5% or 9% at the laser wavelength. Both mirrors were placed close to the crystal resulting in a geometrical cavity length of ~8.5 mm. The pump source comprised a fiber-coupled (fiber core diameter: 200 μm, N.A. = 0.22) AlGaAs diode laser emitting unpolarized output at a central wavelength of 793 nm (emission bandwidth: 5 nm, M^2 > 80). The pump beam was collimated and focused into the laser element by an AR-coated lens

assembly (reimaging ratio: 1:1, f = 30 mm). The pump spot size in the focus $2w_P$ was 200 µm. The measured pump absorption was ~47%. The residual pump was filtered out using a long pass filter (FEL1000, Thorlabs). The spectra of the laser output were measured using a spectrometer (WaveScan, APE). The profile of the laser mode in the far-field was captured using a FIND-R-SCOPE near-IR camera (model 85726).

6.2. Laser performance

The input-output dependences of the diode-pumped Tm:CLTGG laser are shown in Fig. 11(a). The laser generated a maximum output power of 1.08 W at 1995 and 2003 nm with a slope efficiency η of 23.8% (with respect to the absorbed pump power) and a laser threshold of 0.91 W (for TOC = 5%). At the maximum incident pump power of 11.7 W, the optical-to-optical conversion efficiency η_{opt} amounted to 9.2%. Further power scaling was limited by the thermal roll-over in the output dependences. With increasing the output coupling, the laser threshold increased from 0.68 W (TOC = 1.5%) to 1.46 W (TOC = 9%).

5. Results

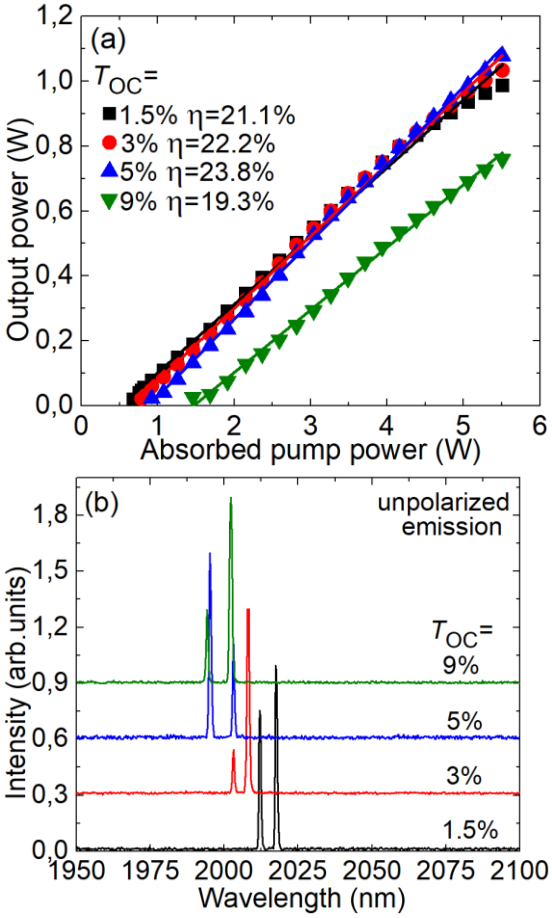

Fig. 11. Diode-pumped Tm:CLTGG laser: (a) input-output dependences, η – slope efficiency; (b) typical spectra of unpolarized laser emission measured at maximum P_{abs}.

The laser generated unpolarized emission. The typical spectra of the laser emission are shown in Fig. 11(b). With increasing TOC from 1.5% to 9%, a blue shift of the emission wavelength was observed from 2012 & 2017 nm to 1994 & 2002 nm. This shift is due to the decreasing reabsorption losses in the crystal being typical for

quasi-three-level Tm lasers. It also agrees with the gain spectra of Tm:CLTGG, cf. Fig. 9(b). The dual-wavelength emission was due to the etalon effect at the crystal / mirror interface and broad and smooth gain profile. The laser mode in the far-field, Fig. 10(b), was nearly circular.

7. Conclusions

To conclude, Tm:CLTGG is a promising crystal for ultrashort pulse generation (sub-100 fs) in the eye-safe spectral range of ~2 μm. It exhibits a structural disorder related to a random site distribution of Ta^{5+}, Ga^{3+} and Li^{+} cations over the same lattice sites, octahedral (16a) and tetrahedral (24d), which leads to a significant inhomogeneous broadening of the absorption and emission bands of Tm^{3+} ions confirmed at low temperature (10 K).

At room temperature, due to a combination of the inhomogeneous broadening and electron-phonon interaction, Tm:CLTGG exhibits smooth and very broad gain profiles owing to the phonon-assisted $^3F_4 \rightarrow {}^3H_6$ transition extending until at least ~2.2 μm. From X-ray diffraction, Raman spectroscopy and optical transmission, it is evident that Li^{+} ions provide charge compensation during the heterovalent doping (as Tm^{3+} ions are replacing Ca^{2+} ones) and almost eliminate the presence of cationic vacancies. Finally, Tm:CLTGG exhibits attractive thermal properties (for a disordered crystal) being superior to those of the CNGG-type crystals.

5. Results

Funding. This work was supported by Spanish Government, Ministry of Science and Innovation (project No. PID2019-108543RB-I00) and by Generalitat de Catalunya (project No. 2017SGR755).

Disclosures. The authors declare no conflicts of interest.

Data Availability. Data underlying the results presented in this paper are not publicly available at this time but may be obtained from the authors upon reasonable request.

References

1. J. M. Cano-Torres, M. Rico, X. Han, M. D. Serrano, C. Cascales, C. Zaldo, V. Petrov, U. Griebner, X. Mateos, P. Koopmann, and C. Kränkel, “Comparative study of crystallographic, spectroscopic, and laser properties of Tm^{3+} in $NaT(WO_4)_2$ (T = La, Gd, Y, and Lu) disordered single crystals,” Phys. Rev. B 84(17), 174207-1-15 (2011).
2. A. Lupei, V. Lupei, L. Gheorghe, L. Rogobete, E. Osiac, and A. Petraru, “The nature of nonequivalent Nd^{3+} centers in CNGG and CLNGG,” Opt. Mater. **16**(3), 403-411 (2001).
3. W. Jing, P. Loiko, J. M. Serres, Y. Wang, E. Vilejshikova, M. Aguiló, F. Díaz, U. Griebner, H. Huang, V. Petrov, and X. Mateos, "Synthesis, spectroscopy, and efficient laser operation of “mixed” sesquioxide $Tm:(Lu,Sc)_2O_3$ transparent ceramics," Opt. Mater. Express **7**(11), 4192-4202 (2017).
4. Yu. K. Voronko, A. A. Sobol, A. Y. Karasik, N. A. Eskov, P. A. Rabochkina, and S. N. Ushakov, “Calcium niobium gallium and calcium lithium niobium gallium garnets doped with rare earth ions – effective laser media,” Opt. Mater. **20**(3), 197–209 (2002).
5. E. Castellano-Hernández, M. D. Serrano, R. J. Jiménez Riobóo, C. Cascales, C. Zaldo, A. Jezowski, and P. A. Loiko, “Na modification

5. Results

of lanthanide doped $Ca_3Nb_{1.5}Ga_{3.5}O_{12}$-type laser garnets: Czochralski crystal growth and characterization," Cryst. Growth Des. **16**(3), 1480–1491 (2016).

6. Yu. K. Voron'ko, A. B. Kudryavtsev, N. A. Es'kov, V. V. Osiko, A. A. Sobol', E. V. Sorokin, and F. M. Spiridonov, "Raman scattering of light in crystals and melt of calcium-niobium gallium garnet," Sov. Phys. Dokl. **32**(1), 70–73 (1988).
7. M. D. Serrano, J. O. Álvarez-Pérez, C. Zaldo, J. Sanz, I. Sobrados, J. A. Alonso, C. Cascales, M. T. Fernández Díaz, and A. Jezowski, "Design of Yb^{3+} optical bandwidths by crystallographic modification of disordered calcium niobium gallium laser garnets," J. Mater. Chem. C **5**(44), 11481–11495 (2017).
8. Z. Pan, J. M. Serres, E. Kifle, P. Loiko, H. Yuan, X. Dai, H. Cai, M. Aguiló, F. Díaz, Y. Wang, Y. Zhao, U. Griebner, V. Petrov, and X. Mateos, "Comparative study of the spectroscopic and laser properties of Tm^{3+}, $Na^{+}(Li^{+})$-codoped $Ca_3Nb_{1.5}Ga_{3.5}O_{12}$-type disordered garnet crystals for mode-locked lasers," Opt. Mater. Express **8**(8), 2287-2299 (2018).
9. J. O. Álvarez-Pérez, J. M. Cano-Torres, A. Ruiz, M. D. Serrano, C. Cascales, and C. Zaldo, "A roadmap for laser optimization of $Yb:Ca_3(NbGa)_5O_{12}$-CNGG-type single crystal garnets," J. Mater. Chem. C **9**(13), 4628-4642 (2021).
10. Z. Pan, Y. Wang, Y. Zhao, H. Yuan, X. Dai, H. Cai, J. E. Bae, S. Y. Choi, F. Rotermund, X. Mateos, J. Maria Serres, P. Loiko, U. Griebner, and V. Petrov, "Generation of 84-fs pulses from a mode-locked Tm:CNNGG disordered garnet crystal laser," Photon. Res. **6**(8), 800-804 (2018).
11. Z. Pan, Y. Wang, Y. Zhao, M. Kowalczyk, J. Sotor, H. Yuan, Y. Zhang, X. Dai, H. Cai, J. E. Bae, S. Y. Choi, F. Rotermund, P. Loiko, J. M. Serres, X. Mateos, U. Griebner, and V. Petrov, "Sub-80 fs mode-locked Tm,Ho-codoped disordered garnet crystal oscillator operating at 2081 nm," Opt. Lett. **43**(20), 5154-5157 (2018).

5. Results

12. Z. Pan, P. Loiko, Y. Wang, Y. Zhao, H. Yuan, K. Tang, X. Dai, H. Cai, J. M. Serres, S. Slimi, E. B. Salem, E. Dunina, A. Kornienko, L. Fomicheva, J. L. Doualan, P. Camy, W. Chen, U. Griebner, V. Petrov, M. Aguiló, F. Díaz, R. M. Solé, and X. Mateos, “Disordered Tm^{3+}, Ho^{3+}-codoped CNGG garnet crystal: Towards efficient laser materials for ultrashort pulse generation at~ 2 μm,” J. Alloys Compd. 853, 157100-1-15.
13. Y. Zhao, Y. Wang, W. Chen, Z. Pan, L. Wang, X. Dai, H. Yuan, Y. Zhang, H. Cai, J. E. Bae, S. Y. Choi, F. Rotermund, P. Loiko, J. M. Serres, X. Mateos, W. Zhou, D. Shen, U. Griebner, and V. Petrov, "67-fs pulse generation from a mode-locked Tm,Ho:CLNGG laser at 2083 nm," Opt. Express **27**(3), 1922-1928 (2019).
14. C. Ma, Y. Wang, X. Cheng, M. Xue, C. Zuo, C. Gao, S. Guo, and J. He, “Spectroscopic, thermal, and laser properties of disordered garnet Nd:CLTGG crystal,” J. Cryst. Growth **504**, 44-50 (2018).
15. G. Q. Xie, D. Y. Tang, W. D. Tan, H. Luo, S. Y. Guo, H. H. Yu, and H. J. Zhang, “Diode-pumped passively mode-locked Nd:CTGG disordered crystal laser,” Appl. Phys. B **95**(4), 691-695 (2009).
16. F. Lou, S. Y. Guo, J. L. He, B. T. Zhang, J. Hou, Z. W. Wang, X. T. Zhang, K. J. Yang, R. H. Wang, and X. M. Liu, “Diode-pumped passively mode-locked femtosecond Yb:CTGG laser,” Appl. Phys. B **115**(2), 247-250 (2014).
17. B. R. Judd, “Optical absorption intensities of rare-earth ions,” Phys. Rev. **127**(3), 750–761 (1962).
18. G. S. Ofelt, “Intensities of crystal spectra of rare-earth ions,” J. Chem. Phys. **37**(3), 511–520 (1962).
19. P. Loiko, A. Volokitina, X. Mateos, E. Dunina, A. Kornienko, E. Vilejshikova, M. Aguilo, and F. Diaz, “Spectroscopy of Tb^{3+} ions in monoclinic $KLu(WO_4)_2$ crystal: application of an intermediate configuration interaction theory,” Opt. Mater. **78**, 495-501 (2018).

5. Results

20. S. Guo, D. Yuan, X. Zhang, X. Cheng, F. Yu, and X. Tao, “Growth and characterizations of calcium tantalum gallium garnet single crystal,” J. Cryst. Growth **311**(1), 214-217 (2008).
21. B. M. Walsh, N. P. Barnes, and B. Di Bartolo, “Branching ratios, cross sections, and radiative lifetimes of rare earth ions in solids: Application to Tm^{3+} and Ho^{3+} ions in $LiYF_4$,” J. Appl. Phys. **83**(5), 2772–2787 (1998).
22. P. S. Peijzel, P. Vergeer, A. Meijerink, M. F. Reid, L. A. Boatner, and G. W. Burdick, “$4f^n-15d \rightarrow 4f^n$ emission of Ce^{3+}, Pr^{3+}, Nd^{3+}, Er^{3+}, and Tm^{3+} in $LiYF_4$ and YPO_4,” Phys. Rev. B **71**(4), 045116-1-9 (2005).
23. A. Lupei, V. Lupei, S. Grecu, C. Tiseanu, and G. Boulon, “Crystal-field levels of Tm^{3+} in gadolinium gallium garnet,” J. Appl. Phys. **75**(9), 4652-4657 (1994).
24. B. Aull and H. Jenssen, “Vibronic interactions in Nd:YAG resulting in nonreciprocity of absorption and stimulated emission cross sections,” IEEE J. Quantum Electron. **18**(5), 925–930 (1982).
25. S. A. Payne, L. L. Chase, L. K. Smith, W. L. Kway, and W. F. Krupke, “Infrared cross-section measurements for crystals doped with Er^{3+}, Tm^{3+}, and Ho^{3+},” IEEE J. Quantum Electron. **28**(11), 2619–2630 (1992).

5. Results

5. Results

5.2. Continuous-wave laser operation at cryogenic temperatures

This section describes the laser generation at cryogenic temperatures (80-140 K) to achieve robust and compact lasers. This represents a challenge in the field of research of diode-pumped SSLs and aims to contribute in a relevant way, to a solution that involves the development of very compact lasers that operate around 1 and 2 microns with high-level performance. The novelty in the cavity design and the cooling strategy of the laser crystal to achieve the desired results.

5.2.1. Laser generation around ~2 μm from Tm

In [P2],[76], [103], we report the laser characteristics of a 5 at.% Tm:YLF crystal using a modular setup at cryogenic temperatures emitting around 2 μm. Continuous wave laser operation was achieved by pumping the laser crystal and a maximum output power of 6.5 W at 80 K corresponding to a slope efficiency of 66.0% with respect to absorbed power was achieved with excellent quality. of beam. We provide the full scientific publication considering that this laser represents the first compact cryogenic laser that operates around a spectral range of 2 μm. The setup and experiments were carried out by the author of the thesis, the leader of the Cryogenic Laboratory at HiLASE and the thesis supervisors.

5. Results

5. Results

Cryogenic Tm:$LiYF_4$ laser around 2 μm

***Appl. Phys. B* 129, 41 (2023)**

Adrian Alles,[1,2] Venkatesan Jambunathan,[3] Sami Slimi[2], Josep M. Serres,[1,2] Magdalena Aguiló[2], Francesc Díaz[2], Xavier Mateos,[2, #,*] Martin Smrz, [3] and Tomas Mocek[3]

[1]Eurecat, Centre Tecnològic de Catalunya, Advanced Manufacturing Systems Unit (AMS), Marcel·lí Domingo 2, 43007 Tarragona, Spain
[2]Física i Cristal·lografia de Materials (FiCMA), Universitat Rovira i Virgili, (URV), Marcel·lí Domingo, 1, 43007 Tarragona, Spain
[3]HiLASE Center, Institute of Physics of the Czech Academy of Sciences, Za Radnicí 828, 25241 Dolní Břežany, Czech Republic
*# Serra Húnter Fellow, *Corresponding author: xavier.mateos@urv.cat*

Abstract

We present the laser characteristics of a 5 at.% Tm:YLF crystal using a modular setup at cryogenic temperatures emitting around 2 μm. Continuous-wave laser operation was achieved by pumping the laser crystal using a Volume Bragg Grating stabilized laser diode emitting at 793 nm. A maximum output power of 6.5 W was achieved at 80 K corresponding to a slope efficiency of 66.0 % with respect to the absorbed power with excellent beam quality.

5. Results

1. Introduction

Lasers operating around 2 microns in the spectral range emit in the so-called eye-safe region having real and commercial application in materials processing (laser welding of transparent plastics), laser radar and atmospheric monitoring, chemical and physical research (nonlinear optics and spectroscopy), as well the favorable absorption in water makes such lasers also very useful for medical applications (surgery and therapy), and in defense [1-4]. All these 2-micron laser applications are relatively young and constantly improving, and some of them need to benefit from better efficiency, shorter pulses (meaning higher peak-power), more energetic pulses, and designs that are more compact. All such novel results represent a challenge in the field of research of diode-pumped solid-state lasers with industrial and scientific applications.

The 2 μm lasers can be achieved by doping the laser host materials with thulium Tm^{3+} ions (Tm). The “Tm” ion absorbs efficiently around 793 nm and can be directly excited using commercial available AlGaAS laser diodes. Moreover, the Tm ion experiences the two for one cross relaxation mechanism, which results in higher slope efficiency than that of the quantum defect [5]. Nevertheless, due to the quasi-three level nature the Tm ion, it suffers from reabsorption losses. In addition, the Tm ion will suffer from other parasitic processes such as energy transfer up-conversion (ETU) and

5. Results

excited state absorption (ESA). All these effects will limit the overall laser performance and suffer from poor beam quality.

To suppress the above-mentioned issues, the active medium has to be cooled down to cryogenic temperatures. The cryogenic cooling will significantly improve the key thermo-optic properties of the active medium, such as increased thermal conductivity, decreasing the variation of the refractive index with temperature, dn / dT and decreasing the thermal expansion coefficient, thus minimizing the thermo-optic effects [6, 7], it will also significantly increase the spectroscopic properties such as absorption & emission cross-sections and lifetime of the emitting electronic level. This will allow greater energy accumulation capacity during the Q-switched technique [8] for pulse generation. To date most of the cryogenic lasers were reported based on Yb doped laser hosts [9-12]. However, only few results based on Tm doped hosts can be seen [13-15].

Bearing in mind all the above mentioned facts, in this work, we paid attention to the Yttrium Lithium Fluoride crystal, $LiYF_4$ (in short YLF), which belongs to the broad fluoride family exhibiting low-phonon energy, broad emission bands and long radiative lifetime, which make these materials very good candidates for high-power laser development in the 2 μm region [16,17]. Many works based on Tm:YLF have been reported mainly at room temperature [18-21]. A

5. Results

preliminary cryogenic laser based on Tm:YLF has been demonstrated using broadband pumping in one of our previous works [22] using a long L-shaped asymmetric cavity. At 100 K, a maximum output power of 2.55 W with a slope efficiency of 22.8% was achieved using 15% output coupling transmission. From that study of absorption spectroscopy and results published in [22], we deduced that a broadband pump source is not suitable for efficient cryogenic laser operation. Stabilized laser diodes should be used to achieve greater efficiency.

This work aims to contribute in a relevant way, to a solution that involves the development of a compact laser that operates around 2 microns with high performance. The novelty of this work lies in the study of a modular cryogenic compact cavity, the cooling strategy of the laser crystal to achieve the desired results, and the pump geometry by a Volume Bragg Grating (BVG) stabilized laser diode as pump source as will be explained below, representing the first cryogenically cooled microchip-like (compact) Tm:YLF laser around 2 microns.

2. Experimental

2.1 Cryogenic continuous-wave (CW) laser setup

Figure 1a) illustrates the schematic diagram of the cryogenic continuous-wave (CW) laser setup. The compact cryogenic cavity

5. Results

includes a plane-plane pump mirror with high-reflective (HR) coating at 1.8-2.1 µm and high transmission (HT) around 800 nm. A set of plane output couplers (OC) with different partial transmission (Toc) of 9, 15, and 30% at 1.8-2.1 µm were used. As active medium a commercial a-cut 5 at. % Tm:YLF crystal with 2 mm thickness and 5×5 mm^2 aperture was mounted in a copper holder at normal incidence and was placed in between the two plane mirrors to form a compact plane – plane cavity inside the modular chamber (see Figure 1b)).

The advantage of this modular chamber is that one can replace any of the optical elements, such as the pump mirror, active medium or output coupler as desired. To conductively cool the active medium, the copper holder along with the sample were fixed to the cold finger of the closed cycle helium cryostat (CH-204, JANIS), that can provide a cooling power of 13.5 W at 100 K. A Lake Shore temperature controller (DT 670) was used to monitor and maintain the sample temperature, which includes 2 silicon diode sensors and a 50 Ω heater. The modular chamber has the provision to tilt and move the distance of both pump and output coupler mirrors using piezo actuators and were controlled by a computer externally. The whole chamber was maintained at a vacuum pressure of 10^{-5} mbar to avoid water vapor condensation on the sample surface. A diode laser emitting around 793 nm was used as pump source, with a bandwidth of 0.5 nm stabilized by a Volume Bragg Grating. The fiber-coupled diode had a core diameter of 105 µm and N.A. = 0.22

5. Results

delivering a maximum output power of 25 W. The radiation from the pump source was imaged to the active medium in a 1:1.5 ratio by two AR- coated achromatic lenses (focal lengths of 100 and 150 mm). The pump spot size was estimated to be ~ 158 μm in the

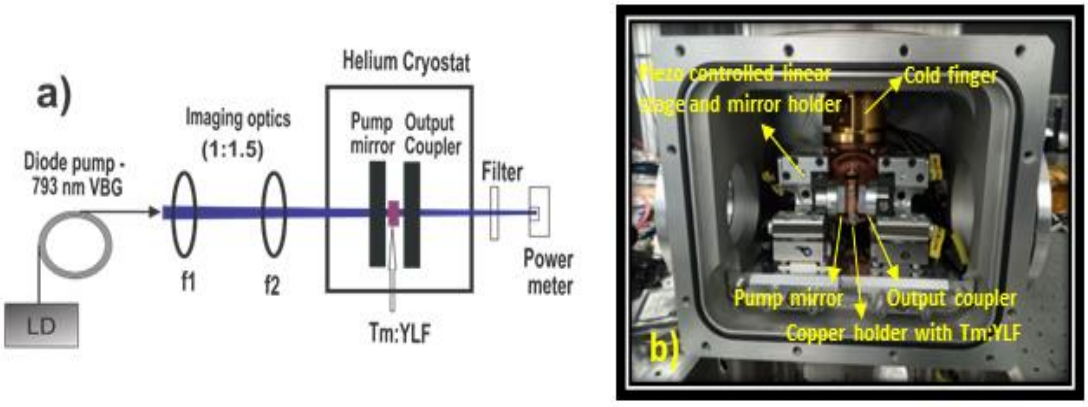

Figure 1. a) Cryogenic compact laser setup; LD—laser diode Imaging optics—achromatic lenses (f1 = 100 mm and f2 = 150 mm). **b)** Modular chamber used for the experiment.

3. Results and discussion

3.1. Cryogenic continuous-wave laser operation of Tm:YLF

The cryogenic continuous-wave (CW) laser was realized and were characterized in two ways. Firstly, by varying the OC transmissions at a fixed temperature and secondly, by varying the temperature of

5. Results

the sample at a fixed OC transmission. Figure 2 a) shows the input–output characteristics of the cryogenic Tm:YLF laser at 80 K by varying the transmission of OC.

From the figure one can infer that Toc = 15% performed better when compared with the others studied transmissions of the OC, and a maximum output power of 6.5 W corresponding to a slope efficiency of 38% was achieved.

The laser emitted at 1876 nm for output coupler transmissions 15 and 30% as shown in figure 2b. However or Toc = 9%, we observed polarization switching between both polarizations π (E//c) and $\boldsymbol{\sigma}$ ($\mathbf{E} \perp \mathbf{c}$). This polarization switching might be due high intracavity power resulting in anisotropic thermal lensing effect on the spot sizes of π and $\boldsymbol{\sigma}$ cavity modes of Tm:YLF.

Figure 2c) shows the measured output wavelengths for different incident pump levels. At low pump levels (< 5 W), the π polarization was dominant and emitted at 1876 nm and at high pump power levels (>13 W), the $\boldsymbol{\sigma}$ polarization was dominant emitting at 1901 & 1912 nm. Intermediate pump power levels provided laser emission with the two-polarization coexisting. The observed laser emission wavelengths are in line with the reported gain cross-section curves for π and $\boldsymbol{\sigma}$ polarizations [23] calculated for different temperatures and inversion rates.

Further investigation on this polarization switching behavior along

5. Results

with cryogenic spectroscopy is under study.

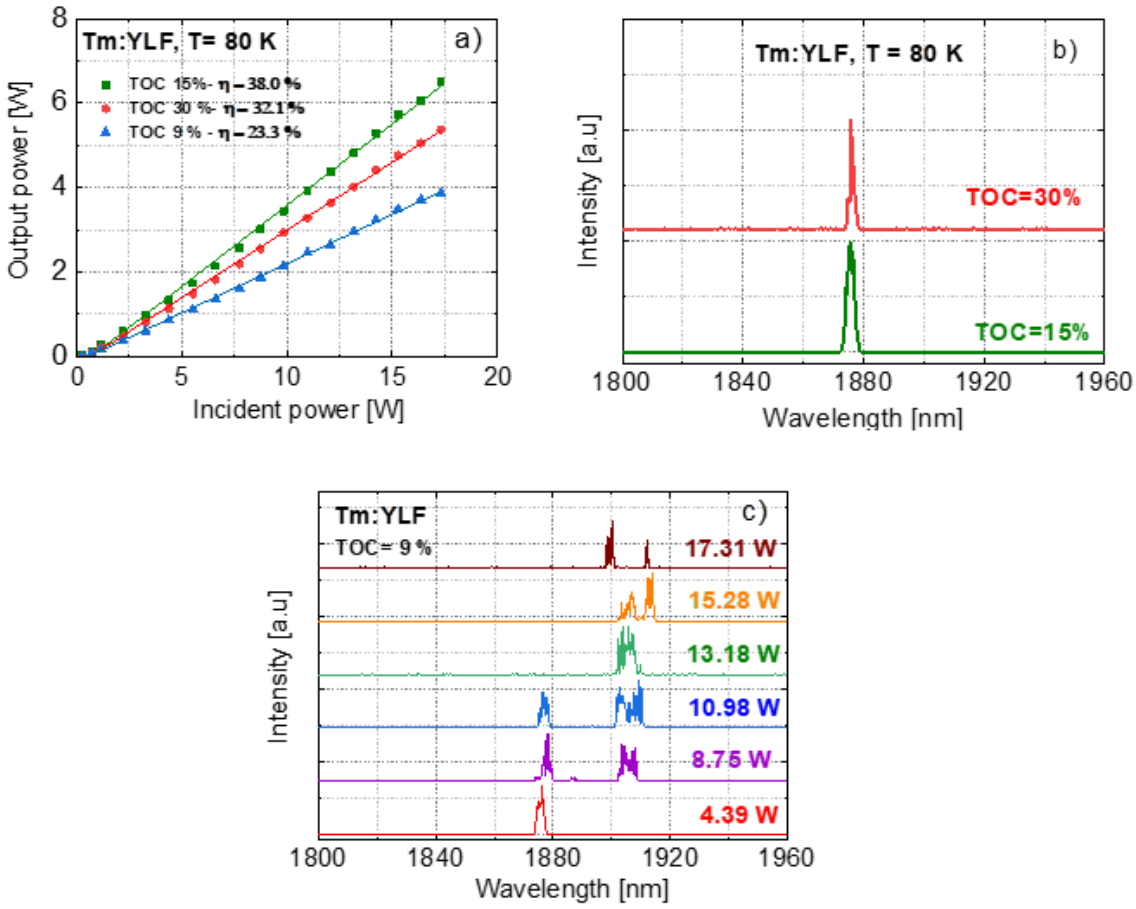

Figure 2. a) Output power vs. input power characteristics of the cryogenic compact Tm:YLF laser for different transmissions of output coupling. **b)** Laser output wavelengths for different Tocs of 15 and 30%. **c)** Laser output wavelength for Toc = 9% with

5. Results

polarization switching.

Figure 3a) shows the input–output characteristics of the cryogenic Tm:YLF laser by varying the temperature and by fixing the OC to 15%. Here, we chose the best performing OC transmission for this study and the temperature of the sample was varied from 80 K to 160 K in step size of 20 K. Laser operation with crystal temperature above 160 K was not considered to avoid the damage of the sample.

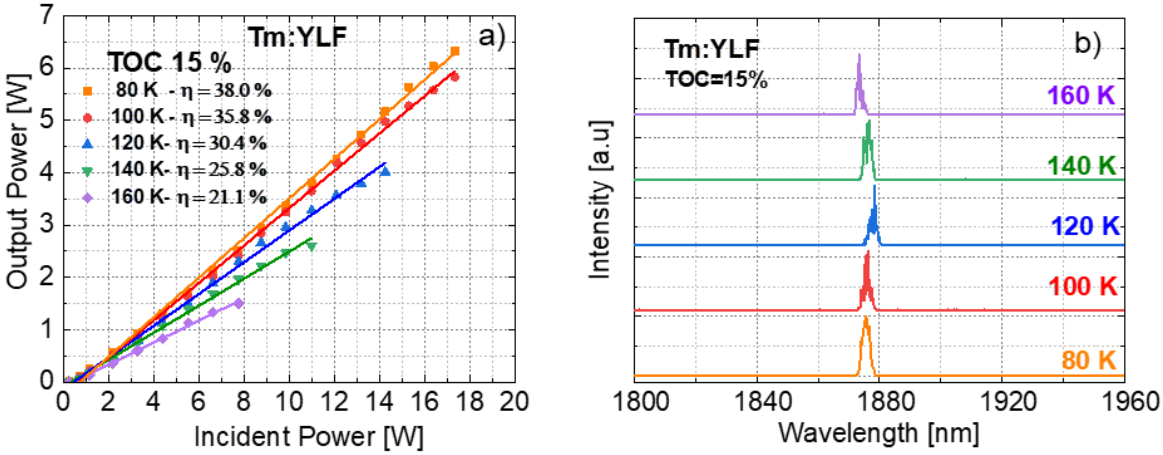

Figure 3. a) Output power vs. input power characteristics of the cryogenic compact Tm:YLF laser for various crystal temperatures. **b)** Corresponding output laser wavelengths for different temperatures

In figure 3a), it is evidenced, that the output power and slope efficiency increase with decrease of temperature. This increase of the output power and slope efficiency is mainly due to the significant reduction of reabsorption at the laser wavelength and improvement

5. Results

of thermo-optic, thermo-mechanical and spectroscopic properties of Tm:YLF. Out of all the temperatures, 80K performed better compared to the other temperatures. We also measured the output laser wavelength for different temperatures and are shown in figure 3b. Figure 3b shows the measured laser spectrum from 80 to 160K. The laser emission was close to 1876 nm corresponding to π (E//c crystallographic axis) polarization in all cases. A short blue shift of the laser wavelength at 160K was observed (3 nm shorter), indicating that at 160K, part of the electronic population of the ground state constituted a quasi-three level laser.

For lower temperatures, the Tm laser acts as a four-level laser without reabsorption losses. We also measured the absorption in the crystal at 80K under non-lasing condition being 57% by taking into consideration the Fresnel losses on the surface crystal as well as a second pass of the pump due to the partial reflection of the non-absorbed pump on the output coupler.

Using this absorption value, we estimated the slope efficiency with respect to the absorbed power (see figure 4a).

A maximum output power of 6.5 W was achieved at an absorbed pump power of 9.97 W. The slope efficiency with respect to the absorbed power amounts to 66.0%.

We also measured a very high quality far field Gaussian beam profile obtained at maximum pump power, shown in figure 4b.

5. Results

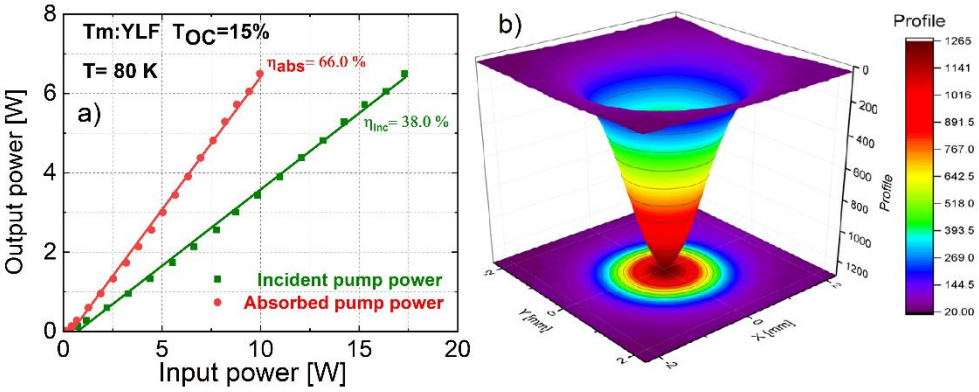

Figure 4 a) Laser performance of the compact cryogenic Tm:YLF laser pumped by the VBG diode at 80 K with Toc=15%. Output power versus incident (green) and absorbed (red) pump power. **b)** far field Gaussian beam profile.

Conclusions

We presented cryogenic laser operation of Tm:YLF using a modular setup pumped by a VBG stabilized laser diode emitting around 793 nm. A maximum output power of 6.5 W corresponding to a slope efficiency of 66% with respect to absorbed power was achieved at 80 K. An excellent performance along with a very good beam quality verifies the advantages of cryogenic cooling. Future work will focus on pulsed laser operation implementing Cr:ZnS and Cr:ZnSe as saturable absorbers in the compact cavity to generate high-energy laser pulses.

Acknowledgements

Grant PID2019-108543RB-I00 funded by MCIN/AEI/10.13

5. Results

039/501100011033. This work has been possible with the support of the Secretaria d'Universitats i Recerca del Departament d'Empresa i Coneixement de la Generalitat de Catalunya, the European Union (UE), and the European Social Fund (ESF) (2021 FI_B1 00170). This work was co-financed by the European Regional Development Fund and the state budget of the Czech Republic (project HiLASE CoE: Grant No. CZ.02.1.01/0.0/0.0/15_006/0000674) and by the European Union's Horizon 2020 research and innovation programme under grant agreement No. 739573.

References

1. K. Scholle, P. Fuhrberg, P. Koopmann, S. Lamrini, 2 μm laser sources and their possible applications, in Frontiers in Guided Wave Optics and Optoelectronics, Ch. 21, ed. by B. Pal (INTECH Open Access Publisher, Rijeka, 2010)
2. J. Yu, B. C. Trieu, M. Petros, Y. Bai, P. J. Petzar, G. J. Koch, U. N. Singh, and M. J. Kavaya: Proc. SPIE 6409 (2006)
3. S.S. Chen, J. Yu, M. Petros, Y. Bai, U.N. Singh, M.J. Kavaya, Proc. SPIE 5653, 175 (2005)
4. Z. Pan, P. Loiko, Y. Wang, Y. Zhao, H. Yuan, K. Tang, X. Dai, H. Cai, J. M. Serres, S. Slimi, E. B. Salem, E. Dunina, A. Kornienko, L. Fomicheva, J. L. Doualan, P. Camy, W. Chen, U. Griebner, V. Petrov, M. Aguiló, F. Díaz, R. M. Solé, and X. Mateos, J. Alloys Compd. 853, 157100 (2021)
5. A. Godard, C R Phys. 8, 1100 (2007)
6. D.C. Brown, IEEE J. Sel. Top. Quantum Electron. 11, 587 (2005)

5. Results

7. R.L. Aggarwal, D.J. Ripin, J.R. Ochoa, T.Y. Fan, J. Appl. Phys., 98, 103514 (2005)
8. J. Koerner, T. Lühder, J. Reiter, I. Uschmann, H. , Marschner, V. Jambunathan, A. Lucianetti, T. Mocek, J. Hein, M.C. Kaluza, J. Lumin. 202, 427 (2018)
9. T.Y. Fan, IEEE J. Sel. Top. Quantum Electron. 13, 448 (2007)
10. D. Rand, D. Miller, D.J. Ripin, T.Y. Fan, Cryogenic Yb^{3+}-doped materials for pulsed solid-state laser applications [Invited]. Opt. Mater. Express 1, 434 (2011)
11. V. Jambunathan, L. Horackova, P. Navratil, A. Lucianetti, T. Mocek, IEEE Photonics Tech. Lett. 28, 1328 (2016)
12. S.P. David, V. Jambunathan, F.X. Yue, B.J.L. Garrec, A. Lucianetti, T. Mocek, , Opt. Mater. Express 9, 4669 (2019)
13. T. Y. Fan, J. R. Ochoa, and P. A. Reed, IEEE J. Quantum Electron. 51(10), 1700605 (2015)
14. Z. Hubka, J. Šulc, H. Jelínková, K. Nejezchleb, V. Škoda SPIE Photonics Eur. Int. Soc. Opt. Photon. 98930Q((2016)
15. F. Yue, V. Jambunathan, S.P. David, X. Mateos, M. Aguiló, F. Díaz, J. Šulc, A. Lucianetti, T. Mocek, Appl. Phys. B 126, 44 (2020)
16. F. Cornacchia, A. Toncelli, M. Tonelli, Prog. Quantum Electron 33, 61 (2009)
17. P. Loiko, J. Serres, X. Mateos, S. Tacchini, M. Tonelli, S. Veronesi, D. Parisi, A. Di Lieto, K. Yumashev, U. Griebner, V. Petrov, Opt. Mater. Express 7(3), 844 (2017)
18. S. So, J.I. Mackenzie, D.P. Shepherd, W.A. Clarkson, J.G. Betterton, E.K. Gorton, Appl. Phys. B 84, 389 (2006)
19. M. Schellhorn, S. Ngcobo, C. Bollig, Appl. Phys. B. 94, 195–198 (2009)
20. A. Berrou, O.J.P. Collett, D. Morris, M.J.D, Opt. Express 26 10559–10572 (2018)

5. Results

21. U. Demirbas, J. Thesinga, E. Beyatli, M. Kellert, M. Pergament, F. X. Kärtner , Opt. Express 30, 41219 (2022)
22. F. Yue, V. Jambunathan, S. P. David, J. Reiter, J. Körner, D. Klöpfel, J. Hein, M. C. Kaluza, A. Lucianetti, T. Mocek, Proc. SPIE 11033, 110330E (2019)
23. U. Demirbas, J. Thesinga, M. Kellert, F. Kärtner, M. Pergament, (2022) Preprint. DOI : 10.13140/RG.2.2.26586.41923

5. Results

5.2.2. Laser generation around ~1 μm from Yb

We report in [P3] the spectroscopy and the first continuous wave laser operation at cryogenic temperatures of Yb:YCOB in a compact modular cavity with a slope efficiency of 69.1 %, with respect to the incident power. In [P4] we investigate the characteristics and continuous wave laser performance of a Yb:$KLu(WO_4)_2$ crystal under cryogenic conditions with a maximum output power of 9.5 W, reached at a temperature of 80 K, with an efficiency slope of 40%. In the same way as in the previous papers the setup and experiments were carried out by the author of the thesis, the leader of the Cryogenic Laboratory in HiLASE and the thesis supervisors. It should be added that the cryogenic spectroscopy in [P3] was measured by one of the authors of the article in the FiCMA laboratories at the URV.

5. Results

5. Results

Cryogenic spectroscopy and continuous-wave microchip Yb:YCOB laser

(In preparation)

Adrian Alles,[1,2] Venkatesan Jambunathan,[3] Ghassen Zin Elabedine,[2] Sami Slimi[2], Josep M. Serres,[1,2] Magdalena Aguiló[2], Francesc Díaz[2], Xavier Mateos,[2, #,*] Martin Smrz, [3] and Tomas Mocek[3]

[1]Eurecat, Centre Tecnològic de Catalunya, Advanced Manufacturing Systems Unit (AMS), Marcel·lí Domingo 2, 43007 Tarragona, Spain
[2]Física i Cristal·lografia de Materials (FiCMA), Universitat Rovira i Virgili, (URV), Marcel·lí Domingo, 1, 43007 Tarragona, Spain
[3]HiLASE Center, Institute of Physics of the Czech Academy of Sciences, Za Radnicí 828, 25241 Dolní Břežany, Czech Republic
 # Serra Húnter Fellow,

**Corresponding author: xavier.mateos@urv.cat*

Abstract

We report the spectroscopy and the first continuous-wave laser operation at cryogenic temperatures of Yb:YCOB in microchip geometry. A VBG diode with stabilized pump emitting at 976 nm matching the zero-phonon line of the gain medium was employed. At 80 K, a maximum output power of almost 8.0 W was achieved. This result provided a a slope efficiency of 69.1%, with respect to incident power using an output coupler transmission of

5. Results

30 %. This value represents twice the output power achieved at 280 K.

1. Introduction

Diode-pumped solid-state lasers find countless applications nowadays. These are used for example in industry (cutting, laser sintering, drilling), medicine, as well as scientific applications (spectroscopy, femtochemistry) and the military industry. Due to the well-known process of thermal lensing as a result of the increase in temperature within the laser medium, the quality of the beam profile and the possibility of focusing the laser light is considerably affected; further resulting in less efficient lasers and significant power scaling limitations. Therefore, strategies should be considered to mitigate these problems.

Cooling the active medium to cryogenic temperatures is a technique used a few months after the discovery of the first ruby laser, when Peter Sorokin and M.J. Stevenson presented the first four-level laser using U^{3+} in a CaF_2 crystal (emission at 2.5 μm), which was cooled to the temperature of liquid helium to lower the threshold of the laser [1].

Numerous publications endorse these advantages and serve as motivation to continue providing scientific knowledge in the area [2-6].

5. Results

One of the challenges associated with lasers is the search for those that are compact. It is precisely this compactness that makes, on many occasions, its use in the dissimilar sectors and applications in industry, medicine, scientific research and in the military industry. This feature, coupled with high beam quality, provides greater laser reliability and long-term stability. The design of compact devices is facing new challenges and at the same time more and more advances are emerging thanks to the achievements and efficiency perspectives both in continuous-wave (CW) and pulsed mode.

The laser generation at 1 micrometer (wavelength) at cryogenic temperatures (80-140 K) in order to achieve a robust and compact laser is our focus of study in this research.

Regarding the active ions, the Ytterbium ion is the simplest system because only one excited state is possible corresponding to the $^2F_{7/2} \rightarrow {}^2F_{5/2}$ transition. At room temperature, RT, Yb -based lasers are said to operate in a 'quasi-three-level' laser scheme. The broadband absorption of Yb^{3+} extends from 880 to 1000 nm depending on the host [7-10]. This in-band pumping system shows very efficient laser generation, reducing the fractional heat load (low losses from non-radiative processes) and very low quantum defect (<10%) providing high slope efficiencies and high optical-to-optical conversions. The simple energy level scheme avoids the up-conversion and the excited-state absorption processes).

5. Results

Cryogenic temperatures have been applied in solid-state lasers essentially in the 1 micron spectral range based on Yb ions because there are improvements in the mitigation of the reabsorption losses over lasers operating at RT [11-14] due to the quasi-three-level scheme. It is remarkable that under cryogenic conditions a reduction of the thermo-optical and thermo-mechanical effects is perceived, as well as an improvement of the spectroscopic properties of the laser materials. An increase in thermal conductivity, a decrease in the thermal expansion coefficient, and a decrease in the thermal dependence of the refractive index, dn/dT are observed [15-16]. Under these conditions, the absorption cross-section of the pump transition increases considerably. No less important is that the radiative life of the emitting level is increased at low temperatures. Quantitative values of absorption and emission cross-sections for Yb-doped laser materials (Yb:YAG and Yb:LuAG) as a function of temperature, between 80 and 340 K, are provided in [17]. Note that for both materials, the emission cross-section at 80 K is about 5 times larger than at RT, while the bandwidth is strongly reduced. In [14] the CW and pulsed laser characteristics of Yb:Y_2O_3 transparent ceramics at cryogenic temperatures are reported. At 100 K, a maximum CW output power of 12 W was achieved, representing around three times higher output than that at 300 K in similar conditions. Further, the slope efficiency of 54.4% improved 2.4 times that at 300 K.

5. Results

The monoclinic oxoborate $Ca_4REO(BO_3)_3$ crystal, where RE = Y (shortly denoted as YCOB), is a promising laser host for doping with Yb^{3+} ions [18]. It can be grown in large volumes, even at high doping levels (up to ~50%) and shows show broad and intense absorption and emission bands with strong polarization-anisotropy [19-24]. As a result, efficient CW [25], passively Q-switched [26,27] and mode-locked [28,29] Yb:YCOB lasers have been realized to date. In [18] the thermal lens in the monoclinic Yb:YCOB was studied at RT for several orientations and laser operation was achieved in microchip geometry reaching a maximum output power of 8.35 W at ~1040 nm with 70% slope efficiency.

Based on the exposed above, this work was devoted to study the spectroscopic and laser characteristics of the Yb:YCOB crystal at cryogenic temperatures in microchip geometry. These results represent the first Yb:YCOB cryogenic laser.

2. Experimental

2.1. Cryogenic spectroscopic characterization

2.2. Cryogenic continuous-wave (CW) laser setup

For the laser operation we employed as active medium, a crystal, x-cut 15 at. % Yb:YCOB crystal (N_{Yb}=6.9 x 10^{20} at/cm^3) with a thickness of 3 mm and an aperture of 3×3 mm^2. The laser setup for the cryogenic continuous-wave (CW) laser experiments was designed by forming a compact modular cavity consisting of a

5. Results

plane-plane pump mirror, with high reflection (HR) coated for 0.9-1.2 μm and high transmission (HT) around 1200 nm. A series of plane output couplers (OC) with different partial transmission (T_{oc} =10, 30, and 50%) were used. The Yb:YCOB crystal was carefully mounted on a brass holder, adjusted to its dimensions, after envelop it in a thin layer of indium; and maintained at normal incidence inside a vacuum chamber. This type of modular cavity allowed greater freedom of movement, that is, it provided the possibility of replacing and/or adjusting, indistinctly, any of the optical elements, namely the output couplers, pumping mirrors and the active medium itself. Figure 1. shows the schematic diagram of the experimental setup. The cryogenic temperatures of the sample were varied with intervals of 20 K starting at 80 K up to 280 K. To achieve an efficient cooling of the active medium, a closed cycle helium cryostat (CH-204, JANIS) was used, which can supply 13.5 W as cooling power at 100 K. To monitor and guarantee that the sample is at the same temperature, a Lake Shore controller (DT 670) was incorporated, which integrates a 50 Ω heater and two sensors of silicon connected to the sample and the cold finger. To prevent water vapor condensation on the sample surface, the entire chamber was kept at a vacuum pressure of 10^{-5}mbar.

From the outside of the modular chamber, a computer-aided system was used, capable of achieving optimized alignment. Piezoelectric actuators have the ability to tilt the mirrors and perform movements at reduced speeds, according to the needs of the operator.

5. Results

A laser diode emitting around 976 nm was used as pump source, with a bandwidth of 0.5 nm stabilized by a Volume Bragg Grating. Diode is coupled by a fiber of core diameter of 105 µm and N.A. = 0.22 delivering a maximum output power of 60 W. The radiation from the pump source was imaged to the active medium in 1:1.5 ratio by two AR-coated achromatic lenses (focal lengths of 100 and 150 mm). The estimated mode size was ~158 µm in the active medium.

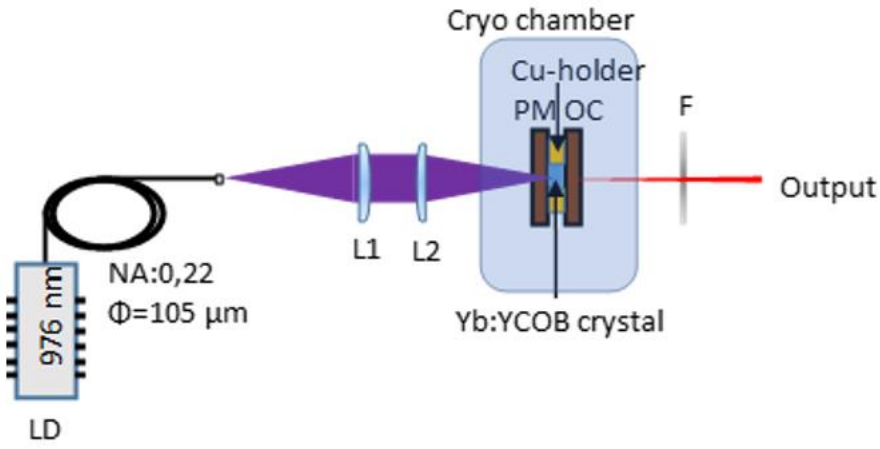

Figure 1. Laser setup: LD—laser diode emitting at ~ 976 nm, core diameter 105 µm, N.A. = 0.22; Imaging optics—achromatic lenses (L1 = 100 mm and L2 = 150 mm).

3. Results and discussion

3.1 Cryogenic continuous-wave laser operation of Yb:YCOB

5. Results

The study followed for the laser operation consisted of varying three parameters: the heat sink temperature (chiller temperature) of the pump, the transmission of the output coupler and finally the temperature of the sample in question: Yb:YCOB.

Firstly, the laser characteristics are studied by varying the heat sink temperature by 5°C from 15 °C to 35 °C, which can be clearly observed in Figure 2 a). The transmission of the output coupler is fixed to 10% and the temperature of the sample is maintained at 80K during this experiment. The highest slope efficiency of 44.2% is achieved with a diode chiller temperature of 30°C. At a temperature of 15°C the slope efficiency is 35,9 %, lower than in the rest of the temperatures studied. The output power linearly increases without the presence of thermal effects up to the highest available pump power.

We have limited the output power of the pump to a maximum of 11.96 W to avoid any damage of the crystal that prevents us from continuing the experiment. For all temperatures of the pump heat sink, the laser wavelength remained centered around 976 nm, as we observe in Figure 2 b). It is vitally important that there is a match between the wavelength as the bandwidth of absorption and emission of the sample. Failure to do so would likely lead to less efficient laser operation.

5. Results

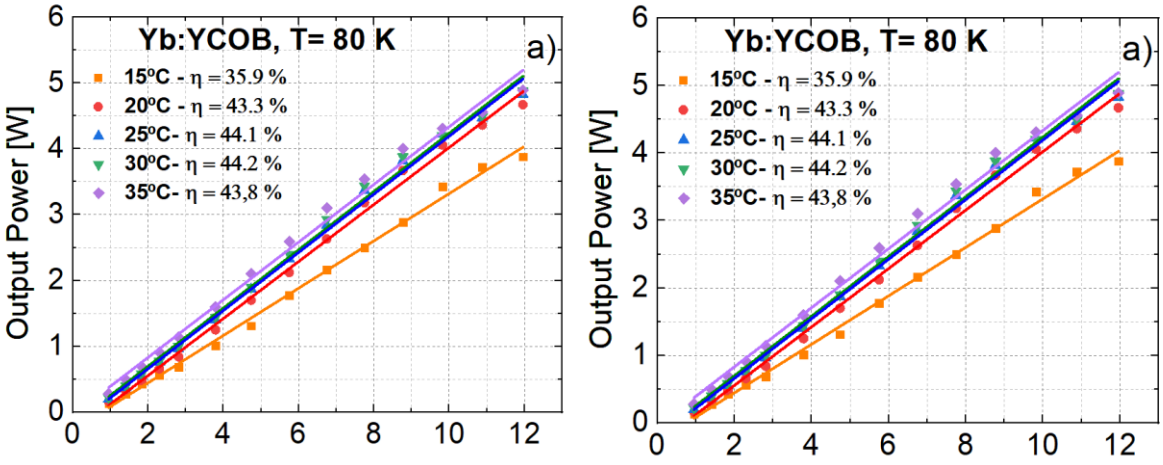

Figure 2 . a) Output power vs. incident power characteristics of the cryogenic compact YbYCOB laser for various heat sink temperature (chiller temperature) of the pump. **b)** Corresponding output laser wavelengths for different temperatures

In the second experiment, we characterize the laser performance (laser threshold, output power and slope efficiency) after varied the following transmissions of the output: (T_{oc} = 10, 30 and 50%). In all cases, we fixed the heat sink temperature at 35 °C and the temperature of the sample at 80 K. Figure 3 a) shows the CW input-output characteristics of the Yb:YCOB laser. The highest slope efficiency is 69,72% achieved at an incident power of 11.92 W for TOC = 50% and the maximum output power 7.91W, with a slope efficiency of 69.16 % is achieved at 80 K for TOC = 30%. The output coupler TOC = 10% showed inferior slope efficiency and output power. It is also noted that regardless of the Toc we used, the behavior of the laser output wavelength was the same in all cases.

5. Results

In Figure 3 b), we observe that it was centered around 1017 nm for the three transmissions of output coupling studied.

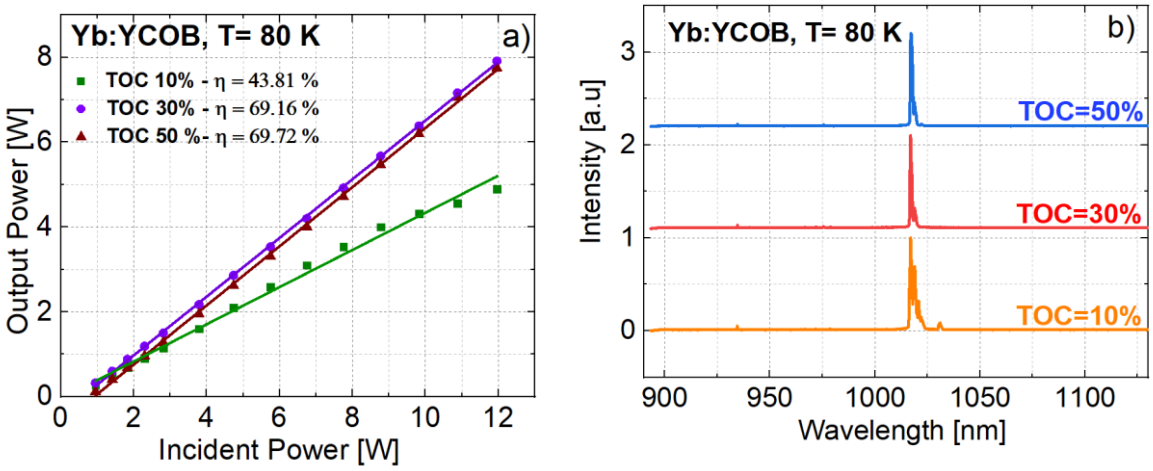

Figure 3. a) Output power vs. incident power characteristics of the cryogenic compact Yb:YCOB laser for different transmissions of output coupling. **b)** Laser output wavelengths for transmissions of output coupling (10,15,50%).

To finish, we study the behavior of the laser operation by varying the temperature of the laser performance. We kept the output coupling fixed at 30% and we varied the temperature of the sample in step sizes of 40 K starting with 80 K up to 280 K. Figure 4 a) shows the input and output characteristics of the Yb:YCOB cryogenic laser after having performed these variations. A maximum output power of 7.91 W with a slope efficiency of almost 70.0 % is achieved at 80 K. It becomes noticeable how the slope

5. Results

efficiency increases by almost 30% when the sample is cooled from room temperature to 80 K. This is essentially due to the fact that there is a reduction in reabsorption and a marked improvement in the thermo-optical, thermo-mechanical and spectroscopic properties of Yb:YCOB. This shows that the results are superior if we compare them with those that we would obtain at room temperature, keeping the rest of the similar conditions in the laser operation. Figure 4 b), shows the corresponding output laser wavelengths for different temperatures. At 80 K the laser wavelength remained centered around 1017 nm. Note the change in wavelength at 280 K, approaching in this case at 1031 nm. This shows that when the YbYCOB sample is cooled, a reduction in reabsorption losses occurs. We summarize that cryogenic temperatures favor laser performance and a marked improvement in thermomechanical and thermooptical properties of Yb:YCOB.

5. Results

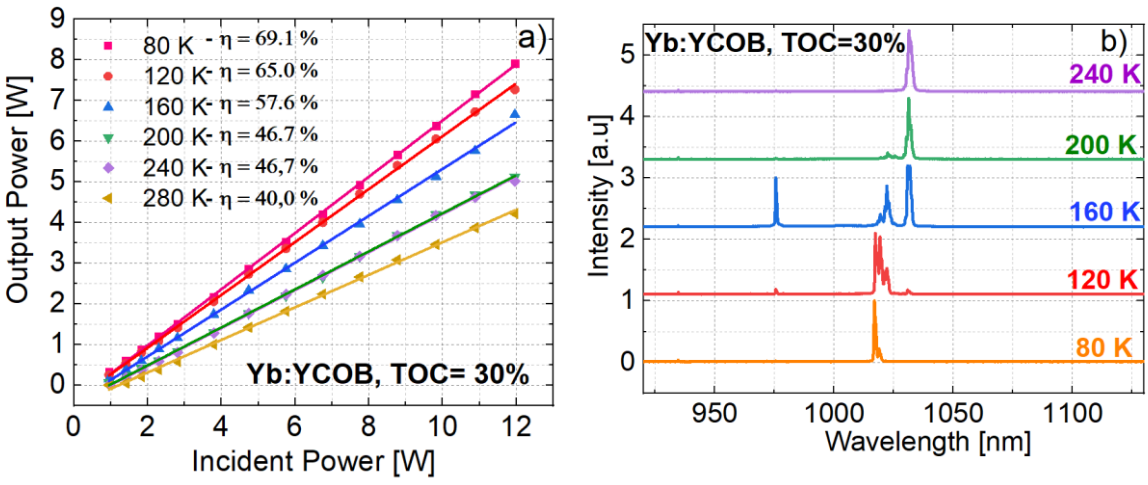

Figure 4. a) Output power vs. input power characteristics of the cryogenic compact Yb:YCOB laser for various crystal temperatures. **b)** Corresponding output laser wavelengths for different temperatures

We also measure the absorption of the sample under non-laser conditions, which amounts to up to 89%. With these values we compare between the absorbed/output power characteristics versus the incident/output power characteristics.

In Figure 5 a), it is illustrated that 7.91 W was obtained as maximum output power. This value corresponds to an absorbed power of 10.64 W. The efficiency of the slope with respect to the absorbed power amounts to 77.7%. It is worth mentioning that the values of the losses due to reflection of the sample in question were not considered for the estimation of the efficiency of the slope. It is worth

5. Results

noting the high quality of the beam profile obtained, which is thanks to the cryogenic temperatures.

Figure 5 b), clearly shows the presence of a far-field Gaussian-shaped beam profile. This beam profile was obtained at the maximum power studied.

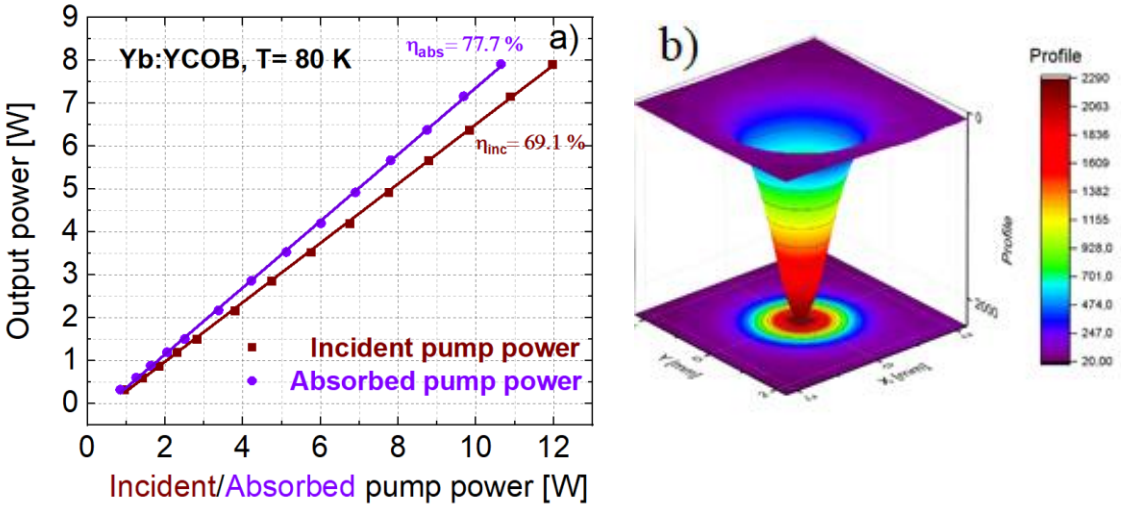

Figure 5. a) Laser performance of the compact cryogenic Yb:YCOB laser pumped by the VBG diode at 80 K with Toc=30%. Output power versus incident (brown) and absorbed (purple) pump power. **b)** Far field Gaussian beam profile.

Conclusions

In conclusion, we study the spectroscopy and continuous-wave laser operation of Yb:YCOB crystal at cryogenic temperatures. For the laser operation a compact cavity of modular type was employed;

5. Results

obtaining 7.91 W as maximum output power, with a temperature of 80 K. Regarding the absorbed power, a slope efficiency of 77.7% was obtained. We highlight the advantages of cryogenic systems by contrasting the high quality of the beam profile and in the same way the use of a VBG stabilized diode pumping.

Acknowledgements

Grant PID2019-108543RB-I00 funded by MCIN/AEI/ 10.13039/501100011033. This work has been possible with the support of the Secretaria d'Universitats i Recerca del Departament d'Empresa i Coneixement de la Generalitat de Catalunya, the European Union (UE), and the European Social Fund (ESF) (2021 FI_B1 00170). Grant PECT "Cuidem el que ens uneix", operation 4 Sensòrica, Act 4 Fotònica" PR15-020174 co-financed by the European Regional Development Fund "ERDF A way of making Europe" through the ERDF Catalonia Operational Programme 2014-2020.

This work was co-financed by the European Regional Development Fund and the state budget of the Czech Republic (project HiLASE CoE: Grant No. CZ.02.1.01/0.0/0.0/15_006/0000674) and by the European Union's Horizon 2020 research and innovation programme under grant agreement No. 739573. This work was also supported by the Ministry of Education, Youth and Sports of the Czech Republic (Programmes NPU I Project No. LO1602).

5. Results

References

1. P.P. Sorokin, M.J. Stevenson, Phys. Rev. Lett. 5, 557–559 (1960)
2. D. Ripin, J. Ochoa, R.L. Aggarwal, T. Fan, Opt. Lett. 29, 2154 (2004)
3. D.C. Brown, IEEE J. Sel. Top. Quantum Electron. 11, 587–599 (2005)
4. S.J. Yoon, J.I. Mackenzie, Opt. Express 22, 8069–8075 (2014)
5. D. V. Seletskiy, R. Epstein, and M. Sheik-Bahae, Rep. Prog. Phys. 79(9), 096401 (2016)
6. U. Demirbas, M. Kellert, J. Thesinga, S. Reuter, Y. Hua, M. Pergament, F. X. Kärtner, Proc. SPIE 12018, Photonic Heat Engines: Science and Applications IV, 1201802 (2022)
7. P.-H. Haumesser, R. Gaumé, B. Viana, E. Antic-Fidancev, D. Vivien, J. Phys.: Condens. Matter 13, 5427 (2001)
8. S. Chenais, F. Druon, F. Balembois, P. Georges, A. Brenier, G. Boulon: Opt. Mater. 22, 99 (2003)
9. J. Liu, W. Han, H. Zhang, J. Wang, V. Petrov, Appl. Phys. B 91, 329 (2008)
10. F. Pirzio, E. Caracciolo, S. D. D. D. Cafiso, M. Kemnitzer, A. Guandalini, F. Kienle, S. Veronesi, M. Tonelli, J.A. d. Au, and A. Agnesi, “Ultrafast Solid-State Oscillators and High-Power Amplifiers Based on Broadband, Multisite Yb-doped Crystals,” European Conference on Lasers and Electro-Optics - European Quantum Electronics Conference, paper CA_2_1, (2015)
11. D.J. Ripin, J.R. Ochoa, R.L. Aggarwal, T.-Y. Fan, IEEE J. Quantum Electron. 41, 1274 (2005)
12. V. Jambunathan, L. Horackova, P. Navratil, A. Lucianetti, T. Mocek, IEEE Photonics Tech. Lett. 28, 1328–1331 (2016)
13. V. Jambunathan, P. Navratil, S.P. David, F. Yue, J.M. Serres, X. Mateos, and T. Mocek. "Diode-pumped cryogenic Yb:KLu(WO4)2 laser," Conference on Lasers and Electro-Optics Europe & European Quantum Electronics Conference

5. Results

(CLEO/Europe-EQEC), pp. 1-1, doi: 10.1109/CLEOE-EQEC.2017.8086319. (2017)
14. S.P. David, V. Jambunathan, F.X. Yue, B. J. Le Garrec, A. Lucianetti, T. Mocek, Appl. Phys. B, 125, 137 (2019)
15. D.C. Brown, IEEE J. Sel. Top. Quantum Electron. 11, 587 (2005)
16. J. Kong, D.Y. Tang, B. Zhao, J. Lu, K. Ueda, H. Yagi, T. Yanagitani, Appl. Phys. Lett. 86, 161116 (2005)
17. J. Körner, V. Jambunathan, J. Hein, R. Seifert, M. Loeser, M. Siebold, U. Schramm, P. Sikocinski, A. Lucianetti, T. Mocek, M.C. Kaluza, Appl. Phys. B 116, 75 (2013)
18. P. Loiko, J. M. Serres, X. Mateos, H. Yu, H. Zhang, J. Liu, K. Yumashev, U. Griebner, V. Petrov, M. Aguiló, F. Díaz, , IEEE Photonics J. 8(3), 1501312 (2016)
19. M. Iwai, T. Kobayshi, H. Furuya, Y. Mori, T. Sasaki: Jpn. J. Appl. Phys. 36 (Pt.2, 3A) L276 (1997)
20. F. Mougel, A. Kahn-Harari, G. Aka, D. Pelenc, J. Mater. Chem. 8, 1619 (1998)
21. Q. Ye, B.H.T. Chai, J. Cryst. Growth 197, 228 (1999)
22. H. Zhang, X. Meng, P. Wang, L. Liu, R. Cheng, J. Dawes, P. Dekker, S. Zhang, L. Sun: Appl. Phys. B 68, 1147 (1999)
23. F. Druon, F. Auge, F. Balembois, P. Georges, A. Brun, A. Aron, ´ F. Mougel, G. Aka, D. Vivien: J. Opt. Soc. Am. B 17, 18(2000)
24. A. Aron, G. Aka, B. Viana, A. Kahn-Harari, D. Vivien, F. Druon, F. Balembois, P. Georges, A. Brun, N. Lenain, M. Jacquet, Opt. Mater. 16, 181 (2001)
25. J. Liu, H. Zhang, J. Wang, V. Petrov, Opt. Lett. 32, 2909 (2007)
26. J. Liu, Q. Dai, Y. Wan, W. Han, X. Tian, Opt. Exp., vol. 21, no. 8, pp. 9365–9376, (2013)
27. H.C. Liang, J.Y. Huang, K.W. Su, H.C. Lai, Y.F. Chen, K.F. Huang, H.J. Zhang, J.Y. Wang, M.H. Jiang, Appl. Opt. 46, 2292 (2007)
28. F. Druon, F. Balembois, P. Georges, A. Brun, A. Courjaud, C. Hönniger, F. Salin, A. Aron, F. Mougel, G. Aka, D. Vivien: Opt. Lett. 25, 423 (2000)

5. Results

29. A. Yoshida, A. Schmidt, V. Petrov, C. Fiebig, G. Erbert, J. Liu, H. Zhang, J. Wang, U. Griebner, Opt. Lett. 36(22), 4425–4427 (2011)

5. Results

5. Results

Continuous-wave laser operation of Yb:KLuW using a modular compact cavity at cryogenic temperatures

(In preparation)

Adrian Alles,[1,2] Venkatesan Jambunathan,[3] Ghassen Zin Elabedine,[2] Sami Slimi[2], Josep M. Serres,[1,2] Magdalena Aguiló[2], Francesc Díaz[2], Xavier Mateos,[2, #,*] Martin Smrz, [3] and Tomas Mocek[3]

[1]Eurecat, Centre Tecnològic de Catalunya, Advanced Manufacturing Systems Unit (AMS), Marcel·lí Domingo 2, 43007 Tarragona, Spain
[2]Física i Cristal·lografia de Materials (FiCMA), Universitat Rovira i Virgili, (URV), Marcel·lí Domingo, 1, 43007 Tarragona, Spain
[3]HiLASE Center, Institute of Physics of the Czech Academy of Sciences, Za Radnicí 828, 25241 Dolní Břežany, Czech Republic
 # Serra Húnter Fellow,

**Corresponding author: xavier.mateos@urv.cat*

Abstract

In the present work we investigate the characteristics and the continuous wave laser operation of a Yb:KLu$(WO_4)_2$ crystal under cryogenic conditions. The pump source consisted of a BWT Beijing LTD laser diode, connected to a fiber with a wavelength centralized at 981 nm due to a volume Bragg grating (VBG). The experiments were carried out using as a design, and for the first time, for this material; a plane-plane compact modular cavity. The maximum

5. Results

power output was 9.5 W, achieved at a temperature of 80 K, with a slope efficiency of 40% with an output coupler, Toc=30%.

1. Introduction

Although it is true that, from the very beginning of the discovery of the laser, a race for its use began, the increase in the applications of solid-state lasers has been even more remarkable in recent decades. There are practically no sectors where these types of lasers are not found. From the high demand in medicine, to the increasingly demanded need in industry, research and military purposes [1] . The benefits that can be obtained from them are unquantifiable; hence, having promising laser materials is essential. Within the group of laser materials that continues to promise encouraging results, we can mention the monoclinic Yb:KLu$(WO_4)_2$ (Yb:KLuW). Results have been demonstrated in both continuous and pulsed modes. This makes it considered a good material.

The studies derived from the Yb:KLuW crystal have found a place in numerous publications [2-6] that seek to improve and increase the results available to date with the aim of having more compact lasers, with higher output powers and better yields. Extensive research has been done on this crystal in our own working group and in collaboration with other relevant research centers and universities. Some of the publications are based on the growth and structural, thermomechanical, and optical properties, as well as spectroscopy and thermal lensing of these crystal matrices. Another

5. Results

study focused on verifying the power scaling capabilities of a Yb:$KLu(WO_4)_2$ laser, both in continuous wave (CW) and passive Q switching, as well as passive Q switching microchip lasers and in passively Q-switched high repetition rate pulsed lasers with Cr^{4+}:YAG or saturable absorbers.

Under room temperature (RT) conditions, a nearly three-level solid-state laser system is observed to partially occupy the Stark levels, which in this case includes the lower level. A clear model of this type of system is based on the presence of the trivalent ytterbium ion (Yb^{3+}). It is precisely the simplicity of this type of solid-state laser systems with the presence of Yb^{3+} that prevents two of the harmful phenomena in laser generation that cause a rise in the power threshold of the pump and a reduction in the slope efficiency: the excited state absorption (ESA) and upconversion (UC) process. If it were laser ions with multiple electronic levels, such as erbium or thulium, it would be more likely that the ESA would be more relevant, but not in the case of Yb^{3+}. Due to the simple structure in this type of system, the quantum defect is very bass. Precisely this leads to the favorable power scaling in laser operation.

At cryogenic temperatures number results are reported at 1 micron based on Yb ions. These results amply demonstrate that lasers operating under these conditions show improvements over those at room temperature [7-10]. In 2017, the authors of this research carried out a study on the functioning and laser operation under

cryogenic conditions of a Yb-doped $KLu(WO_4)_2$ crystal in which the pump source consisted of a diode emitting at 981 nm both in continuous regime as in pulsed. In the before mentioned work at 80 K, an output power of 4.31 W was produced, with a slope efficiency of almost 45% with respect to the incident power, in which an L-shaped cavity was used [11].

The present work tries to resolve the recommendations that were previously raised and tries to optimize the results. The main novelty of this study then lies in the design of a compact modular cavity to carry out the experiments.

2. Experimental setup

This section describes the configuration for the continuous wave cryogenic laser operation that was used. Figure 1 shows the scheme implemented with the compact modular cavity. It is made up of two plane mirrors: a high reflection (HR) pump mirror and the output coupler, which have room inside the vacuum chamber. Different transmissions in the output coupling with TOC=10, 20 and 30%. The laser material used consisted of a Yb:KLuW crystal with a thickness of 3 mm and an aperture of 3 mm^2. The active medium was covered with a thin indium foil and placed on a suitable copper support according to the dimensions of the crystal.

Note that, as shown in Figure 1, both crystals and the active

5. Results

material are located inside the chamber, forming a plane-plane cavity. The pump source consisted of a BWT Beijing LTD laser diode, connected to a fiber with a wavelength centralized at 981 nm due to a volume Bragg grating (VBG). The maximum output power of the diode is 27.8 W and it has a 0.4 nm spectral bandwidth. The fiber was designed with a diameter of 105 µm and NA = 0.22 numerical aperture. The active medium received the radiation from the pump in a ratio of 1:1.5. Two achromatic lenses with focal lengths of 100 and 150 mm respectively with ~210 µm as pump spot were placed on the laser material.

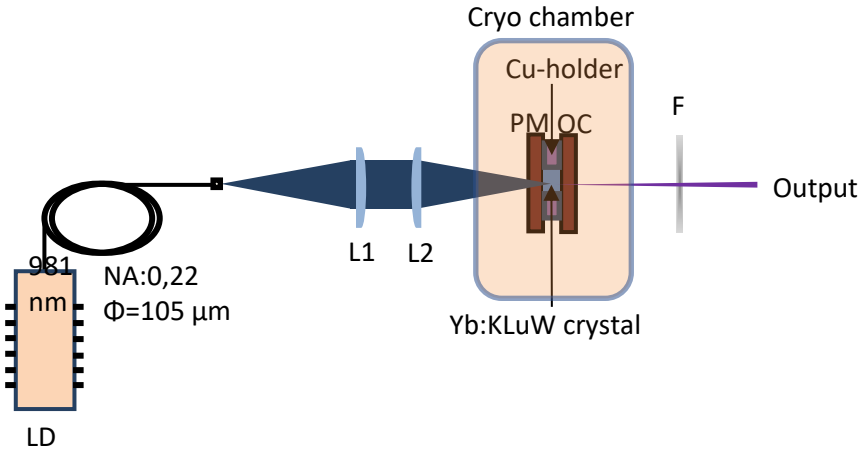

Figure. 1 Laser setup: LD—laser diode emitting at ~ 981 nm, core diameter 105 µm, N.A. = 0.22; Imaging optics—achromatic lenses (L1 = 100 mm and L2 = 150 mm)

Once placed and sealed inside the vacuum chamber, the laser material was guaranteed a pressure of around 10^{-5} mbar to avoid

any type of condensation. Cryogenic temperatures were possible to maintain due to the use of a JANIS helium cryostat, model CH-204. The closed cycle system at 100 K supplied a cooling power of 13.5 W. Temperature was constantly monitored using a Lake Shore controller (DT 670). The controller has two silicon sensors and a 50 Ω heater.

3. Results and discussion

3.1 Cryogenic continuous-wave laser operation of Yb:KLuW

In this section we discuss the main results derived from continuous laser operation. The first study basically consisted of making two variations: in the first one we observed the performance of the laser by varying the temperature, keeping the output coupler fixed. As a second study, we vary the different transmissions of the output couplers keeping the temperature fixed.

We initially decided to look at how sample temperature influences laser performance. To do this, we continue to vary the temperature from 80 to 160 K, in that order, and by increments of 40 K in each measurement. We set the TOC=10% in all cases. It can be clearly seen in Figure 2, that at the first fixed temperature of 80 K, the highest efficiency of the slope was obtained with a value close to

5. Results

40%. We attribute that higher laser yields are obtained at cryogenic temperatures. Under these conditions, the decrease in reabsorption in the laser wavelength is favored, among other factors such as that favor the improvement of the thermooptical, thermomechanical and spectroscopic properties of Yb:KLuW. To avoid any type of damage to the crystal and to continue with the experiment successfully, it was decided not to continue with the power scaling with temperatures above 160 K.

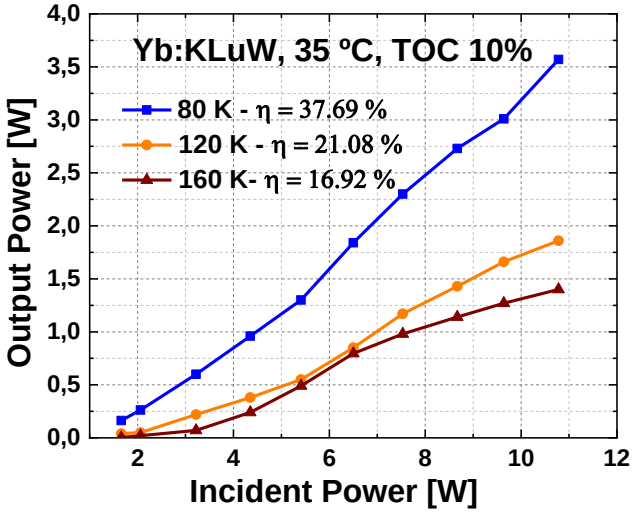

Figure. 2 Output power vs. input power characteristics of cryogenic Yb:KLuW laser for various crystal temperatures

5. Results

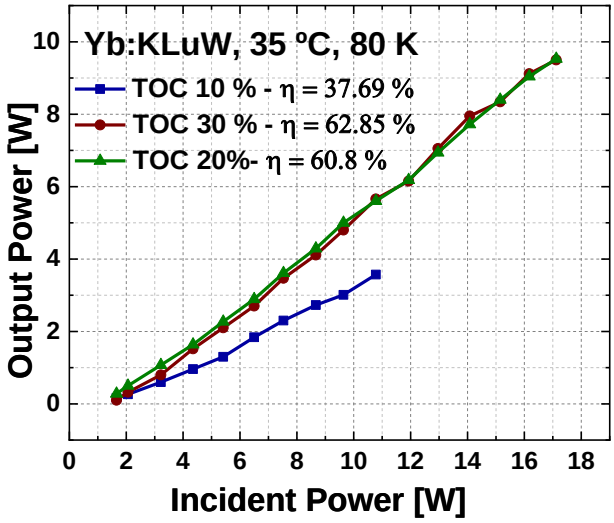

Figure. 3 Output power vs. input power characteristics for different TOCs

As a second study and once the optimum temperature of 80 K was known, it was decided to keep it permanent, in this case varying the transmittance of the TOC of the output coupler = 10%, 20% and 30%, obtaining the results as shown in Figure. 3

From the CW input-output characteristics of the Yb:KLuW material, it is observed in this graph that the behavior of the output power is linear. The highest output power value was 9.50 W with high slope efficiency amounting to 62.85%. In this case, the TOC with which this value was obtained was 30% with an incident power of 17.12 W. We obtained lower output power and efficiency values for the slopes of the other two TOCs. In the case of TOC=10%, the efficiency of the slope was notably lower with a value below 40%.

5. Results

We have measured the profile of the beam at 80 K at maximum power, resulting in high quality, and in Gaussian form, as shown in Figure 4 b). The quality of the beam is evidently attributable to the cryogenic temperatures under which the experiments were developed.

For its part, the wavelength of the laser remained centered throughout the experiment. It is observed in Figure 4 a) that both at 30°C and at 35°C, the wavelength was centered at approximately 981 nm. Note that the chiller temperature was maintained at 30°C for the experiment.

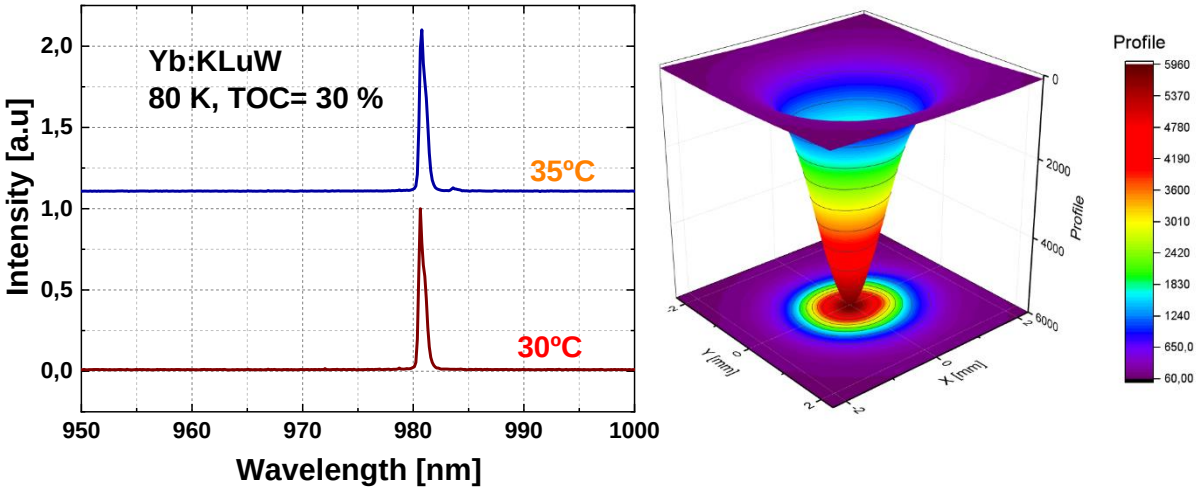

Figure 4. **a)** Laser wavelength for various sample temperatures **b)** Far field beam Gaussian profile

5. Results

Conclusions

Once the study is finished, it allows us to conclude that we have managed to optimize the Yb:$KLu(WO_4)_2$ laser operation compared to previous published works. The use of cryogenic temperatures and the pumping source with a centered wavelength, were important keys to carry out the experiments in continuous operation, which for the first-time benefit from a plane-plane modular compact cavity for this type. of laser material. The maximum output power amounted to almost 10.0 W, which is more than double that obtained using the previous configuration L. Cryogenic temperatures were shown to substantially improve the results usually obtained at room temperature. In this case, at 80 K, the best slope of the efficiency was obtained with about 40% and the quality of the beam profile presented a high quality. Future work will use the compact modular cavity to introduce saturable absorbers in a pulsed regime.

Acknowledgements

This work has been possible with the support of the Secretaria d'Universitats i Recerca del Departament d'Empresa i Coneixement de la Generalitat de Catalunya, the European Union (UE), and the European Social Fund (ESF) (2021 FI_B1 00170). This work was co-financed by the European Regional Development Fund and the

state budget of the Czech Republic (project HiLASE CoE: Grant No. CZ.02.1.01/0.0/0.0/15_006/0000674) and by the European Union's Horizon 2020 research and innovation programme under grant agreement No. 739573. This work was also supported by the Ministry of Education, Youth and Sports of the Czech Republic (Programmes NPU I Project No. LO1602).

References

[1] A. Sennaroglu, ed. Solid-state lasers and applications. CRC press, (2017).

[2] A. Schmidt, S. Rivier, G. Steinmeyer, J. H Yim, W. Bae Cho, S. Lee, F. Rotermund, M. C. Pujol, X. Mateos, M. Aguiló, F. Díaz, V. Petrov, and U. Griebner, "Passive mode locking of Yb:KLuW using a single-walled carbon nanotube saturable absorber," Opt. Lett. **33**, 729-731. (2008)

[3] V. Petrov, M. C. Pujol, X. Mateos, Ò. Silvestre, S. Rivier, M. Aguiló, R. M. Solé, J. Liu, U. Griebner, and F. Díaz, “Growth and properties of $KLu(WO_4)_2$, and novel ytterbium and thulium lasers based on this monoclinic crystalline host,” Laser Photonics Rev. **1**(2), 179–212. (2007)

[4] J. Zhang, K. Wang, J. Wang, H. Zhang, W. Yu, X.Wang, H.R. Xia. Anisotropic thermal properties of monoclinic Yb: K Lu $(WO_4)_2$ crystals. Applied Physics Letters, **87**(6), 061104. (2005)

[5] J. Liu, V. Petrov, H. Zhang. Power scaling of a continuous-wave

5. Results

and passively Q-switched Yb:KLu(WO_4)$_2$ laser end-pumped by a high-power diode. Appl. Phys. B **88**, 527–530 (2007). https://doi.org/10.1007/s00340-007-2745-0

[6] Z. Hongyang, W. Jiyang, L. Jing, Z. Jianxiu , Z. Huaijin ,J. Minhua, Growth, optical and thermal properties of Yb, Tm:KLu(WO4)2,Journal of Crystal Growth,Volume **293**, Issue 1,Pages 223-227,ISSN 0022-0248,https://doi.org/10.1016/j.jcrysgro.2006.05.010. (2006)

[7] S.P. David, V. Jambunathan, F.Yue, B. Jean Le Garrec, A. Lucianetti, and T. Mocek. "Laser performances of diode pumped Yb:Lu_2O_3 transparent ceramic at cryogenic temperatures," Opt. Mater. Express **9**, 4669-4676 (2019)

[8] Y. Lei, B. Zhong, T. Yang. X. Duan, M. Xia, C. Wang, and J, Yin . Laser cooling of Yb^{3+}: LuLiF4 crystal below cryogenic temperature to 121 K. Applied Physics Letters, **120**(23), 231101. (2022)

[9] V. Jambunathan, P. Navratil, S.P. David, F. Yue, J.M. Serres, X. Mateos, and T. Mocek. "Diode-pumped cryogenic Yb:KLu(WO_4)$_2$ laser," Conference on Lasers and Electro-Optics Europe & European Quantum Electronics Conference (CLEO/Europe-EQEC), 2017, pp. 1-1, doi: 10.1109/CLEOE-EQEC.2017.8086319. (2017)

[10] V. Jambunathan, L. Horackova, P. Navratil, A. Lucianetti, and T. Mocek. "Cryogenic Yb:YAG Laser Pumped by VBG-Stabilized Narrowband Laser Diode at 969 nm," in IEEE Photonics Technology Letters, vol. **28**, no. 12, pp. 1328-1331.(2016)

5. Results

[11] P. Navratil, V. Jambunathan, S. P. David, F. Yue, J. M. Serres, X. Mateos, M. Aguiló, F. Díaz, U. Griebner, V. Petrov, A. Lucianetti, and T. Mocek, "Continuous-wave and passively Q-switched cryogenic Yb:KLu(WO_4)$_2$ laser," Opt. Express **25**, 25886-25893. (2017)

5. Results

Chapter 6

Study of lasers in additive manufacturing

Current times demand new green alternatives. Without a doubt, 3D printing is essential if we want to talk about sustainability. Beyond a trend or "fashion" it happens to play a fundamental role in the world in which we live today. It is vital to take advantage of natural resources, reduce energy consumption and emissions, recycling and the use of waste and the search for sustainable manufacturing materials that favor a reduction in environmental impact.

This thesis has been focused on developing a new additive manufacturing technology, with speeds higher than the existing ones, with a broader catalog of materials and superior mechanical properties than the most similar technologies and with the

6. Study of lasers in additive manufacturing

innovation that, being a new technology, it could be patented, in addition to generating new scientific knowledge. The technology allows the use of new materials that cannot be used with polymeric powder bed technologies and to penetrate new high-potential sectors such as medical. In this chapter we present the main results and future challenges of the LASUV3D project, commercial name of the project.

6.1. Additive manufacturing technologies.

Additive manufacturing (AM) [104] [105] [106][107], commonly known as 3D printing, is a set of techniques and technologies for creating physical objects in space, layer by layer. There are different ways to superimpose these layers: laser fusion, UV polymerization of the material, fusion of the material or even bonding with adhesives.

6. Study of lasers in additive manufacturing

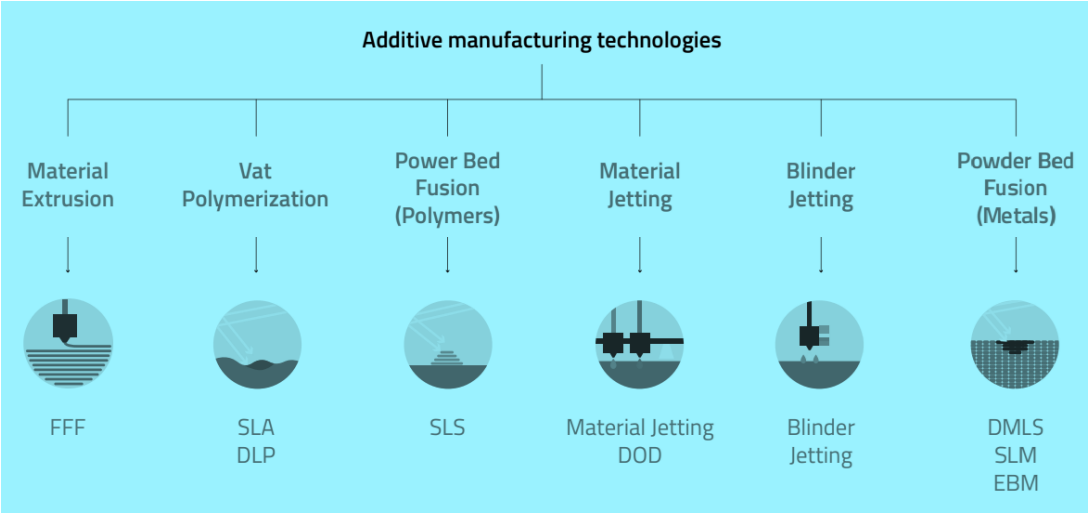

Figure 21. Additive manufacturing technologies.

Today, the potential of 3D printing is very high, since there are many different applications in different sectors [99], [108]–[112]. The main feature is the flexibility it offers, which makes it a very valuable tool to produce short series. However, it takes a long time to make a piece, layer by layer, and available commercial equipment can only handle certain materials with one machine, not different materials.

6. Study of lasers in additive manufacturing

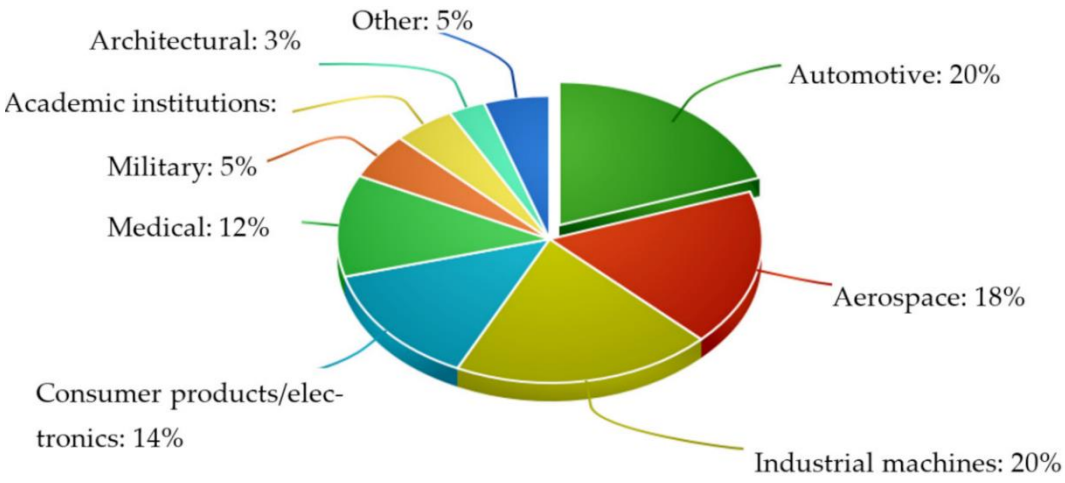

Figure 22. Industrial Adoption of additive manufacturing (AM).

6.2. LASUV3D

The main objective of the LASUV3D project is to research and develop new technologies for plastic (powder) 3D printing to overcome some of the problems with existing technologies on the market. To carry out this project, its basic principles will first be conceptualized and tested on a test bench, which will allow demonstrating the initial assumptions to assess feasibility, characterize it and decide what the configuration of the machine will be. In the LASUV3D project, the goal is to create a new additive manufacturing technology by combining two existing technologies. The principal advantage of combining the two technologies is that the combination overcomes the respective disadvantages of each technology.

6. Study of lasers in additive manufacturing

The first technology, Large Area Sintering (LAS)[32], allows higher production volumes than any other additive manufacturing technology that uses polymer powders, produces pieces with excellent mechanical properties, and can use large amounts of material. However, the final definition of the pieces is poor, especially the contours of each layer.

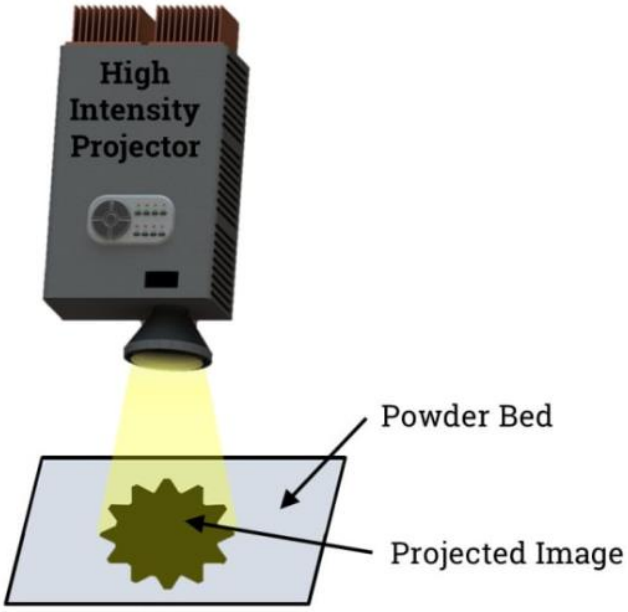

Figure 23. Large Area Sintering (LAS)

Selective Laser Sintering (SLS) technology is the most widely used polymer pulse technology on the market [113], [114], providing high-resolution pieces and the ability to generate any type of geometry

6. Study of lasers in additive manufacturing

without limitations. However, it is a low-speed technology, the pieces have preferential directions over mechanical behavior and the available materials are limited. In this way, the combination of the two technologies eliminates the respective disadvantages and increases the potential superiorities.

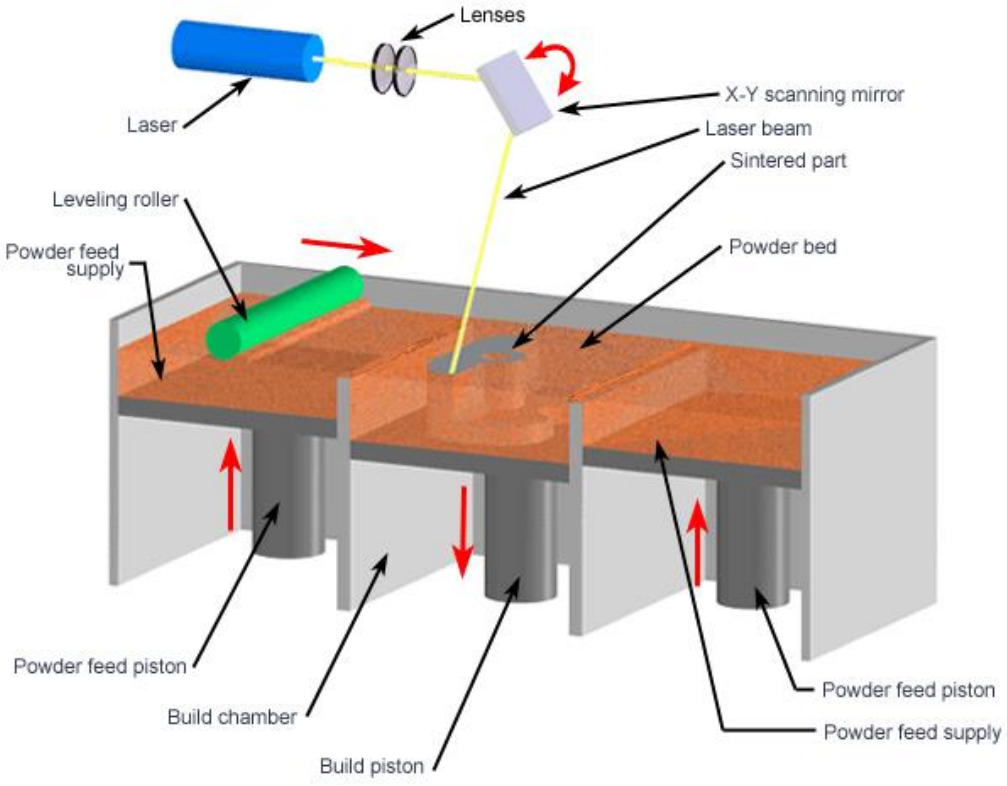

Figure. 24 Selective Laser Sintering (SLS)

The objective of the project is to make the contours of the pieces with SLS technology and the interior with LAS technology to obtain

a fast piece with a good surface finish. For the contours, the SLS surface finishing technique will be used, slower but more precise, and for the interiors the LAS technique, which is very fast because it uses image projection, but with a weaker surface finish. Therefore, it will take advantage of each technology and eliminate its disadvantages. On the other hand, it is expected that the mechanical properties of the part could be higher, but this should be investigated when the project is completed.

6.2.1. Definition of the LASUV3D project

This project proposes to develop an additive printing prototype that combines two new technologies. In this way, the production process of 3D pieces can be accelerated using large area sintering technology (LAS) and laser technology (SLS), combining their respective advantages to avoid the disadvantages of each. The project deals with the investigation of new laser materials using different light sources. The development of new light sources will allow the equipment's laser to be customized to the material to be processed. In addition, the design and development of test benches for new technologies will be carried out. The test facility will provide an opportunity to gain control knowledge for two technologies that require different control systems at the same time. LAS technology requires control over the image emitted by the projector, while SLS technology requires control over the laser path. In addition to

6. Study of lasers in additive manufacturing

knowing how to control both technologies, there are also many process conditions, such as the apparent temperature of the structure, the surface temperature, the placement of a new layer of material of a certain thickness, the speed of the laser, and the image must be perfectly controlled to get a high-quality print.

The specific objectives of the project are broken down into each area of action as follows:

- ✓ Explore new laser materials using different light sources.
- ✓ Define different light sources for different materials.
- ✓ Manufacture and characterize various compact laser prototypes and additive manufacturing materials.
- ✓ Prototyping of 3D machines compatible with different materials.
- ✓ Research and characterization of high-power laser projection for plastic powder printing.
- ✓ Combination of LAS technology (UV projector) + UV laser to develop a 3D printer prototype.
- ✓ Design and development of test benches for new technologies.
- ✓ Design and development of the structure of the machine: It includes all the mechanical parts necessary for the movement of the machine, as well as the light source and the housing of the heat source.
- ✓ Design and development of the machine control program: writing of

a simple firmware that allows controlling all the movements of the machine and the heat source. When determining the production parameters of the selected material, different machine parameters that will strengthen the coating must be determined for each material: chamber temperature, powder layer surface temperature, layer height, exposure time, etc.

- ✓ Parts manufacturing: part integration technology demonstration.

6.2.2. Current state of additive manufacturing technology

The generation of CW or pulsed laser is very interesting in various fields of application. In the second case, short (nanosecond timescale) and ultrashort (picosecond and femtosecond timescale) laser pulses are needed because high energy output and maximum power achieved in such a short time can be achieved in many fields; for example: material processing, laser interaction on human tissue, etc. Two related areas where such lasers are used are: the medical field for tissue or eye treatment and the industrial area for advanced manufacturing applications to produce 3D pieces.

3D printing, or additive manufacturing, is a series of processes that generate objects by adding material layer by layer corresponding to successive cross sections of a 3D model. Additive manufacturing of 3D pieces now makes it possible to produce pieces with complex geometries, allowing parts to be produced at an economical cost. However, layer-by-layer manufacturing takes a long time to create

6. Study of lasers in additive manufacturing

a piece, and commercial equipment can only process certain materials and cannot use the same machine to process different materials.

Two new additive manufacturing technologies, SLS and LAS, promise to speed up the manufacturing process, improving the cost, quality, and manufacturing time of each piece. While these technologies have their drawbacks in terms of cost and improved quality time, combining the two technologies allows us to pick their respective strengths and avoid their drawbacks, resulting in high processing speed, scalable resolution micrometer and a reduction in the price per unit.

SLS technology [115]–[119] was invented and patented by Carl Deckard and Joe Beaman at the University of Texas at Austin in the mid-1980s. In this technique, a laser is used to melt, fuse, or sinter particles to create an object. SLS printers will have different laser powers that determine what materials the machine can print on. SLS printers print the material in powder form with a roller mechanism inside the machine that continuously deposits new layers of "primary" material on top of the partially sintered material. The advantage of this method is that no impression support is required as the surrounding not sintered material acts as a support during the entire impression process. As a result, pieces can be more complex in terms of geometry and locking components. This is a technique in which plastic powder is sintered in a working

chamber. At the end of the processing, the objects are separated from the recyclable powder, which makes SLS technology one of the production processes with the least waste of raw materials. Since the introduction of SLS technology in the manufacturing industry, it has been widely used by engineers and designers to create aesthetic prototypes with a high level of finish and functional components that benefit from low manufacturing costs and a wide variety of materials. As usually happens in innovations, SLS technology is also experiencing a very interesting moment of evolution, which aims to expand the fields of application of selective laser sintering. The main advantages of this technology are high resolution, high resolution of details, good surface finish, absence of support structures and a lot of design freedom. But it also has several limitations: the amount of material is limited, and the production speed is low, because the laser must take different paths to complete the entire cross section of the layer.

By contrast, LAS technology [120] is a relatively a new technology developed in 2017 by Christopher J. Gardiner at the University of Florida. The technology uses a high-power, high-resolution DLP (digital light processing) projector to send an image of focused white light onto a bed of powder to heat and fuse layers of powder particles in a two-dimensional cross section over a previous layer. 3D pieces are created by sequential sintering of powder layers and assembling these thin 2D parts. This radiation first heats the inner

6. Study of lasers in additive manufacturing

regions of the cross section because the heat is more concentrated and there is less powder around to dissipate the heat at lower temperatures. This creates an area of molten powder that is then spread out to fill the entire sintered cross-sectional shape. Using the digital capabilities of the projector, any radiation pattern can be projected onto the powder bed. This new technology presents the following advantages: speed of production, since the entire cross section of the layer is projected directly; it is possible to use more materials because the sintering zone has a longer heating time; and in this way, the mechanical properties of the part can also be controlled more (less degradation of the material), it does not require support structures, and the design freedom is great. At the same time, it also has disadvantages, such as poorly defined layer outlines.

The patent status of the LAS technology has been investigated and it is verified that the patent has been applied for, but the existence of previous publications invalidates the possibility of applying for a patent of the LSA technology. It has been found that thicker layers can be obtained using the LAS technique compared to SLS. It was also found that the pieces made with this technique had a higher degree of sintering due to the increase in light intensity and exposure time, but there is no direct correlation between these parameters and performance, so it is worth mentioning that there are these two parameters into account. Different additive manufacturing methods were compared by sintering PA12 [113].

6. Study of lasers in additive manufacturing

The results showed that the different processes produced similar degrees of crystallization, but there were significant differences in mechanical properties between them, especially in terms of elongation and fracture. The pieces produced with LAS have a higher mechanical resistance than other processes. The SLS and MJF (Multi Jet Fusion, HP) processes keep the bed at a high temperature during production to avoid recrystallization and slow cooling at the end of part production. Both processes also showed lower porosity and higher elongation at break than the processes produced with LAS. However, the LAS process (as implemented in the post) may not be able to maintain temperatures above recrystallization during the process, which would lead to faster production approvals, resulting in higher temperature differences and microstructures elongation at break. It can be seen that very little research has been done on LAS technology and therefore it can be concluded that it is a new technology with many advantages that can give a very high competitive advantage when combined with SLS. The combination of the two technologies is expected to result in stronger pieces and reduced production time.

6.2.3. Technological potential

The great potential of this new technology lies in the use of materials that cannot be used with polymer powder coating technology.

6. Study of lasers in additive manufacturing

Therefore, the medical market, which has great potential for additive manufacturing technology, will be one of the target markets. Schemes using photonic technologies are one of the most promising concepts due to their physical properties and multiple applications in any industry or market. Many technological devices already use laser technology, and many more are working to replace traditional methods. Part of this project is based on research, innovation, and exploration of new laser light sources, opening new research opportunities, and improving the properties of existing devices. Solid-state lasers allow CW and pulsed laser operation at wavelengths where there are currently no devices on the market with these capabilities. The potential of the technology developed in this project should allow a qualitative leap with respect to current technologies.

6.3. Discussion of the main results of the project

6.3.1 Materials

To achieve satisfactory results, it is necessary to understand the materials and characterize them correctly. The characterization of the polyamides was used using a reflectance spectrometer (Varian Cary 5000 UV-VIS-IR). The results obtained show that the material has strong reflectance in the visible to near-infrared range, but almost no reflectance in the ultraviolet (<400 nm) and mid-infrared (>1800 nm) range. To this extent, the device partly projects light

6. Study of lasers in additive manufacturing

through the material, partly absorbs it, and partly reflects it. This means 100%= %T + %A+ %R. As an opaque material, the percentage of the transmitted portion is 0%, leaving 100% = %A + %R. To have a strong absorption, we need the reflectance value to be the lowest value, so that we obtain a strong absorption, we can use equipment with less power, with a saving of energy consumption and greater efficiency in the manufacturing of the pieces. Selected additive manufacturing materials, including polyamides [121], resins, and other forms, were characterized spectroscopically to identify those with the best print performance and understand which light source is required for light-matter behavior.

6. Study of lasers in additive manufacturing

Figure 25. Additive manufacturing materials

Within this task we studied two different samples of polyamide. Both small vials with the polyamide SWPXU13 and SWPXU20 were placed inside a laboratory desiccator to keep the substances clean and dehydrated by means of vacuum. The powder was then compacted into tablets.

The SWPXU20 polyamide presented a more humid behavior, making its compaction more difficult.

Figure 25. Polyamides (SWPXU13 y SWPXU20)

Reflectance spectra (%) were measured using the spectrophotometer (Varian CARY 5000 UV-VIS-IR). Resulting in the following:

6. Study of lasers in additive manufacturing

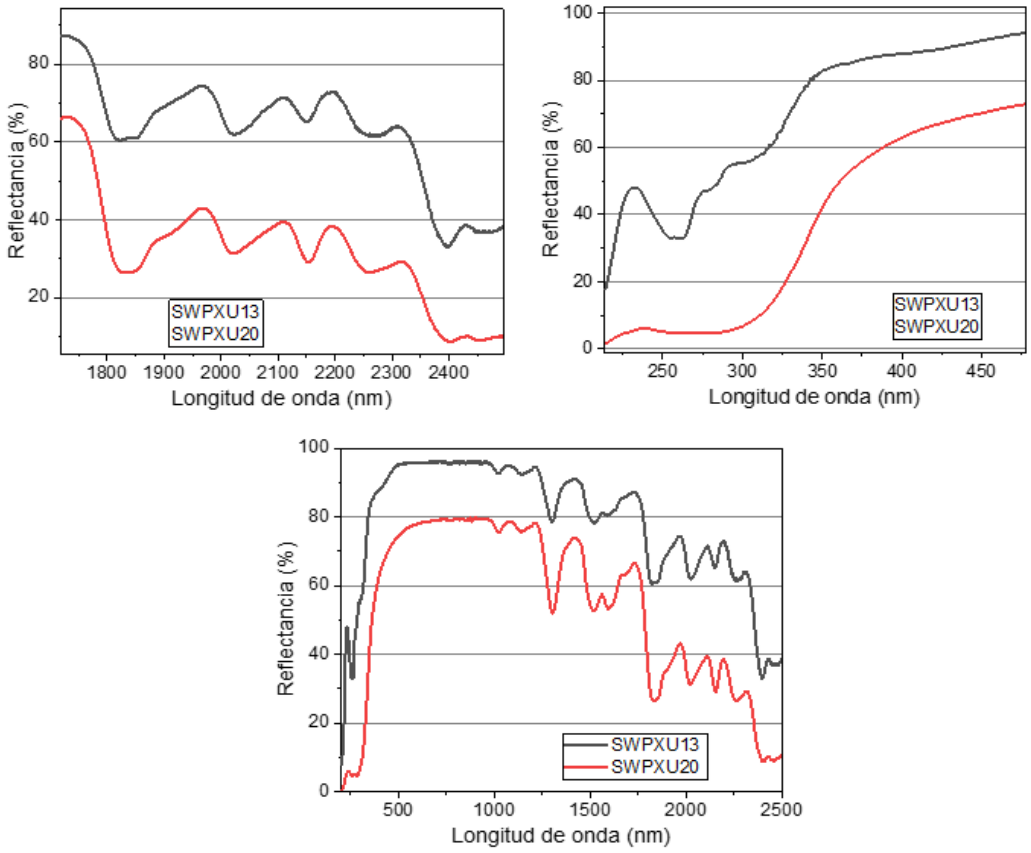

Figure 26. Spectroscopic characterization of polyamides (SWPXU13 and SWPXU20)

It turned out that the most interesting spectral bands to irradiate with light are between 200 and 450 nm and between 1800 and 2500 nm. The ideal would be to use 250 nm or 2400 nm to improve the efficiency of the device, reduce consumption and power of the laser. With a 450nm laser, less intensity will be absorbed by the material, much more residual light will be reflected by the material (use

goggles or a screen with a 450nm filter), and a higher power laser must be available.

It can be seen from the spectra that the peak ratio between the two materials is similar, indicating that their composition is nearby. Some of them appeared with greater and/or less intensity, indicating minor changes in the analyzed material. With such reflectance studies, it is not possible to characterize the material to understand its composition. Compared to SWPXU20, the reflectance of the SWPXU13 sample is much higher. This indicates that the absorption of the sample is higher in the case of SWPXU20. It is expected to absorb more current than the SWPXU13, but since it is not generally comparable, it has a higher scattering loss due to the retention of the grainier pickups. The available reflectance kit has an integrating sphere to prevent this from happening and has a more matte finish than the SWPXU20 sample. To resolve doubts about the material, the samples were allowed to dry to see if the pellets were more compressed. One of the problems that will be found is that the material will not have the original properties, but it will be possible to verify that the absorption is due to scattering losses.

6.3.2. Development of alternative washing solutions for pieces printed by SLA.

6. Study of lasers in additive manufacturing

Piece post-finishing is an essential part of the SLA 3D printing workflow. Rinsing, washing, and curing pieces[122] gives them a high degree of functionality and detail and helps make the finishing process more efficient. If the resin residue left in the grooves of the part is not effectively removed as it hardens, the resin residue will also harden, destroying the part and leaving it amorphous.
There is not many scientific research on rinsing and washing SLA printed pieces. 3D printing resin manufacturers often recommend isopropanol as a finishing solvent [123]. Due to the Covid-19 crisis, isopropyl alcohol sales have skyrocketed, and prices have more than tripled, creating shortages. Plus, other disadvantages, such as a highly volatile and flammable product with possible health effects, ventilation conditions for its use and limitations related to the fact that it cannot be used in ultrasonic tanks; they make it necessary to look for other solutions that allow us to achieve a high quality, the result is more economical, easy to dispose of and more respectful with the environment.

We carried out a study to evaluate the quality of the pieces after cleaning with each solution, at different time intervals and in all cases with the same resin. To do this, we analyze the roughness of the printed pieces, and, after the finishing process, we carry out the superficial physical characterization of the parts using FESEM. In this study, we used LCD-based SLA technology and the Anycubic Photon Mono printer.

6. Study of lasers in additive manufacturing

The different pieces (test tubes) were printed with the same type of 405 nm UV resin in all cases.

Figure 27. SLA printed tubes

As previously mentioned, the pieces after being printed usually remain with a certain amount of resin on the surface. To have a good result, cleaning is necessary. If the 3D printed object is not cleaned properly, the resin on the surface can distort the shape of the model, cured blobs can be found, and the piece can end up sticky. Two cleaning containers have been used. In the first bath most of the resin can be removed. The second, cleaner bath can be

6. Study of lasers in additive manufacturing

used for optimal cleaning of the piece. In this case, the second can be the ultrasonic bath. Sufficient rinse solution has been used in each case to completely cover the piece. After this cleaning step, a correct drying of the parts has been ensured before subsequent curing. This can be done by placing the part in a well-ventilated area for at least 30 minutes or by using compressed air for 2 minutes.

Figure 28. Spinning and pieces washing

Two solutions were used to bath the parts: isopropyl alcohol (90% concentration) and laboratory detergent.

6. Study of lasers in additive manufacturing

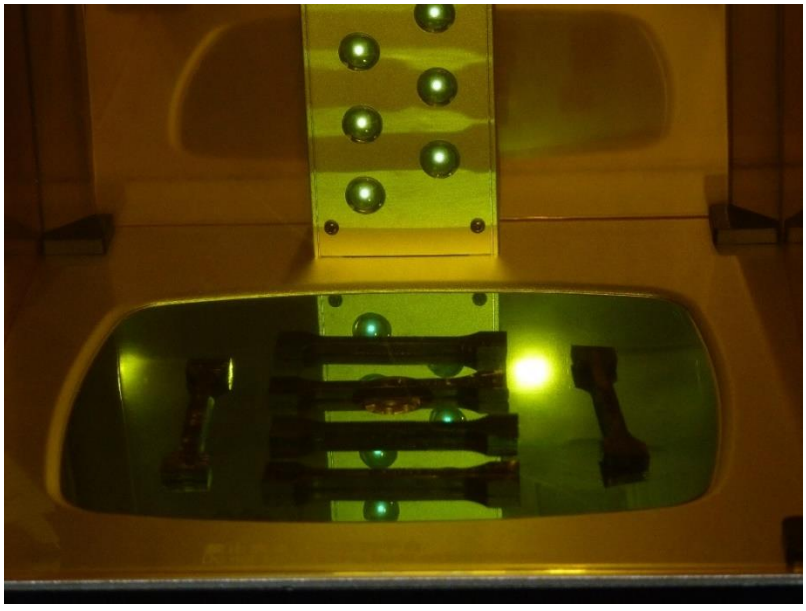

Figure 29. Pieces curing

The Figure. 30 shows high resolution images of the surface of a sample using electron-matter interactions in the FESEM.

6. Study of lasers in additive manufacturing

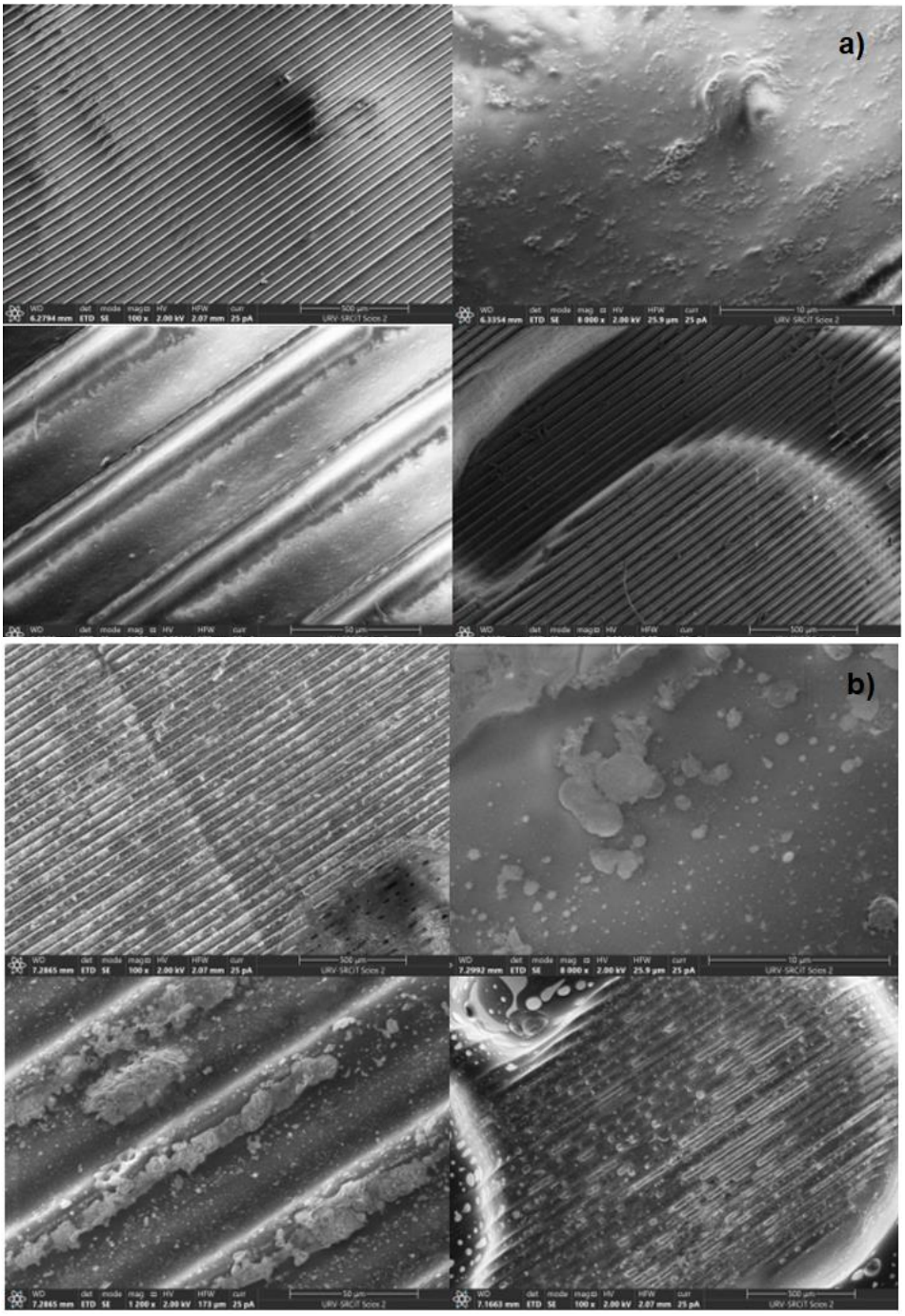

Figure 25. High resolution images of the surface of a sample using FESEM.

We evidenced for the isopropyl alcohol solution, Figure. 30 a), a superior quality of the washed pieces in relation to the quality offered by the laboratory detergent, Figure. 30 b). Better coloring and finishing with less wear. We recommend carrying out a detailed study of the tension and resistance of parts using a universal testing machine.

In any case, solvents and resins should be disposed of according to regulations and water and solvents that have been contaminated with alcohol and liquid resin should never be flushed down the sink drain. However, considering the ease of disposal, the cheapest price, and the safety in the use of laboratory detergent, we believe that if we do not need pieces with a higher quality, this option should be chosen.

6.3.3. Light sources

With the use of a laser, a lot of energy irradiated per cm^2 can be quickly merged without any problem since high power lasers with very good stability are commercially available. In this case, good results are achieved with commercial 385 to 445 nm lasers. It is interesting for heating resins and could be used for disinfection work.

6. Study of lasers in additive manufacturing

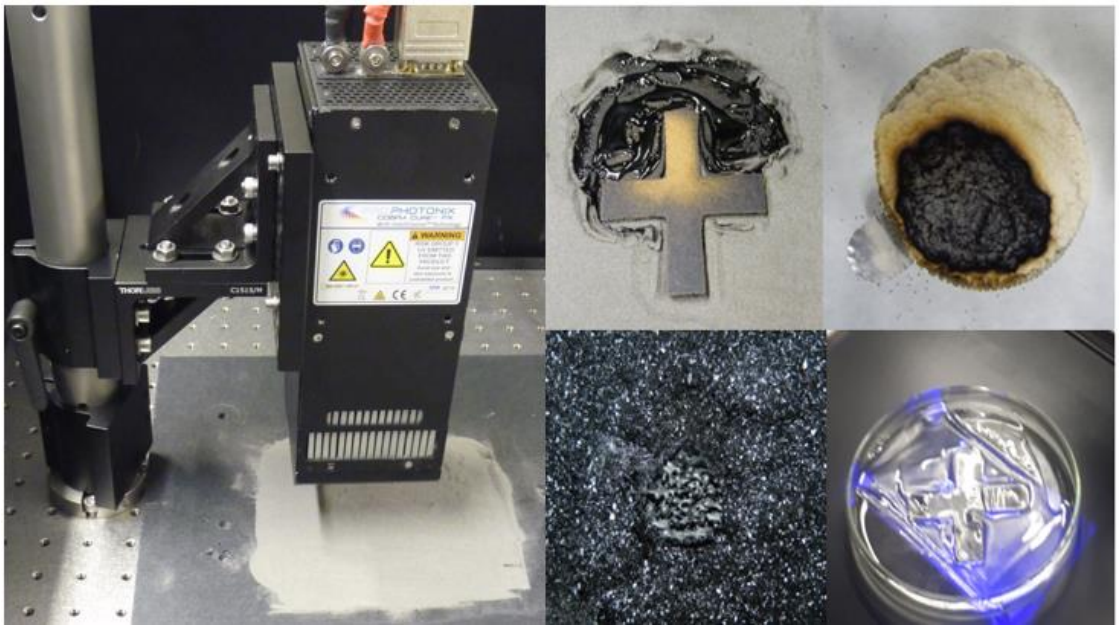

Figure 26. Light source and material curing

For the search of projectors on the market, only projectors that have at least the following characteristics as minimum values were considered: brightness 2,000 lumens and contrast 10,000:1, resolution 1024 x 768 pixels. The price range is very wide, but for 300-500 EUR you can usually find projectors. It is also noticeable that the price depends more on the resolution than on the brightness or contrast. The feasibility of some commercial projectors was investigated, but so far, no projector with sufficient performance to melt the powders was found on the market. The options are to develop a personalized one or go to a very professional market with very high prices. Eurecat has decided to develop its own.

6. Study of lasers in additive manufacturing

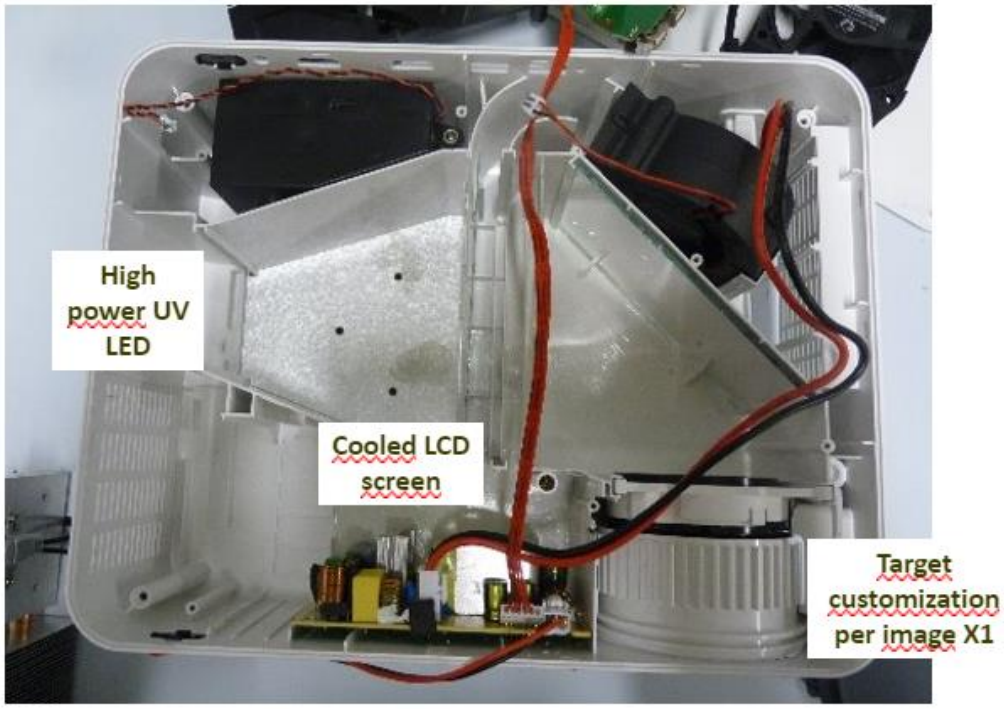

Figure 27. Testing with one of the commercial projectors

For the projection of light with LAS technology, there is no commercially available equipment that allows obtaining high values of energy per cm^2. The technologies that are viable to be implemented are LCD projection and DLP. Each of them has advantages and disadvantages.

LCD projection is a system that allows image formation by transmittance. That is, the pixels are transparent and opaque to form an image with a low contrast from white to black. The contrast allows us to control the residual light that the screen lets through despite being an opaque pixel. On the other hand, it is also observed that the LCD screen by high-power light is greatly heated,

6. Study of lasers in additive manufacturing

and non-linear effects start to happen. The screen is observed to darken. With a long exposure time the screen stops working.

The standard polarizers lose transmittance for wavelengths greater than 400 nm and specific polarizers are necessary for this application that allow transmitting light with a value close to 100% to avoid heating in this optical element.

To solve this point of absorption in the screen and in polarizers, a water-cooling system has been proposed, thus allowing the generated heat to be dissipated more quickly and being able to increase the energy per surface unit and also allowing the separation of the polarizer from the screen. LCD.

However, LCD displays are of high interest since they allow 4K resolutions based on the number of DPIs (densities per pixel), limiting their resolution to the pixel size.

6. Study of lasers in additive manufacturing

Figure 27. Water cooled LCD display

DLP projection is a system that allows image formation by reflectance. In other words, pixels are small micromirrors that move through a certain angle to form an image. In this case, the contrast of black and white is greater and allows a sharper image. This system is more complicated to control due to its mechanics of use and they are also limited in the resolution of the sensor. However, they do not present as many problems to scale in power/energy per unit area and allow a wide spectral range to operate in light from the visible ultraviolet to the infrared range.

For fast curing, the highest value of power is necessary. Commercially, DLP equipment with light sources in the UV range, are about 30mW/cm^2, for this application it would be necessary to reach values higher than 500mW/cm^2. On the other hand, these

6. Study of lasers in additive manufacturing

continuous systems also have limitations in the thermal part, in a usual screen projection this is a problem, but with this technology the projection system will be discontinuous allowing dissipation of the heat generated in the DLP chip without get to burn it. To reach the melting point of the particles, an IR light heating system has been proposed with tube lights of 200W consumption, Figure 29, where the highest irradiation power is in the infrared range. This means that the build surface is only a few degrees below always fusing temperature and LCD/DLP is only used to raise the temperature a maximum of five degrees.

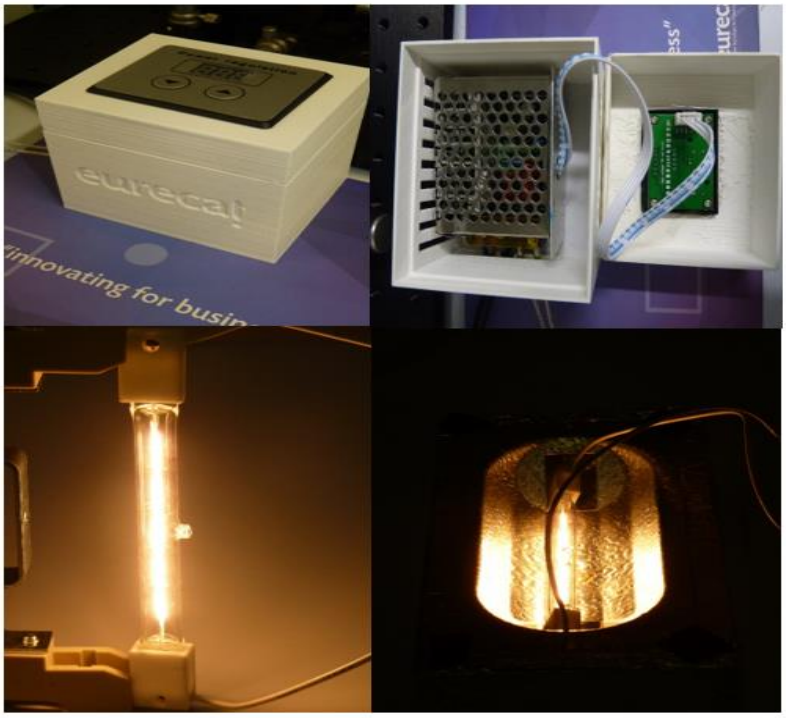

Figure 28. Heating system with halogen lamps

6. Study of lasers in additive manufacturing

Currently, the two possibilities are being studied and obtaining good results in both, but it has not yet been decided which may have a higher performance for this application. But it should be added that due to positioning in the machine, DLP technology is more feasible since it can be more separated from the powder.

It is vitally important to increase the power with IR heating lamps [124]. For the projector, a maximum power of 240mW has been obtained by eliminating the internal color filters and obtaining a monochrome image. In the case of LCD screens, a power per square centimeter of about 200mW has been obtained. Note that the monochrome display has a high transmittance for IR light and high absorption when illuminating UV light below 400nm. There are difficulties with certain materials and other solutions must be sought in order to achieve 1W minimum for efficient curing in LAS 3D printing. Among the main limitations is that the lamps only reach 13W, and for an area of 10x10cm^2, they would result in around 130mW. It is necessary to find new systems with a power of 1W/cm^2 for a better curing of powdered materials. This has already been found in the case of resin prints because any projector can cure with the desired times. However, for curing powders much more power is required. For example, with the projector at 24mW/cm^2, a curing of the powder has already been obtained, but long times have been required.

There are few companies on the market that have high power

6. Study of lasers in additive manufacturing

projection systems. Phoenix is the first system based on Texas Instruments' DLP670S chipset. This In-Vision system offers superior optical performance reaching 6.5 W of output power for additive manufacturing.

The laser has a power of 5.5 W and a wavelength of 450 nm, which has been selected with the help of experts in the field who have validated the choice, Figure 30.

This must be a few centimeters from the powder to speed up the process. This is a laser that is currently used for 3D printing and therefore only a market study had to be carried out to select the most suitable one.

6. Study of lasers in additive manufacturing

Model	XSS05
Supply Voltage	12VDC
Working Current	2.0A Max
Output Optical Power	>5.5W
Laser Power	5.5W
Laser Wavelength	445nm-455nm
Facula Type	Dot (Adjustable Focus)
Driving Mode	Built in ACC Constant Current Drive
Laser Output Control	PWM/TTL
Power Supply & Control Interface	2.54 3PIN
Shell Material	Aluminum Surface Anode Blue
Module Material	Brass
Collimating Lens	K9 Optical Glass & High Antireflection Coating
Heat Dissipation Mode	Aluminum Alloy Shell Forced Air Cooling
Net Weight	0.34 lbs / 153 g
Product Size	3.9 x 1.3 x 1.3 in / 9.9 x 3.3 x 3.3 cm

Figure 29. Laser characteristics

For the SLS lighting part [125][126], we have studied the possibility of mounting a galvanometer with which a lot of processing speed could be gained [127], [128]. Currently, the laser is installed on X-Y axes and is moved by various motors, but to reduce manufacturing time, it would be optimal if it worked with galvos. This fact would make the weight less and the printing time would be reduced. The

6. Study of lasers in additive manufacturing

programming would be more complex, however, the benefits of using the galvos would be great.

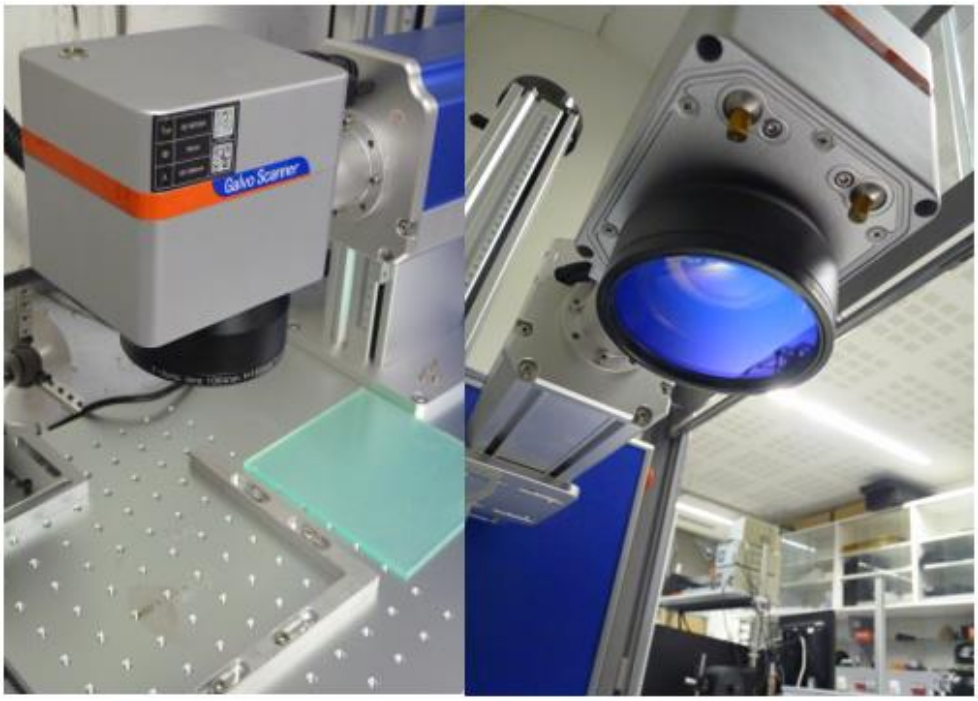

Figure 30. Galvo Scanner System.

As mentioned before, the main objective of this project is to validate the LASUV3D machine technology, which is in the development phase, this means that many of the pieces can be improved and changed in future versions. The material unification system is based on Selective Laser Sintering (SLS) and Large Area Sintering (LAS) technology. The first is the more traditional version of 3D printing with plastic powder using a laser and the second sinters the material

6. Study of lasers in additive manufacturing

using a projector. Therefore, in no case will this point be modified, there is only the possibility of incorporating a laser and/or a projector with better features or modifying the current ones, as is the case of the projector that wants to increase its power by means of a superior light source., if it can be refrigerated with good results. This is one of the most critical points of the current and future project.

A common point currently, of most prototypes, is the use of pieces manufactured in 3D printing. In the following versions, the use of other materials that have a higher tolerance than the afore mentioned technology will be sought. It should be noted that currently the tolerances of 3D printing are improving day after day, but they still cannot be equaled to that of other technologies, such as machining; this will make it necessary to redesign some pieces, especially those of the trays.

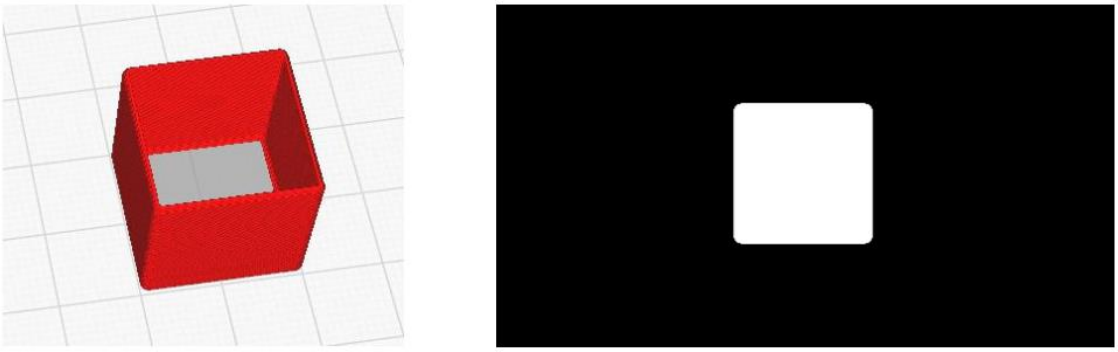

Figure 31. Left: Contour made by laser (SLS), Right: internal part performed by projector (LAS)

6. Study of lasers in additive manufacturing

When it comes to design by assembly, once the prototype has been correctly validated and the way to launch the product to the market is being sought, all the pieces that can be standardized will be used to the same extent in all parts of the machine, always that is possible. This fact will help both the optimization of the machine and the assembly time. This has already been done at this point in the project, but once there is a redesign of the machine it will have to be reviewed again. To go on the market, the aesthetic part of the machine is essential.

Currently the closures are made with steel plates, to improve aesthetics they will be redesigned with more pleasant shapes for the consumer and that can be manufactured by injection. It will only improve the aesthetics if it will not decrease the manufacturing cost, as long as the production is in series, since the injection of plastic begins to be profitable from a minimum amount of units/year.

6. Study of lasers in additive manufacturing

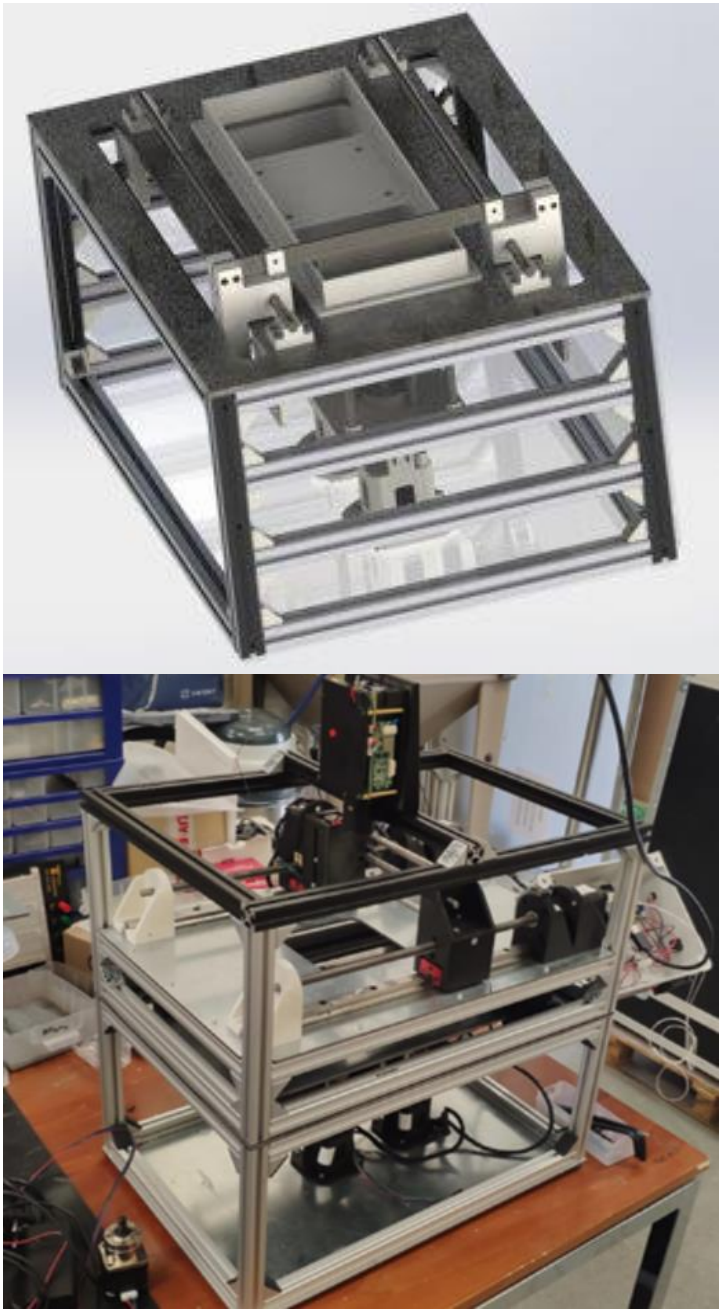

Figure 32. Assembling the test bench

Chapter 7

Conclusions

Throughout this doctoral thesis, the laser operation of novel crystals doped with rare earths, in a continuous wave regime, has been studied. The main achievements for each active ion studied here are listed below. It has designed and developed the creation and implementation of new additive manufacturing technologies for applications in various sectors. As it has been observed, different contributions have been made in laser performance cavities, compact cryogenic lasers, and systems to solve the growing needs of the industry in the field of 3D printing, particularly new light sources, and the study of materials.

7. Conclusions

- **Laser generation around ~2 μm from Tm+3 doped Tm:CLTGG**

✓ Tm:CLTGG is a promising crystal for ultrashort pulse generation (sub-100 fs) in the eye-safe spectral range of ~2 μm. It exhibits a structural disorder, which leads to a significant inhomogeneous broadening of the absorption and emission bands of Tm^{3+} ions confirmed at low temperature (10 K).

✓ At room temperature, due to a combination of the inhomogeneous broadening and electron-phonon interaction, Tm:CLTGG exhibits smooth and very broad gain profiles owing to the phonon-assisted $^3F_4 \rightarrow {}^3H_6$ transition extending until at least ~2.2 μm.

✓ Tm:CLTGG exhibits attractive thermal properties (for a disordered crystal) being superior to those of the CNGG-type crystals.

✓ The laser generated a maximum output power of 1.08 W at 1995 and 2003 nm with a slope efficiency of 23.8% and a laser threshold of 0.91 W.

✓ In conclusion, this study has shown that the microchip configuration is a good option for efficient laser generation.

7. Conclusions

- **Continuous-wave laser operation at cryogenic temperatures**

✓ The laser potential of the Tm:YLF was confirmed by demonstrating a cryogenic CW laser at 80 to 200 K. At 80 K, a maximum output of 6.5 W was obtained, corresponding to a slope efficiency of 66.0 % with respect to absorbed power.

✓ An excellent performance along with a very good beam quality verifies the advantages of cryogenic cooling.

✓ Future work will focus on pulsed laser operation implementing Cr:ZnS and Cr:ZnSe as saturable absorbers in the compact cavity to generate high-energy laser pulses.

✓ This work also reported the first demonstration of a cryogenically cooled 2 μm laser based on the Tm:YLF.

✓ We reported the spectroscopy and the first continuous wave laser operation at cryogenic temperatures of Yb:YCOB in a compact modular cavity with a slope efficiency of 69.1 %, with respect to the incident power.

✓ We investigated the characteristics and continuous wave laser performance of a Yb:$KLu(WO_4)_2$ crystal under cryogenic conditions with a maximum output power of 9.5 W, reached at a temperature of 80 K, with an efficiency slope of 40%.

7. Conclusions

- **Study of lasers for additive manufacturing**

As part of the LASUV3D project, led by the AMS group, a new additive manufacturing technology has been designed and developed, which combines two existing technologies.

✓ Additive manufacturing materials such as resins and polyamides have been studied to expand the catalog of printing materials. For curing powders much more power is required. With the projector at 24mW/cm^2, a curing of the powder has already been obtained, but long times have been required.
  ✓ It is vitally important to increase the power with IR heating lamps.
  ✓ The laser speed, projection time of the projector, and efficient control of heat sources have been studied to achieve higher printing speeds. It must be clarified that the projector is still in the development phase and may undergo changes.
  ✓ Small samples have been obtained to validate the technology. This was one of the goals main aspects of the project since it is a project to study the feasibility of the technology.
  ✓ Successful printing of pieces in short series has been done with the machine. We are currently working on the search for a new projector with higher power and therefore less overheating. At the same time, alternative ways are being developed, such as working with a high-power LCD or DLP screen. Considering the limitations of each of them and their high prices in the market,

the development of their own models that can even be patented is studied.

- ✓ Considering the particularities of the machine, it was considered to request protection through a utility model, which protects inventions with a less inventive range than those protected with a patent, but which would also be a considerable achievement.

References

[1] J. P. Padilla-Martinez, C. Berrospe-Rodriguez, G. Aguilar, J. C. Ramirez-San-Juan, and R. Ramos-Garcia, “Optic cavitation with CW lasers: A review,” *Physics of Fluids*, vol. 26, no. 12, Dec. 2014, doi: 10.1063/1.4904718/1013829.

[2] “Pulsed laser,” Oct. 1989.

[3] J.M. Serres Serres, M. Aguiló and X. Mateos, “Continuous-wave and passively Q-switched solid-state microchip lasers in the near-infrared Doctoral thesis Tarragona 2017.

[4] Q. Peng *et al.*, “Lasers in medicine,” *Reports on Progress in Physics*, vol. 71, no. 5, p. 056701, Apr. 2008, doi: 10.1088/0034-4885/71/5/056701.

[5] H. Lee, C. H. J. Lim, M. J. Low, N. Tham, V. M. Murukeshan, and Y. J. Kim, “Lasers in additive manufacturing: A review,” *International Journal of Precision Engineering and Manufacturing - Green Technology*, vol. 4, no. 3, pp. 307–322, Jul. 2017, doi: 10.1007/S40684-017-0037-7.

[6] D. F. Welch, “A brief history of high-power semiconductor lasers,” *IEEE Journal on Selected Topics in Quantum Electronics*, vol. 6, no. 6, pp. 1470–1477, 2000, doi: 10.1109/2944.902203.

[7] J. Hecht, “Short history of laser development,” *Optical Engineering*, vol. 49, no. 9, p. 091002, Sep. 2010, doi: 10.1117/1.3483597.

[8] J. M. White, H. E. Goodis, and C. L. Rose, “Use of the pulsed Nd:YAG laser for intraoral soft tissue surgery,” *Lasers Surg Med*, vol. 11, no. 5, pp. 455–461, Jan. 1991, doi: 10.1002/LSM.1900110511.

References

[9] J. R. Deepak, R. P. Anirudh, and S. Saran Sundar, “Applications of lasers in industries and laser welding: A review,” *Mater Today Proc*, 2023, doi: 10.1016/j.matpr.2023.02.102.

[10] K. Scholle *et al.*, “2 µm Laser Sources and Their Possible Applications,” *Frontiers in Guided Wave Optics and Optoelectronics*, Feb. 2010, doi: 10.5772/39538.

[11] A. Barazanchi, K. C. Li, B. Al-Amleh, K. Lyons, and J. N. Waddell, “Additive Technology: Update on Current Materials and Applications in Dentistry,” *Journal of Prosthodontics*, vol. 26, no. 2, pp. 156–163, Feb. 2017, doi: 10.1111/JOPR.12510.

[12] Y. Tian *et al.*, “A Review of 3D Printing in Dentistry: Technologies, Affecting Factors, and Applications,” *Scanning*, vol. 2021, 2021, doi: 10.1155/2021/9950131.

[13] A. Gebhardt, F. M. Schmidt, J. S. Hötter, W. Sokalla, and P. Sokalla, “Additive Manufacturing by Selective Laser Melting: The realizer desktop machine and its application for the dental industry,” *Phys Procedia*, vol. 5, no. PART 2, pp. 543–549, 2010, doi: 10.1016/j.phpro.2010.08.082.

[14] K. Wang, Y. Wang, J. O. Strandhagen, and T. Yu, Eds., “Advanced Manufacturing and Automation VIII,” vol. 484, 2019, doi: 10.1007/978-981-13-2375-1.

[15] N. Werkheiser, “In-space Manufacturing Project Manager Marshall Space Flight Center NIKI.WERKHEISER@NASA.GOV”, Accessed: Jun. 28, 2023. [Online]. Available: www.nasa.gov

[16] S. Jonuzakov, “Economic aspects of additive manufacturing,” Mar. 2023.

[17] B. Garrett, “3D printing: New economic paradigms and strategic shifts,” *Glob Policy*, vol. 5, no. 1, pp. 70–75, Feb. 2014, doi: 10.1111/1758-5899.12119.

[18] T. D. Ngo, A. Kashani, G. Imbalzano, K. T. Q. Nguyen, and D. Hui, “Additive manufacturing (3D printing): A review of materials, methods, applications and

References

challenges," *Compos B Eng*, vol. 143, pp. 172–196, Jun. 2018, doi: 10.1016/J.COMPOSITESB.2018.02.012.

[19] D. C. Brown, "The promise of cryogenic solid-state lasers," *IEEE Journal on Selected Topics in Quantum Electronics*, vol. 11, no. 3, pp. 587–599, May 2005, doi: 10.1109/JSTQE.2003.850237.

[20] D. Rand, J. Hybl, and T. Y. Fan, "Cryogenic lasers," *Handbook of Solid-State Lasers: Materials, Systems and Applications*, pp. 525–550, Feb. 2013, doi: 10.1533/9780857097507.2.525.

[21] A. Yoshida *et al.*, "Diode-pumped mode-locked Yb:YCOB laser generating 35 fs pulses," *Opt Lett*, vol. 36, no. 22, p. 4425, Nov. 2011, doi: 10.1364/OL.36.004425.

[22] H. Jiang, J. Wang, H. Zhang, X. Hu, P. Burns, and J. A. Piper, "Spectral and luminescent properties of Yb3+ ions in YCa4O(BO3)3 crystal," *Chem Phys Lett*, vol. 361, no. 5–6, pp. 499–503, Aug. 2002, doi: 10.1016/S0009-2614(02)00989-2.

[23] S. Chénais *et al.*, "Thermal lensing measurements in diode-pumped Yb-doped GdCOB, YCOB, YSO, YAG and KGW," *Opt Mater (Amst)*, vol. 22, no. 2, pp. 129–137, 2003, doi: 10.1016/S0925-3467(02)00356-7.

[24] J. M. Serres *et al.*, "Prospects of monoclinic Yb:KLu(WO_4)_2 crystal for multi-watt microchip lasers," *Opt Mater Express*, vol. 5, no. 3, p. 661, Mar. 2015, doi: 10.1364/OME.5.000661.

[25] L. Shah *et al.*, "Laser tunability in Yb3+:YCa4O(BO3)3 {Yb:YCOB}," *Opt Commun*, vol. 167, no. 1, pp. 149–153, Aug. 1999, doi: 10.1016/S0030-4018(99)00293-X.

[26] J. Kawanaka *et al.*, "Highly efficient cryogenically-cooled Yb:YAG laser," *Laser Phys.*, vol. 20, no. 5, p. 1079, May 2010, doi: 10.1134/s1054660x10090252.

[27] P. Navratil, V. Jambunathan, L. Horackova, A. Lucianetti, and T. Mocek,

References

"Diode pumped compact cryogenic Yb:YAG/Cr:YAG pulsed laser," *Solid State Lasers XXV: Technology and Devices*, vol. 9726, p. 97261G, Mar. 2016, doi: 10.1117/12.2210960.

[28] S. P. David, V. Jambunathan, F. Yue, A. Lucianetti, and T. Mocek, "Efficient diode pumped Yb:Y2O3 cryogenic laser," *Appl Phys B*, vol. 125, no. 7, pp. 1–5, Jul. 2019, doi: 10.1007/S00340-019-7250-8/METRICS.

[29] P. Loiko *et al.*, "Thermal Lensing and Multiwatt Microchip Laser Operation of Yb:YCOB Crystals," *IEEE Photonics J*, vol. 8, no. 3, Jun. 2016, doi: 10.1109/JPHOT.2016.2555584.

[30] D. V. Seletskiy, S. D. Melgaard, S. Bigotta, A. Di Lieto, M. Tonelli, and M. Sheik-Bahae, "Laser cooling of solids to cryogenic temperatures," *Nature Photonics 2010 4:3*, vol. 4, no. 3, pp. 161–164, Jan. 2010, doi: 10.1038/nphoton.2009.269.

[31] F. Yue, "DEVELOPMENT OF A CRYOGENIC 2 MM MULTI-PASS AMPLIFIER IN NANOSECOND REGIME."

[32] by J. Christopher Gardiner, M. Professor, N. B. Crane, D. Murphy, and T. Yucelen, "Large Area Sintering Test Platform Design and Preliminary Study on Cross Sectional Resolution," 2017.

[33] "The History of the Laser - Mario Bertolotti - Google Libros." https://books.google.la/books?hl=es&lr=&id=JObDnEtzMJUC&oi=fnd&pg=PP11&dq=lasers+history&ots=tAP8cz9gM2&sig=YDwo8IX7fjn5_JdyUg2S88IEOBk&redir_esc=y#v=onepage&q=lasers%20history&f=false (accessed Jun. 28, 2023).

[34] P. P. Sorokin, "Contributions of IBM to Laser Science—1960 to the Present," *IBM J Res Dev*, vol. 23, no. 5, pp. 476–489, Sep. 1979, doi: 10.1147/RD.235.0476.

[35] C. H. Townes, "Theodore H. Maiman (1927–2007)," *Nature 2007 447:7145*, vol. 447, no. 7145, pp. 654–654, Jun. 2007, doi: 10.1038/447654a.

References

[36] T. H. Maiman, “Stimulated optical radiation in Ruby,” *Nature*, vol. 187, no. 4736, pp. 493–494, 1960, doi: 10.1038/187493A0.

[37] T. H. Maiman, “Stimulated optical radiation in Ruby,” *Nature*, vol. 187, no. 4736, pp. 493–494, 1960, doi: 10.1038/187493A0.

[38] S. Scholtz, M. Becker, L. MacMorris, and A. Langenbucher, “LASER. ‘A solution in search of a problem,’” *Curiosities in Medicine*, pp. 181–184, 2023, doi: 10.1007/978-3-031-14002-0_49.

[39] “Optical maser having terminal level above ground state,” Dec. 1960.

[40] M. I. Nathan, W. P. Dumke, G. Burns, F. H. Dill, and G. Lasher, “Stimulated emission of radiation from GaAs p-n junctions,” *Appl Phys Lett*, vol. 1, no. 3, pp. 62–64, 1962, doi: 10.1063/1.1777371.

[41] H. Haken, “Laser Theory,” pp. 1–304, 1970, doi: 10.1007/978-3-662-22091-7_1.

[42] J. J. Zayhowski, “Microchip lasers,” *Opt Mater (Amst)*, vol. 11, no. 2–3, pp. 255–267, 1999, doi: 10.1016/S0925-3467(98)00048-2.

[43] C. Bostedt *et al.*, “Linac Coherent Light Source: The first five years,” *Rev Mod Phys*, vol. 88, no. 1, p. 015007, Mar. 2016, doi: 10.1103/REVMODPHYS.88.015007/FIGURES/44/MEDIUM.

[44] R. Powell, Powell, and Richard, “Types of Lasers,” *sham*, p. 1035, 2006, doi: 10.1007/978-0-387-26308-3_71.

[45] H. Kubbinga, “A tribute to Max Planck,” *Europhysics News*, vol. 49, no. 4, pp. 27–30, Jul. 2018, doi: 10.1051/EPN/2018405.

[46] J. M. Dudley, “Light, Lasers, and the Nobel Prize,” *https://doi.org/10.1117/1.AP.2.5.050501*, vol. 2, no. 5, p. 050501, Oct. 2020, doi: 10.1117/1.AP.2.5.050501.

[47] A. Marino, “Physics, lasers and the nobel prize,” *Europhysics News*, vol. 50, no. 2, pp. 26–28, Mar. 2019, doi: 10.1051/EPN/2019205.

[48] “Photonics and Lasers: An Introduction - Richard S. Quimby - Google Libros.”

References

https://books.google.la/books?hl=es&lr=&id=82f-gIvtC7wC&oi=fnd&pg=PR7&dq=photonics+lasers&ots=ApERJc-U_r&sig=vNvJJu59M-5Frej0VPIQnLTQMXo&redir_esc=y#v=onepage&q=photonics%20lasers&f=false (accessed Jun. 29, 2023).

[49] V. Philipps *et al.*, “Development of laser-based techniques for in situ characterization of the first wall in ITER and future fusion devices,” *Nuclear Fusion*, vol. 53, no. 9, p. 093002, Aug. 2013, doi: 10.1088/0029-5515/53/9/093002.

[50] F. W. Cummings, “Stimulated Emission of Radiation in a Single Mode,” *Physical Review*, vol. 140, no. 4A, p. A1051, Nov. 1965, doi: 10.1103/PhysRev.140.A1051.

[51] W. Krupke and R. Byer, “Solid-State Lasers,” 1960.

[52] F. Díaz *et al.*, “Diode-pumped microchip Tm:KLu(WO_4)$_2$ laser with more than 3 W of output power,” *Optics Letters, Vol. 39, Issue 14, pp. 4247-4250*, vol. 39, no. 14, pp. 4247–4250, Jul. 2014, doi: 10.1364/OL.39.004247.

[53] J. M. Serres *et al.*, “Diode-pumped microchip Tm:KLu(WO_4)_2 laser with more than 3 W of output power,” *Opt Lett*, vol. 39, no. 14, p. 4247, Jul. 2014, doi: 10.1364/OL.39.004247.

[54] J. P. Wittke, Z. J. Kiss, R. C. Duncan, and J. J. McCormick, “Uranium-Doped Calcium Fluoride as a Laser Material,” *Proceedings of the IEEE*, vol. 51, no. 1, pp. 56–62, 1963, doi: 10.1109/PROC.1963.1659.

[55] Z. Liu, A. Ikesue, and J. Li, “Research progress and prospects of rare-earth doped sesquioxide laser ceramics,” *J Eur Ceram Soc*, vol. 41, no. 7, pp. 3895–3910, Jul. 2021, doi: 10.1016/J.JEURCERAMSOC.2021.02.026.

[56] K. Petermann *et al.*, “Rare-earth-doped sesquioxides,” *J Lumin*, vol. 87–89, pp. 973–975, May 2000, doi: 10.1016/S0022-2313(99)00497-4.

References

[57] O. J. Beck, “The use of the Nd-YAG and the CO2 laser in neurosurgery,” *Neurosurgical Review 1980 3:4*, vol. 3, no. 4, pp. 261–266, Dec. 1980, doi: 10.1007/BF01650032.

[58] T. M. Aslam, H. Devlin, and B. Dhillon, “Use of Nd:YAG laser capsulotomy,” *Surv Ophthalmol*, vol. 48, no. 6, pp. 594–612, Nov. 2003, doi: 10.1016/J.SURVOPHTHAL.2003.08.002.

[59] S. Urfalıoglu, G. Özdemir, M. Güler, B. Daghan, and F. Öz, “The evaluation of the effect of Nd-YAG capsulotomy on posterior ocular vascular structures by Optical coherence tomography angiography,” *Photodiagnosis Photodyn Ther*, vol. 42, Jun. 2023, doi: 10.1016/J.PDPDT.2023.103323.

[60] K. F. Wall and A. Sanchez, “TItanium Sapphire Lasers”.

[61] W. R. Rapoport and C. P. Khattak, “Titanium sapphire laser characteristics,” *Applied Optics, Vol. 27, Issue 13, pp. 2677-2684*, vol. 27, no. 13, pp. 2677–2684, Jul. 1988, doi: 10.1364/AO.27.002677.

[62] M. G. Kovalsky, J. R. Tredicce, and A. A. Hnilo, “Extreme events in the Ti:sapphire laser,” *Optics Letters, Vol. 36, Issue 22, pp. 4449-4451*, vol. 36, no. 22, pp. 4449–4451, Nov. 2011, doi: 10.1364/OL.36.004449.

[63] G. A. Massey, “CRITERION FOR SELECTION OF cw LASER HOST MATERIALS TO INCREASE AVAILABLE POWER IN THE FUNDAMENTAL MODE,” *Appl Phys Lett*, vol. 17, no. 5, pp. 213–215, Sep. 1970, doi: 10.1063/1.1653370.

[64] L. Zheng *et al.*, “Determination of cross-relaxation efficiency based on spectroscopy in thulium-doped rare-earth sesquioxides,” *Ceram Int*, vol. 49, no. 7, pp. 11060–11066, Apr. 2023, doi: 10.1016/j.ceramint.2022.11.301.

[65] C. Krankel, “Rare-earth-doped sesquioxides for diode-pumped high-power lasers in the 1-, 2-, and 3-μm spectral range,” *IEEE Journal of Selected Topics in Quantum Electronics*, vol. 21, no. 1, pp. 250–262, Jan. 2015, doi: 10.1109/JSTQE.2014.2346618.

References

[66] X. Mateos *et al.*, “Efficient Micro-Lasers Based on Highly Doped Monoclinic Double Tungstates,” *IEEE J Quantum Electron*, vol. 53, no. 3, Jun. 2017, doi: 10.1109/JQE.2017.2681626.

[67] M. Yamile and S. Sarmiento, “MONOCLINIC TM:KLU(W04)2: A NEW CRYSTAL FOR EFFICIENT DIODE-PUMPED CONTINUOUS-WAVE AND Q-SWITCHED LASERS.”

[68] V. Jambunathan, X. Mateos, and M. A. Díaz, “Infrared lasers based on Ho 3+ :KRE(WO 4) 2 crystals with Tm 3+ or Yb 3+ as sensitizers UNIVERSITAT ROVIRA I VIRGILI INFRARED LASERS BASED ON HO3+:KRE(WO4)2 CRYSTALS WITH TM3+OR YB3+ AS SENSITIZERS,” 2011.

[69] S. P. David *et al.*, “Laser performances of diode pumped Yb:Lu_2O_3 transparent ceramic at cryogenic temperatures,” *Optical Materials Express, Vol. 9, Issue 12, pp. 4669-4676*, vol. 9, no. 12, pp. 4669–4676, Dec. 2019, doi: 10.1364/OME.9.004669.

[70] V. Jambunathan *et al.*, “Spectroscopic characterization of various Yb 3+ doped laser materials at cryogenic temperatures for the development of high energy class diode pumped solid state lasers,” *High-Power, High-Energy, and High-Intensity Laser Technology; and Research Using Extreme Light: Entering New Frontiers with Petawatt-Class Lasers*, vol. 8780, p. 87800G, May 2013, doi: 10.1117/12.2016915.

[71] O. Silvestre, M. C. Pujol, M. Rico, F. Güell, M. Aguiló, and F. Díaz, “Thulium doped monoclinic KLu(WO4)2 single crystals: Growth and spectroscopy,” *Appl Phys B*, vol. 87, no. 4, pp. 707–716, Jun. 2007, doi: 10.1007/S00340-007-2664-0/METRICS.

[72] M. D. Serrano *et al.*, “Broadly tunable laser operation near 2μm in a locally disordered crystal of Tm^{3+}-doped $NaGd(WO_4)_2$,” *JOSA B, Vol. 23, Issue 12, pp. 2494-2502*, vol. 23, no. 12, pp. 2494–2502, Dec. 2006, doi: 10.1364/JOSAB.23.002494.

References

[73] J. M. Cano-Torres *et al.*, “Infrared spectroscopic and laser characterization of Tm in disordered double tungstates,” *Materials Science and Engineering: B*, vol. 146, no. 1–3, pp. 22–28, Jan. 2008, doi: 10.1016/J.MSEB.2007.07.040.

[74] S. P. David, V. Jambunathan, F. Yue, A. Lucianetti, and T. Mocek, “Efficient diode pumped Yb:Y2O3 cryogenic laser,” *Applied Physics B 2019 125:7*, vol. 125, no. 7, pp. 1–5, Jun. 2019, doi: 10.1007/S00340-019-7250-8.

[75] F. Yue *et al.*, “Diode-pumped cryogenic Tm:LiYF4 laser,” *https://doi.org/10.1117/12.2517734*, vol. 11033, no. 26, pp. 34–39, Apr. 2019, doi: 10.1117/12.2517734.

[76] A. Alles *et al.*, “Cryogenic Tm:LiYF 4 laser around 2 μm,” vol. 129, p. 41, 2023, doi: 10.1007/s00340-023-07970-8.

[77] J. Körner *et al.*, “Spectroscopic characterization of Yb3+-doped laser materials at cryogenic temperatures,” *Appl Phys B*, vol. 116, no. 1, pp. 75–81, 2014, doi: 10.1007/S00340-013-5650-8.

[78] T. Y. Fan *et al.*, “Cryogenic Yb3+-doped solid-state lasers,” *IEEE Journal on Selected Topics in Quantum Electronics*, vol. 13, no. 3, pp. 448–458, May 2007, doi: 10.1109/JSTQE.2007.896602.

[79] S. P. David, V. Jambunathan, F. Yue, A. Lucianetti, and T. Mocek, “Diode - pumped efficient cryogenic Yb:Y2O3 transparent ceramic laser,” *2019 Conference on Lasers and Electro-Optics Europe and European Quantum Electronics Conference, CLEO/Europe-EQEC 2019*, Jun. 2019, doi: 10.1109/CLEOE-EQEC.2019.8872979.

[80] S. Chakraborty and M. C. Biswas, “3D printing technology of polymer-fiber composites in textile and fashion industry: A potential roadmap of concept to consumer,” *Compos Struct*, vol. 248, p. 112562, Sep. 2020, doi: 10.1016/J.COMPSTRUCT.2020.112562.

[81] A. S. Elakkad and A. shams university, “3D Technology in the Automotive Industry,” *International Journal of Engineering Research and*, vol. V8, no. 11.

References

ESRSA Publications Pvt. Ltd., Nov. 19, 2019. doi: 10.17577/ijertv8is110122.

[82] B. J. Tuazon, N. A. V. Custodio, R. B. Basuel, L. A. D. Reyes, and J. R. C. Dizon, "3D Printing Technology and Materials for Automotive Application: A Mini-Review," *Key Eng Mater*, vol. 913, pp. 3–16, 2022, doi: 10.4028/P-26O076.

[83] S. Negi, R. Kumar Sharma, and S. Dhiman, "Basics, applications and future of additive manufacturing technologies: A review Numerical modelling of temperature rise generation at tool , chip and workpiece in metal cutting View project Optimization for the density of laser sintered parts View project BASICS, APPLICATIONS AND FUTURE OF ADDITIVE MANUFACTURING TECHNOLOGIES: A REVIEW," *Article in Journal of Manufacturing Technology Research · March*, vol. 5, no. 1, 2013, Accessed: Jun. 29, 2023. [Online]. Available: https://www.researchgate.net/publication/281004567

[84] J. Delgado, L. Serenó, K. Monroy, and J. Ciurana, "Selective Laser Sintering," *Modern Manufacturing Processes*, pp. 481–499, Aug. 2019, doi: 10.1002/9781119120384.CH20.

[85] "Method of selective laser sintering with improved materials," Aug. 2006.

[86] F. Fina, A. Goyanes, S. Gaisford, and A. W. Basit, "Selective laser sintering (SLS) 3D printing of medicines," *Int J Pharm*, vol. 529, no. 1–2, pp. 285–293, Aug. 2017, doi: 10.1016/J.IJPHARM.2017.06.082.

[87] S. Yuan, F. Shen, C. K. Chua, and K. Zhou, "Polymeric composites for powder-based additive manufacturing: Materials and applications," *Prog Polym Sci*, vol. 91, pp. 141–168, Apr. 2019, doi: 10.1016/J.PROGPOLYMSCI.2018.11.001.

[88] A. Alles *et al.*, "Growth, Spectroscopy and Laser Operation of Tm3+, Li+-Codoped Ca3Ta1.5Ga3.5O12-Type Disordered Garnet Crystal," *2021 Conference on Lasers and Electro-Optics Europe and European Quantum Electronics Conference (2021), paper ca_9_4*, p. ca_9_4, Jun. 2021,

References

Accessed: Jun. 28, 2023. [Online]. Available: https://opg.optica.org/abstract.cfm?uri=CLEO_Europe-2021-ca_9_4

[89] M. Cañellas and A. Pérez, “EURECAT centre tecnològic de Catalunya.,” vol. Notícies, Mar. 2017, Accessed: Jun. 29, 2023. [Online]. Available: https://rdi.dtes.scipedia.com/s/Canellas_Perez_2017a

[90] A. : Adrián and M. Pedregosa, “Disseny i desenvolupament d’una nova tecnologia per l’àmbit de la fabricació additiva.”

[91] H. E. Martn, “Solid state differential input chopper,” *1* \, Jul. 1967.

[92] T. Y. Fan and A. Sanchez, “Pump Source Requirements for End-Pumped Lasers,” *IEEE J Quantum Electron*, vol. 26, no. 2, pp. 311–316, 1990, doi: 10.1109/3.44963.

[93] D. Psaltis, K. Buse, G. Steckman, C. Moser, F. Havermeyer, and W. Liu, “Volume Bragg Grating Devices,” *Optical Fiber Communication Conference (2003), paper FC6*, p. FC6, Mar. 2003, Accessed: Jun. 29, 2023. [Online]. Available: https://opg.optica.org/abstract.cfm?uri=OFC-2003-FC6

[94] J. Chen, B. Gu, E. J. LeBoeuf, H. Pan, and S. Dai, “Spectroscopic characterization of the structural and functional properties of natural organic matter fractions,” *Chemosphere*, vol. 48, no. 1, pp. 59–68, Jul. 2002, doi: 10.1016/S0045-6535(02)00041-3.

[95] D. F. Swinehart, “The Beer-Lambert Law,” *J Chem Educ*, vol. 39, no. 7, pp. 333–335, 1962, doi: 10.1021/ED039P333.

[96] S. P. Mulvaney and C. D. Keating, “Raman spectroscopy,” *Anal Chem*, vol. 72, no. 12, Jun. 2000, doi: 10.1021/A10000155/ASSET/A10000155.FP.PNG_V03.

[97] K. Jiao *et al.*, “The characterization and quantitative analysis of nanopores in unconventional gas reservoirs utilizing FESEM–FIB and image processing: An example from the lower Silurian Longmaxi Shale, upper Yangtze region, China,” *Int J Coal Geol*, vol. 128–129, pp. 1–11, Aug. 2014, doi:

References

10.1016/J.COAL.2014.03.004.

[98] D. Bourell *et al.*, “Materials for additive manufacturing,” *CIRP Ann Manuf Technol*, vol. 66, no. 2, pp. 659–681, 2017, doi: 10.1016/j.cirp.2017.05.009.

[99] X. Tian, Z. Zhao, H. Wang, X. Liu, and X. Song, “Progresses on the additive manufacturing of functionally graded metallic materials,” *J Alloys Compd*, vol. 960, Oct. 2023, doi: 10.1016/j.jallcom.2023.170687.

[100] C. Tombling and M. Tillin, “Innovations in LCD technology,” *Synth Met*, vol. 122, no. 1, pp. 209–214, May 2001, doi: 10.1016/S0379-6779(00)01339-4.

[101] E. Huerta, J. E. Corona, A. I. Oliva, F. Avilés, and J. González-Hernández, “Universal testing machine for mechanical properties of thin materials,” *Revista mexicana de física*, vol. 56, no. 4, pp. 317–322, 2010, Accessed: Jun. 29, 2023. [Online]. Available: http://www.scielo.org.mx/scielo.php?script=sci_arttext&pid=S0035-001X2010000400008&lng=es&nrm=iso&tlng=en

[102] A. Lucianetti *et al.*, “HiLASE: a scalable option for Laser Inertial Fusion Energy,” *J Phys Conf Ser*, vol. 688, no. 1, p. 012060, Mar. 2016, doi: 10.1088/1742-6596/688/1/012060.

[103] A. Alles *et al.*, “Compact cryogenic Tm:LiYF4 laser”, doi: 10.1051/epjconf/202226701023.

[104] D. L. Bourell, “Perspectives on Additive Manufacturing,” *https://doi.org/10.1146/annurev-matsci-070115-031606*, vol. 46, pp. 1–18, Jul. 2016, doi: 10.1146/ANNUREV-MATSCI-070115-031606.

[105] F. P. W. Melchels, M. A. N. Domingos, T. J. Klein, J. Malda, P. J. Bartolo, and D. W. Hutmacher, “Additive manufacturing of tissues and organs,” *Prog Polym Sci*, vol. 37, no. 8, pp. 1079–1104, 2012, doi: 10.1016/j.progpolymsci.2011.11.007.

[106] C. Chu, G. Graf, and D. W. Rosen, “Design for additive manufacturing of cellular structures,” *Comput Aided Des Appl*, vol. 5, no. 5, pp. 686–696, 2008,

References

doi: 10.3722/CADAPS.2008.686-696.

[107] N. Guo and M. C. Leu, “Additive manufacturing: Technology, applications and research needs,” *Frontiers of Mechanical Engineering*, vol. 8, no. 3, pp. 215–243, Sep. 2013, doi: 10.1007/S11465-013-0248-8.

[108] M. Vaezi, H. Seitz, and S. Yang, “A review on 3D micro-additive manufacturing technologies,” *International Journal of Advanced Manufacturing Technology*, vol. 67, no. 5–8, pp. 1721–1754, 2013, doi: 10.1007/S00170-012-4605-2.

[109] S. H. Huang, P. Liu, A. Mokasdar, and L. Hou, “Additive manufacturing and its societal impact: A literature review,” *International Journal of Advanced Manufacturing Technology*, vol. 67, no. 5–8, pp. 1191–1203, Jul. 2013, doi: 10.1007/S00170-012-4558-5.

[110] S. A. M. Tofail, E. P. Koumoulos, A. Bandyopadhyay, S. Bose, L. O’Donoghue, and C. Charitidis, “Additive manufacturing: scientific and technological challenges, market uptake and opportunities,” *Materials Today*, vol. 21, no. 1. Elsevier B.V., pp. 22–37, Jan. 01, 2018. doi: 10.1016/j.mattod.2017.07.001.

[111] W. Gao *et al.*, “The status, challenges, and future of additive manufacturing in engineering,” *CAD Computer Aided Design*, vol. 69, pp. 65–89, Dec. 2015, doi: 10.1016/j.cad.2015.04.001.

[112] T. DebRoy *et al.*, “Additive manufacturing of metallic components – Process, structure and properties,” *Prog Mater Sci*, vol. 92, pp. 112–224, Mar. 2018, doi: 10.1016/j.pmatsci.2017.10.001.

[113] B. Özbay Kısasöz, I. E. Serhatlı, and M. E. Bulduk, “Selective Laser Sintering Manufacturing and Characterization of Lightweight PA 12 Polymer Composites with Different Hollow Microsphere Additives,” *Journal of Materials Engineering and Performance 2021 31:5*, vol. 31, no. 5, pp. 4049–4059, Jan. 2022, doi: 10.1007/S11665-021-06481-X.

References

[114] S. Terekhina, T. Tarasova, S. Egorov, L. Guillaumat, and M. L. Hattali, "On the difference in material structure and fatigue properties of polyamide specimens produced by fused filament fabrication and selective laser sintering," *International Journal of Advanced Manufacturing Technology*, vol. 111, no. 1–2, pp. 93–107, Nov. 2020, doi: 10.1007/S00170-020-06026-X/METRICS.

[115] "Apparatus and method for producing parts with multi-directional powder delivery," Nov. 1991.

[116] P. Fischer, V. Romano, A. Blatter, and H. P. Weber, "Highly precise pulsed selective laser sintering of metallic powders," *Laser Phys Lett*, vol. 2, no. 1, pp. 48–55, Jan. 2005, doi: 10.1002/LAPL.200410118.

[117] S. Das, "Physical Aspects of Process Control in Selective Laser Sintering of Metals," *Adv Eng Mater*, vol. 5, no. 10, pp. 701–711, Oct. 2003, doi: 10.1002/ADEM.200310099.

[118] "Modern Manufacturing Processes," *Modern Manufacturing Processes*, Sep. 2019, doi: 10.1002/9781119120384.

[119] E. O. Olakanmi, R. F. Cochrane, and K. W. Dalgarno, "A review on selective laser sintering/melting (SLS/SLM) of aluminium alloy powders: Processing, microstructure, and properties," *Prog Mater Sci*, vol. 74, pp. 401–477, Oct. 2015, doi: 10.1016/J.PMATSCI.2015.03.002.

[120] R. Paul *et al.*, "Rapid Prototyping of High-resolution Large Format Microouidic Device Through Maskless Image Guided In-situ Photopolymerization," 2022, doi: 10.21203/rs.3.rs-2109926/v1.

[121] C. Yan, L. Hao, L. Xu, and Y. Shi, "Preparation, Characterisation and Processing of Carbon Fibre/Polyamide-12 Composites for Selective Laser Sintering," *Compos Sci Technol*, vol. 71, no. 16, pp. 1834–1841, Nov. 2011, doi: 10.1016/j.compscitech.2011.08.013.

[122] A. Schmitz, "Effect of Curing Parameters on Warp in the SLA Printing

References

Process," *ASME International Mechanical Engineering Congress and Exposition, Proceedings (IMECE)*, vol. 4, Feb. 2023, doi: 10.1115/IMECE2022-88495.

[123] T. W. Bacha, D. C. Manuguerra, R. A. Marano, and J. F. Stanzione, "Hydrophilic modification of SLA 3D printed droplet generators by photochemical grafting," *RSC Adv*, vol. 11, no. 35, pp. 21745–21753, Jun. 2021, doi: 10.1039/D1RA03057D.

[124] C. O'Hara, "Development of UV LED Based Lamps with Modular Optical Heads," *Theses*, Jan. 2019, Accessed: Jun. 29, 2023. [Online]. Available: https://sword.cit.ie/allthe/140

[125] C. Basu, M. Meinhardt-Wollweber, and B. Roth, "Lighting with laser diodes," *Advanced Optical Technologies*, vol. 2, no. 4, pp. 313–321, Aug. 2013, doi: 10.1515/AOT-2013-0031/MACHINEREADABLECITATION/RIS.

[126] K. Senthilkumaran, P. M. Pandey, and P. V. M. Rao, "Influence of building strategies on the accuracy of parts in selective laser sintering," *Mater Des*, vol. 30, no. 8, pp. 2946–2954, Sep. 2009, doi: 10.1016/J.MATDES.2009.01.009.

[127] H. W. Yoo, S. Ito, and G. Schitter, "High speed laser scanning microscopy by iterative learning control of a galvanometer scanner," *Control Eng Pract*, vol. 50, pp. 12–21, May 2016, doi: 10.1016/J.CONENGPRAC.2016.02.007.

[128] T. Hegna, H. Pettersson, K. M. Laundal, and K. Grujic, "3D laser scanner system based on a galvanometer scan head for high temperature applications," *https://doi.org/10.1117/12.888985*, vol. 8082, pp. 1195–1203, May 2011, doi: 10.1117/12.888985.

References

List of publications

The results of this thesis are based on the work of following publications in indexed international journals and conferences:

[P1] **Adrian Alles**, Zhongben Pan, Pavel Loiko, Josep Maria Serres, Sami Slimi, Shawuti Yingming, Kaiyang Tang, Yicheng Wang, Yongguang Zhao, Elena Dunina, Alexey Kornienko, Patrice Camy, Weidong Chen, Li Wang, Uwe Griebner, Valentin Petrov, Rosa Maria Solé, Magdalena Aguiló, Francesc Díaz, and Xavier Mateos, **"Tm^{3+}-doped calcium lithium tantalum gallium garnet (Tm:CLTGG): novel laser crystal,"** Opt. Mater. Express 11, 2938-2951 (2021)

https://doi.org/10.1364/OME.435238

[P2] **Adrian Alles**, Venkatesan Jambunathan, Sami Slimi, Josep M. Serres, Magdalena Aguiló, Francesc Díaz, Xavier Mateos, Martin Smrz, and Tomas Mocek, **"Cryogenic Tm:LiYF4 laser around 2 μm"**, Appl. Phys. B 129, 41 (2023)

https://doi.org/10.1007/s00340-023-07970-8

[P3] **Adrian Alles**, Venkatesan Jambunathan, Ghassen Zin Elabedine, Sami Slimi, Josep M. Serres, Magdalena Aguiló, Francesc Díaz, Xavier Mateos, Martin Smrz, and Tomas Mocek, **"Cryogenic spectroscopy and continuous-wave microchip Yb:YCOB laser"**, (In preparation).

[P4] **Adrian Alles**, Venkatesan Jambunathan, Ghassen Zin Elabedine, Sami Slimi, Josep M. Serres, Magdalena Aguiló, Francesc Díaz, Xavier Mateos, Martin Smrz, and Tomas Mocek, **"Continuous-wave laser operation of Yb:KLuW using a modular compact cavity at cryogenic temperatures"**, (In preparation).

[C1] **A. Alles**, Z. Pan, J. M. Serres, P. Loiko, K. Tang, S. Yingming, Y. Wang, Y. Zhao, E. Dunina, A. Kornienko, P. Camy, W. Chen, L. Wang, U. Griebner, V. Petrov, R. M. Solé, M. Aguiló, F. Díaz, and X. Mateos, "Growth, Spectroscopy and Laser Operation of Tm^{3+}, Li^{+}-Codoped $Ca_3Ta_{1.5}Ga_{3.5}O_{12}$-Type Disordered Garnet Crystal," *Conference on Lasers and Electro-Optics Europe and European Quantum Electronics Conference*, OSA Technical Digest (Optica Publishing Group, 2021), paper ca_9_4. (2021)

[C2] **A. Alles**, V. Jambunathan, S. Slimi, J. M. Serres, M. Aguiló, F. Díaz, X. Mateos, M. Smrz, T. Mocek, **"Compact cryogenic Tm: LiYF4 laser"**. In European Physical Journal Web of Conferences (Vol. 267, p. 01023). (2022) https://doi.org/10.1051/epjconf/202226701023

UNIVERSITAT ROVIRA I VIRGILI
INFRARED LASERS WITH NOVEL GEOMETRIES
Adrian Alles Leal